May 2001

Indicoat Final Report
Determination of Hardness and Modulus of Thin Films and Coatings by Nanoindentation

N M Jennett, A S Maxwell, K Lawrence, L N McCartney, R Hunt,
J Koskinen, J Meneve, W Wegener, T Muukkonen, F Rossi, N Gibson,
Zhihui Xu, A J Bushby, S Brookes, A Cavaleiro, K Herrmann,
B Bellaton, R Consiglio, F Augereau, O Kolosov, D Schneider, T Chudoba

NPL Materials Centre
National Physical Laboratory
Teddington
Middlesex
TW11 0LW

ABSTRACT

This report describes the work that has been conducted during the European Indicoat project into the nanoindentation of coatings. The project determined the sensitivity of hardness and modulus values to: instrument calibration and environment; indenter geometry calibration; the instrumental parameters of the detailed loading cycles; and material effects such as coating type and thickness. Selected models have been compared, tested, validated and the limits of their applicability determined. The models used independent traceable values of the coatings Young's modulus obtained by acoustic methods. Validation involved comparing the modelled response with the experimentally determined indentation response.

© Crown copyright 2001
Reproduced by permission of the Controller, HMSO

ISSN 1473-2734

National Physical Laboratory
Teddington, Middlesex, TW11 0LW, UK

Extracts from this report may be reproduced provided that the source is acknowledged and the extract is not taken out of context.

Approved on behalf of Managing Director, NPL by Dr C Lea,
Head of NPL Materials Centre

Determination of Hardness and Modulus of Thin Films and Coatings by Nanoindentation (INDICOAT)

Contract No. SMT4-CT98-2249
1 October 1998 - 1 May 2001
Co-ordinator: N M Jennett, NPL, UK

Final Report
October 1998 to May 2001

N M Jennett [a], L N McCartney [a], K Lawrence [a], R Hunt [a], A Maxwell[a], J Koskinen [b], J Meneve [c], W Wegener [d], N Gibson [e], Zhihui Xu [f], A J Bushby [g], T Chudoba [h], A Cavaleiro [i], K Herrmann [j], R Consiglio [k], F Augereau [l], D Schneider [m].

[a] NPL, UK; [b] VTT, Finland; [c] VITO, Belgium; [d] JRC ISPRA, Italy; [e] KTH, Sweden; [f] QMW, UK; [g] TUC, Germany; [h] FETUC, Portugal; [i] PTB, Germany; [j] CSEM, Switzerland; [k] LAIN, France; [l] UOX-MAT, UK; [m] FhG-IWS, Germany.

May 2001

Summary of Project

Background
Nanoindentation [depth sensing indentation (DSI)] is one of the few methods capable of measuring both the elastic and plastic properties of small volumes of material such as coatings. However, nanoindentation into thin (less than about 2μm thick) coatings or at high loads is unable to determine coating properties such as hardness and Young's modulus directly. The measured response is not a pure coating response but contains a component from the substrate. Current standards can only suggest various maximum indentation depths as a "rules of thumb" to obtain a 'coating-only' response.

Objectives
The objective was to derive and validate from experimental measurement, intercomparison and analysis, procedures that will enable the extraction of the coating properties from indentation into a coated substrate. The results have been used to produce a draft ENV for use by CEN/TC 184 WG5 and CEN/TC 262/SC1/WG1.

Work Programme
An extensive experimental programme of work has been undertaken using six different types of commercial instrument, five indenter geometries, four different coating systems and three bulk reference materials. The project has determined the sensitivity of hardness and modulus values to: instrument calibration and environment; indenter geometry calibration; the instrumental parameters of the detailed loading cycles; and material effects such as coating type and thickness. Selected models have been assessed to calculate coating properties from the measured composite indentation response. These models have been compared, tested, validated and the limits of their applicability determined. Validation consisted of comparing the modelled response with the experimentally determined indentation response.

Results and Achievements
Procedures for the measurement and analysis of coating properties from the nanoindentation of coated substrates have been produced. These procedures are to be used by CEN/TC 184 WG5 and CEN/TC 262/SC1/WG1 to develop new standards nanoindentation. Methods for calculating instrument compliance and area function from indentation data have been developed. The indentation area function results have been compared favourably with direct measurements of indenter shape obtained using a metrological AFM. Intercomparison results demonstrate that different test parameters need to be used for ductile and brittle coatings. Results show that it is relatively easy to accurately measure the hardness of ductile coatings or the elastic modulus of brittle coatings. However, it is more difficult to accurately determine the hardness of brittle coatings or the elastic moduli of ductile coatings. It is recommended that to measure the hardness of brittle coatings a sharp indenter should be used to ensure yield occurs in the coating rather than the substrate. However, it is recommended that a spherical indenter should by used when measuring the modulus of soft coatings with a long maximum hold period to eliminate the effects of creep.

Content

Summary of Project 4
Content 5
Glossary 7
Description of Work 9
Partners' roles 10
Results 13
1 Environmental effects 13
1.1 Introduction 13
1.2 Results 13
1.2 Conclusions 15
2 Zero point uncertainty 16
2.1 Zero Point Methods 16
2.2 Results 16
2.3 Conclusion 17
3 Calibration of instrument and indenter 18
3.1 Introduction 18
3.2 Calibration methods for nanoindentation instruments 18
3.2.1 Indenter tip geometry 18
3.2.2 Measuring deviation of the depth measuring system 27
3.2.3 Compliance of the nanoindentation instrument 27
3.3 Summarization of measurement uncertainties 30
4 AFM images 33
4.1 Introduction 33
4.2 Results 33
4.3 Summary 33
5 Intercomparison of indentation experiments 37
5.3 Discussion 50
5.3.1 Ductile coatings 50
5.4 Conclusions 51
6 Intercomparison results 52
6.1 Protocol 52
7 Data Analysis 58
7.1 Hardness calculation 58

7.1.1 Comparison of different hardness definitions 58
7.1.2 Uncertainty estimation of the hardness measurement 61

7.2 Modulus calculation 62
7.2.1 Experiment 62
7.2.2 Analysis and results 62
7.2.3 Discussion 63
7.2.4 Conclusions 64

8 MODELLING 66

8.1 Objectives and approach 66

8.2 Elastic modelling 67
8.2.1 Introduction 67
8.2.2 Types of modelling 68
8.2.3 Results 69
8.2.4 Conclusions from elastic modelling investigation 75

8.3 2D elastic/plastic FE solutions 76
8.3.1 Introduction 76
8.3.2 Results of 2D elastic-plastic analyses 78
8.3.3 Hardness results 80
8.3.4 Direct comparison of NPL and KTH predictions of E^*_{IT} and H_{IT} 81
8.3.5 Conclusions regarding elastic-plastic modelling 83
8.3.6 Other conclusions 84

Technology Implementation Plan 85

Appendix 1 List of Publications 88

Appendix 2 Guidelines for Use of the Test Method 89

Appendix 3 Intercomparison Instructions 119

Appendix 4 Research Profile of Partners 121

Appendix 5 Partners Contact Details 130

Glossary

ρ	density
$\hat{\sigma}$	deviatoric stress
σ_{EFF}	effective stress
$\bar{\varepsilon}_{pl}$	plastic strain
ε_o	plastic strain parameter
σ_o	plasticity stress parameter
μ	coefficient of friction
ε	elastic strain
ν	Poisson ratio
σ	stress
ν_c	Poisson ratio of coating
ν_i	Poisson ratio of indenter
ν_{IT}	Poisson ratio of specimen
ν_s	Poisson ratio of substrate
a	radius of contact area
a/t_c	contact radius (in plane) / film thickness
$A_c(h)$	contact area
AFM	atomic force microscopy
Al	Aluminium
Al_2O_3	Alumina
AM	acoustic microscopy
$A_p(h)$	projected area function
$A_s(h)$	surface area function
Au	Gold
BK7	Borosilicate BSC517642 glass
C	specimen compliance
C_c	coating compliance
C_f	frame compliance
C_s	substrate compliance
C_t	total compliance
d	diagonal length of indentation
DLC	diamond like carbon
D_r	radial displacement correction
E	Young's Modulus
E_c	indentation modulus of coating
E_i^*	reduced modulus of indenter
E_{IT}	indentation modulus of specimen
E_r	reduced modulus
E^*_{IT}	reduced modulus of specimen
E_s	indentation modulus of substrate
F	force
FEA	finite element analysis
FFT	fast fourier transform

	force maximum
h	measured depth under load
H_c	Coating Hardness
h_c	contact depth
H_c	Substrate Hardness
H_{IT}	Indentation Hardness
HM	Martin's Hardness (see note 1 below)
	maximum depth
h_p	remnant indent depth
H_{pl}	Plastic Hardness
h_r	depth intercept of tangent to unloading curve
HV	Vicker's Hardness
IIT	Instrument indentation test
LSAW	laser surface acoustic wave
N	Newton
Ni	Nickel
Pa	Pascal
PACVD	Plasma Assisted Chemical Vapour Deposition
PVD	Physical Vapour Deposition
r	sphere radius of indenter (Great circle radius)
R_a	measurement of surface roughness (average amplitude of surface roughness)
S	contact stiffness
s	second
sd	standard deviation
SEM	scanning electron microscope
S_f	instrument frame stiffness
T	temperature
	time
U	uncertainty
UTS	Ultimate Tensile Strength
$V_{(Z)}$	velocity as a function of depth
V1	velocity of peak 1
V2	velocity of peak 2
VL	longitudinal wave velocity
VR	Rayleigh wave velocities
VT	transverse wave velocity
W	Tungsten
σ_Y	yield stress

Note 1 The term HU "Universal Hardness has recently been superseded in ISO14577 after a decision by ISO/TC164/SC3 to rename this elasto-plastic hardness scale as "Martens' hardness" HM in honour of the foundational work of Martens in the field.

Description of Work

There were five scientific WPs and two supporting WPs: a Coatings Procurement work package and a Management and Co-ordination work-package in the Indicoat project. The overall structure of the project was therefore as follows:

WP 1 This was concerned with material procurement and coatings production.

WP 2 Direct modulus and hardness validation measurements and all the modelling work was conducted in this work-package. Firstly, independent traceable determination of coating Young's modulus was required to give validity to the final results (hardness can only be determined by indentation methods). Secondly, various models which exist to facilitate calculation of coating properties from the measured composite response were compared, tested and validated. Initially, a semi-empirical approach was followed whereby the onset of substrate effects were determined experimentally and all measured coating properties were restricted to a region where only coating values were measured or an empirical rule for interpolation can be used; this was only applicable for the determination of hardness. Next, existing analytical models were used to compute the coating response, but even the most advanced models are only applicable to elastic deformation. Finally, numerical models have been developed to allow a complete elastic plastic solution, thereby allowing derivation of hardness and Young's modulus values. Each of these approaches have been examined using the most advanced models that are currently available and the limits of their applicability determined.

WPs 3-6 are predominantly experimental but also consider data analysis and results comparison. Experimentally two important issues have been addressed. Firstly, an extensive experimental programme of work was undertaken with four different coating systems to examine the effects of coating type and thickness and indenter geometry on the indentation response and compare this with the values determined from the modelling phase. Secondly, the effect of instrumental parameters was investigated by examining the influence of six different commercial instrument types and the detailed loading cycles that were used upon the final result. WP 6 brought together all of the project output in the form of test protocols for hardness and modulus measurements which were tested in a round robin intercomparison. The final conclusions of all this work have been incorporated into a draft ENV.

Partners' roles

National Physical Laboratory (NPL):

WP1: Specify Materials; Procure substrates and Coatings; Contributing to reports.
WP2: Task Leader; Theoretical Modelling (analytical and FEA); Contributing to reports.
WP3: Indentation Experiments and data analysis; Contributing to reports.
WP4: Indentation Experiments; Data analysis; Temperature measurements; Contributing to reports.
WP5: AFM Measurements, analysis software and data analysis; Indentation Experiments; Data analysis; Contributing to reports.
WP6: Task Leader; Results analysis; Protocol drafting; Indentation Experiments; Data analysis; Standards drafting; Contributing to reports.
WP7: Overall Project Coordinator; Project management; Report collation

VTT Manufacturing Technology (VTT):

WP1: Specify Materials; Procure substrates and Coatings; Contributing to reports.
WP2: Theoretical Modelling (analytical and FEA); Contributing to reports.
WP3: Task Leader; Indentation Experiments and data analysis; Contributing to reports.
WP4: Indentation Experiments; Data analysis; Temperature measurements; Contributing to reports.
WP6: Indentation Experiments; Data analysis; Standards drafting; Contributing to reports.
WP7: Project management; Report collation.

Vlaamse Instelling vor Technologisch Onderzoek (VITO):

WP1: Specify Materials; Procure substrates and Coatings; Contributing to reports.
WP3: Indentation Experiments and data analysis; Contributing to reports.
WP4: Task Leader; Indentation Experiments; Data analysis; Temperature measurements; Contributing to reports.
WP5: Indentation Experiments; Data analysis; Contributing to reports.
WP6: Results analysis; Protocol drafting; Indentation Experiments; Data analysis; Standards drafting; Contributing to reports.
WP7: Project management; Report collation

Joint Research Centre Ispra (JRC):

WP1: Specify Materials; Procure substrates and coatings; Contributing to reports.
WP2: Theoretical Modelling (analytical and FEA); Contributing to reports.
WP4: Indentation Experiments; Data analysis; Temperature measurements; Contributing to reports.
WP5: Indentation Experiments; Data analysis; Contributing to reports.
WP6: Indentation Experiments; Data analysis; Contributing to reports.

Royal Institute of Technology (KTH):

WP2: Theoretical Modelling (analytical and FEA); Contributing to reports.
WP3: Indentation Experiments and data analysis; Contributing to reports.
WP4: Indentation Experiments; Data analysis; Temperature measurements; Contributing to reports.
WP6: Indentation Experiments; Data analysis; Contributing to reports.

Queen Mary and Westfield College (QMW):

WP2: Theoretical Modelling (analytical and semi-empirical); Statistical analysis; Contributing to reports.
WP3: Indentation Experiments and data analysis; Contributing to reports.
WP4: Indentation Experiments; Data analysis; Temperature measurements; Contributing to reports.
WP5: Indentation Experiments; Data analysis; Contributing to reports.
WP6: Indentation Experiments; Data analysis; Contributing to reports.

Technishe Universitat Chemnitz (TUC):

WP2: Theoretical Modelling (analytical and semi-empirical); Contributing to reports.
WP3: Indentation Experiments and data analysis; Imaging of indents; Contributing to reports.
WP4: Indentation Experiments; Data analysis; Temperature measurements; Contributing to reports.
WP5: AFM measurements and data analysis; Indentation Experiments; Data analysis; Contributing to reports.
WP6: Indentation Experiments; Data analysis; Contributing to reports.

Tecnologia da Universidade de Coimbra (TUC):

WP2: Theoretical Modelling (analytical and FEA); Contributing to reports.
WP3: Indentation Experiments and data analysis; Contributing to reports.
WP4: Indentation Experiments; Data analysis; Temperature measurements; Contributing to reports.
WP5: Indentation Experiments; Data analysis; Contributing to reports.
WP6: Indentation Experiments; Data analysis; Contributing to reports.

Physikalisch-Technische Bundesanstalt (PTB):

WP2: Specify Materials; Procure and test hardness blocks; Contributing to reports.
WP3: Imaging of indents; Contributing to reports.
WP4: Indentation Experiments; Data analysis; Temperature measurements; Contributing to reports.
WP5: Task Leader; AFM Measurements, analysis software and data analysis; Contributing to reports.
WP6: Indentation Experiments; Data analysis; Standards drafting; Contributing to reports.
WP7: Project management; Report collation

Centre Suisse d'Electronique et de Microtechnique (CSEM):

WP3: Indentation Experiments; Data analysis; Imaging of indents; Contributing to reports.
WP4: Indentation Experiments; Data analysis; Temperature measurements; Contributing to reports.
WP5: Indentation Experiments; Data analysis; Contributing to reports.
WP6: Indentation Experiments; Data analysis; Contributing to reports.

Laboratoire d'Analyse des Interfaces et de Nanophysique (LAIN):

WP2.1: Sub-task Leadership; Acoustic Microscopy modulus measurements of reference samples and substrates; Contributing to and collating reports.

University of Oxford (UOX):

WP2.1: Surface Brillouin Spectroscopy modulus measurements of some reference samples, substrates and coatings; Contributing to reports.

Fraunhofer Institut fur Werkstoff und Strahltechnik (FhG-IWS):

WP2.1: Laser Surface Acoustic Wave modulus measurements of reference samples, substrates and coatings; Contributing to reports.

Results

1 Environmental effects

1.1 Introduction

The objectives of this work were to determine:

a) the sensitivity of the drift rate to environmental temperature changes

b) the uncertainty of the drift rate for normal environments for each instrument.

The drift Δh of the indentation depth h changes with time and temperature. To assess the drift rate uncertainty the "time drift rate" $\Delta h/\Delta t$ and the "temperature drift rate" $\Delta h/\Delta T$ have been determined, over a range of temperatures. The temperature sensitivity has been determined for a wide range of instruments by analysing the response of the machine while heating or cooling the surrounding environment.

1.2 Results

Tables 1.1 and 1.2 give the experimental conditions and results of the drift measurements, including $\delta(\Delta h/\Delta t)$, the uncertainty of the time drift rate.

Table 1.1 Experimental conditions for drift rate measurements.

Partner	Instrument	Indenter	Sample	Hmax /nm	Pmax /mN
NPL	nanoindenter II	Berkovich	FS	-	50
VTT	NanoTest550	Berkovich	FS	-	80
VITO	NanoTest600	Berkovich	FS	200	10
JRC	nanoindenter II	Berkovich	FS	200	-
KTH	nanoindenter II	Berkovich	FS	5200	10
QMW	UMIS	spherical	BK7	70	10
TUC	Fischerscope	Vickers	FS		20
TUC	UMIS 2000	spherical	FS	≥175	50
UC	Fischerscope	Vickers	Glass, FS	-	-
PTB	Fischerscope	Vickers	BK7	3000	10,200,1000
CSEM	nano-HT	Berkovich	FS	-	10, 50

Table 1.2 Results from the drift rate experiments

Part-ner	Temperature recorded	ΔT °C	Location of heating	Heat time (min)	Cool time (min)	Δh/Δt T-dep.	δ(Δh/Δt) (μm/min)	Δh/ΔT (μm/°C)
NPL	enclosure, nanoindenter II	1.2	outside box	281	279	Yes	-	(b)
VTT	room, box, NanoTest 550	1.4	inside box	15	45	(e)	-	-7 to -11
VITO	Stage NanoTest 660	1.8	inside box	60	140	No	0.002 (a)	-3 to -4
JRC	Stage Nanoindenter II	2.2	inside box	100	260	No	-	5
KTH	Nanoindenter II	7	inside box	60	120	-	-	0.81
QMW	6 locations near UMIS	-	none	n.a.	120	-	-	-0.84 to -1.05
TUC	room, Fischerscope	6	room	15		Yes	-	0.16 (c)
TUC	room, UMIS 2000	3	outside box	100	200	-	-	1.2
UC	Fischerscope	3-4	near nano	120	120	yes (d)	-	0.2
PTB	sample, head, air Fischerscope	2	near sample	116	116	(e)	-	-10,0.23 -8
CSEM	sample, air near nano-HT	4	inside box	30	30	No	-	0.4 to 0.6

Notes

(a) : from routine thermal drift determinations; the value is the maximum change to be expected during an indentation

(b) Δh/ΔT is T dependent

(c): average value

(d) also dependence of Δh/Δt on maximum load determined

(e): average values given only

Partners (NPL, VITO, JRC, KTH, TUC, UC and CSEM) produced curves showing the time dependence of T and Δh during heating and/or cooling. These curves allow the T-dependence of Δh/Δt or Δh/ΔT to be determined in a given T-interval. While VITO, JRC and CSEM found there to be no significant temperature dependence, NPL found a quadratic temperature dependence associated with Δh/Δt.

Knowing $|\Delta h/\Delta T|$ to be in the range 1 to 10 μm/°C, one can obtain an estimation of the admissible rate of temperature change: if one allows for a thermal drift of $|\Delta h| = 5$ nm during a scan of 60 s duration, the rate of change in instrument temperature has to be smaller than (0.005 to 0.0005) °C/min.

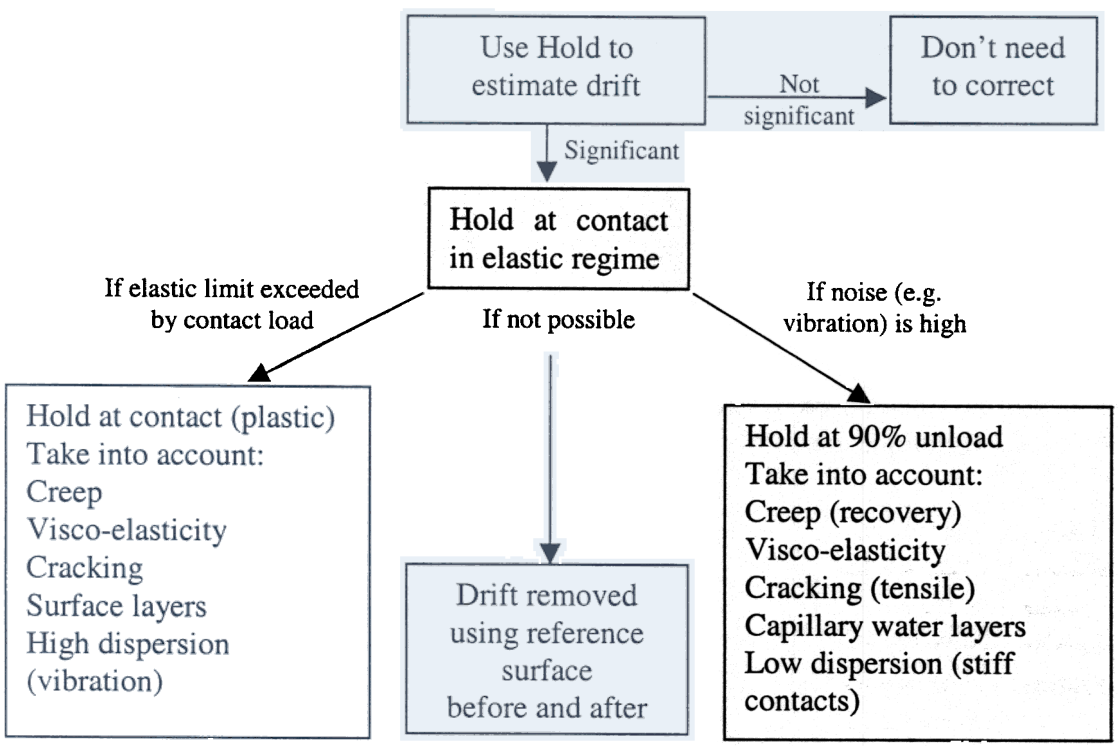
During a routine measurement, for each individual indent the time drift rate was determined automatically during a hold period. The value obtained was used for a correction of the depth

values of the corresponding scan. UC's results for this procedure show that this correction effectively removes the influence of temperature from the hardness values. Experiments showed that the optimum position in a cycle for a hold period was at low loads either immediately before or after the indentation. NPL showed that there was a systematic difference in drift rate between these two positions in the same cycle, which is attributed to material effects, for example creep. It is important that instruments are insulated from thermal fluctuations and /or the environment temperature controlled. Such measures are, however, unlikely to remove thermally induced drift to the levels required unless very soft, low modulus materials are to be tested.

1.2 Conclusions

It is recommended that drift in displacement should be determined using a hold period either at contact or at 90% unload. The results determined during this hold period may then be assumed to result from temperature changes, which, in the absence of a better model, are assumed to be linear. It is recommended that the hold period is approximately the same length of time as loading or unloading. It is also suggested that at least the first 10 seconds (20 seconds if possible) of the hold period data are discarded prior to linear regression. The reason for this is that the start of the hold period is characterised by much more rapid changes in the indentation depth, probably caused by surface and/or instrument settling effects.

The decision tree that is proposed to determine the influence of environmental effects upon nanoindentation is shown below:



2 Zero point uncertainty

The objective of this work was to determine the uncertainty in the zero height definition as a function of surface detection and post facto zero height determination methods.

2.1 Zero Point Methods

Several different methods can be used to determine the true zero point depth in nanoindentation:

"Automatic" surface detection by software belonging to the instrument. During the surface approach phase of the indentation process, the force, depth and time data is monitored and recorded. When a user defined change in the slope of h=h(P) occurs, the approach is stopped. The zero point is then determined by interpolating between data to determine the first excursion in applied force or contact stiffness from the background level during approach. Recorded approach data after the determined zero point is then included in the indentation data.

"User" definition of the contact surface. On some machines a small preload is used to define the zero, this is the method that has been used by TUC. Alternatively it is possible on some instruments to terminate an approach after a sudden decrease in the velocity has been detected. The zero point is estimated by extrapolating back using a polynomial fit.

- **"Post facto" definition of contact surface**. In this case the correction is not done during the measurement but during the analysis. In this category it is common to use a larger preload. The zero point is found by the user simply defining the surface or taking the first 5-10% of the indentation data above the preload and extrapolating back to zero over the region of missing data. The uncertainty of this method increases with the amplitude of the noise in the initial data and the size of the preload (i.e distance to extrapolate).

2.2 Results

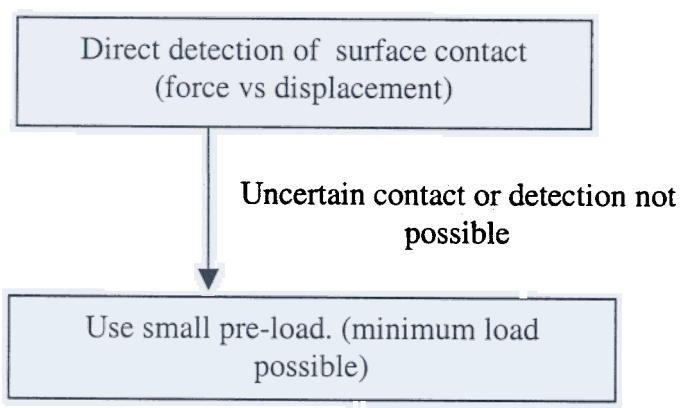
The techniques that have been used by each of the partners and the degree of uncertainty associated with each technique are shown in the table below (Table 2.1).

Table 2.1 Overview of the applied methods and zero height uncertainties

Partner	Instrument	Method	Uncertainty (nm)	Remark
(VITO)	NanoTest 600	post facto fit power law	5 to 10	comparison to corrected data (P4,FS)
(VITO)	NanoTest 600	user	5 to 10	comparison to corrected data (P4,FS)
(JRC)	Nanoindenter II	automatic slope change	≤1	Zero of h and F made Test performed on FS
(TUC)	UMIS 2000	post facto	1 to 4 0.3	Berkovich and Spherical used
(PTB)	Fischerscope	automatic fit (polynomial)	1 to 2	Large influence of roughness observed
(CSEM)	NHT	automatic slope change	3	Depends on approach speed
(CSEM)	NHT	user	3	Test performed on FS

2.3 Conclusion

Using a slope or velocity monitoring methods, the surface detection uncertainty can be as low as 1 to 3 nm. "Post facto" methods appear to result in higher uncertainties (NanoTest 600: ±5 nm, UMIS-2000: <4 nm). The zero point uncertainty depends on inter alia: the environmental noise (e.g. vibration); upon the size of the preload (which determines the length of extrapolation); surface properties of the sample, in particular roughness, oxide layers and water films. The decision tree that is proposed for zero point detection is as follows:



3 Calibration of instrument and indenter

3.1 Introduction

For the calibration of nanoindentation instruments the following main influences have to be considered:

1) Indenter tip geometry
2) Measurement uncertainty and calibration offset of the depth measuring system
3) Uncertainty of the zero point determination
4) Compliance of the nanoindentation instrument
5) Measurement uncertainty and calibration offset of the force measuring system
6) Thermal drift of the nanoindentation instrument

Between them the calibration methods for the uncertainty of the zero point determination and for the thermal drift of the nanoindentation instrument are described in sections 1 and 2.

Calibration methods for nanoindentation instruments

Indenter tip geometry

3.2.1.1 Determination of the geometry of indenters used for nanoindentation with a metrological SFM

Many Scanning Force Microscope (SFM) systems perform poorly at absolute shape measurement on the micron scale, due to the non-linearity, creep and hysteresis of their open loop scan system. Metrological SFMs now exist, which have closed loop scanners and linear displacement sensors on all axes. These sensors are capable of sub-nm resolution. In this project PTB used a Veritekt 3 SFM with a measuring range $x = 70$ µm, $y = 15$ µm, $z = 15$ µm. This SFM is used like a miniaturized three-coordinate measuring device. In cooperation with the Technical University of Ilmenau [1] the SFM was fitted with three miniature laser interferometers along the coordinate axes x, y, z. to correct the capacitive displacement sensors on each axis of movement. The laser interferometers at the $\lambda/2$-zero points of the interference signals have an uncertainty of measurement $U \leq 1$ nm.

Tthe long shafts of the indenters can cause significant Abbe errors, thus an arrangement of the laser interferometers which avoids the Abbe error was developed [2]. Here the 3D-uncertainty of the SFM is reduced to $U = 1{,}5$ nm + $10^{-4} \cdot L$ (L – measured length)[3]. Fig. 3.1 shows the scheme of this SFM with integrated laser interferometers.

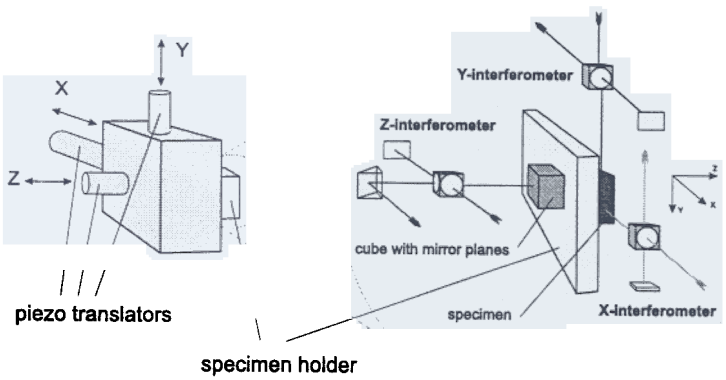


Fig. 3.1: Scheme of the metrological SFM with integrated laser interferometers

The geometry of the indenter is measured by a series of scans each containing 256 x 256 or 512 x 512 scan points. A first scan in the range $x = y = 10$ µm is made to determine the overall indenter geometry. Then follows a scan in the range $x = y = 1.5$ µm in order to investigate the geometry in the immediate surrounding of the indenter tip. Each scan is repeated at least 3 times. If necessary a further scan in the range $x = y = 0.5$ µm is carried out in order to measure the geometry close to the tip with as high as possible resolution. Table 3.1 summarizes the measurement conditions for the indenter measurements

Table 3.1 Measurement conditions of the indenter measurements

Criterion	Value in x-axis	Value in y-axis
Position of the tip at Vickers indenter	0.5 of the x-range	0.5 of the y-range
Position of the tip at Berkovich indenter	0.5 of the x-range	0.33 of the y-range
Scan range for the determination of the overall geometry	10 µm	10 µm
Corresponding scan point distance for: 256 x 256 scan points 512 x 512 scan points	 39.06 nm 19.53 nm	 39.06 nm 19.53 nm
Scan range for the determination of the geometry in the tip region	1.5 µm	1.5 µm
Corresponding scan point distance for: 256 x 256 scan points 512 x 512 scan points	 5.86 nm 2.93 nm	 5.86 nm 2.93 nm
Scan range for the determination of the geometry In nearest tip surrounding	0.5 µm	0.5 µm
Corresponding scan point distance for: 256 x 256 scan points 512 x 512 scan points	 1.95 nm 0.98 nm	 1.95 nm 0.98 nm

3.2.1.2 Determination of area functions of indenters

The projected area of the indenter is calculated from the two-dimensional data sets by the summation of projected triangle areas from neighbouring scan points. The data A_i; h_i are then fitted with a suitable regression curve $A = f(h)$, the so-called area function. This area function describes the contact area A_c of the indenter as function of the vertical distance from the indenter tip. This distance is equivalent to the contact depth h_c. Fig. 3.2 shows the area functions of a Berkovich indenter (three-sided pyramid made of diamond) in two ranges of

the contact depth $h_c < 100$ nm and 100 nm $\leq h_c \leq 1000$ nm together with the theoretical curve for the contact area $A_c = 24{,}5\ h_c^2$.

The representation $\sqrt{A_c} = a = f(h_c)$ was chosen because this function should deliver a straight line running through the zero point. The area function for $h_c > 100$ nm runs approximately linear and parallel to the theoretical curve. The linearity of the curve implicitly shows that the indenter in this range is practically without error. Typically the real area of the indenter mainly due to tip rounding is larger than the specified area. The area function in the contact depth range $h_c < 100$ nm is non-linear and can be used for the correction of the values obtained at the indentation measurement. Fig. 3.3 shows the area functions of a Vickers and a Knoop indenter.

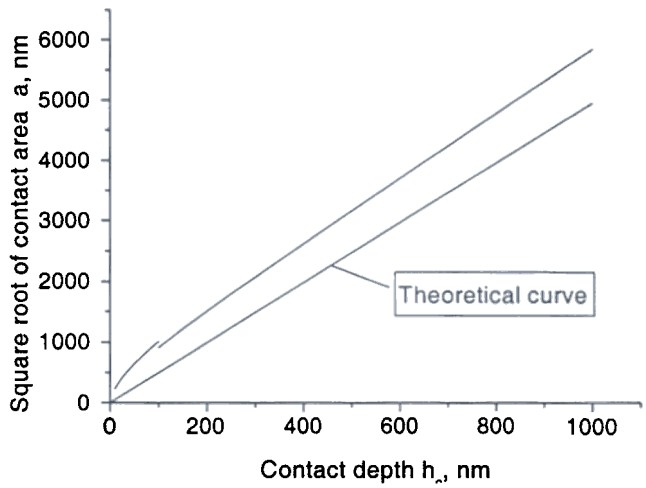


Fig. 3.2: Area functions of a Berkovich indenter

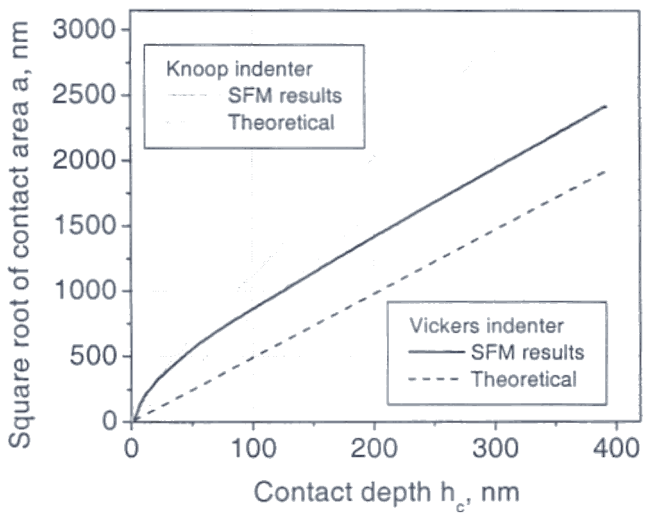


Fig. 3.3: Area functions of Vickers and Knoop indenters

Being pyramidal, Knoop and Vickers indenters have similar area functions to Berkovich indenters. In contrast with a Berkovich indenter, however, they suffer from the so-called „roof edge error", which is due to both pairs of facets not meeting at a single point. In nanoindentation, ball-shaped diamond indenters are gaining increasing importance. Indenting with a tip radius of the order of several µm can generate purely elastic deformations described by the Hertzian equations. Diamond spheres are hard to make, however. Fig. 3.4 shows the ball radius, *r*, as a function of the distance from the indenter tip, *h*, for a ball-shaped indenter with 20 µm nominal ball diameter.

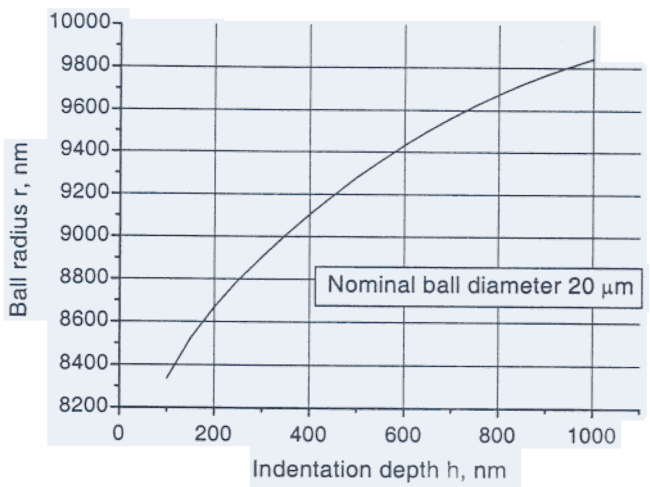


Fig. 3.4: Ball radius as function of the distance from the indenter tip for a ball-shaped indenter with 20 µm diameter

One can see that the ball radius is not constant and only approaches the nominal value of 10 µm at $h \approx 1000$ nm. This is typical and strategies for coping with a depth dependent radius have been developed [10].

3.2.1.3 Uncertainty of area functions of various indenters types

The uncertainty of the indenter area U_A mainly depends on the following influences: [4,5]

- relative standard deviation of repeated measurements of the indenter area, s_{rel}
- area deviation due to the scan point distance, f_{pd}
- area deviation due to the tip radius of the SFM tip, f_{tr}

Fig. 3.5 represents the relative standard deviation of the mean area

$$s_{rel} = \frac{s_A}{\sqrt{n} A_c} \qquad (1)$$

where s_A is the standard deviation in each height of repeated measurements (n = 8 measurements in each of the two ranges) of the indenter area.

It is assumed here, that the pixellation uncertainty is randomly distributed and contained in the values of s_{rel}. The relative standard deviation s_{rel} which contains the overall effect of sensing the indenter's pyramid planes with large inclination angles, already gives a rough indication of the relative measurement uncertainty.

The influences of the pixel distance and the tip radius of the SFM tip have been investigated in [5].

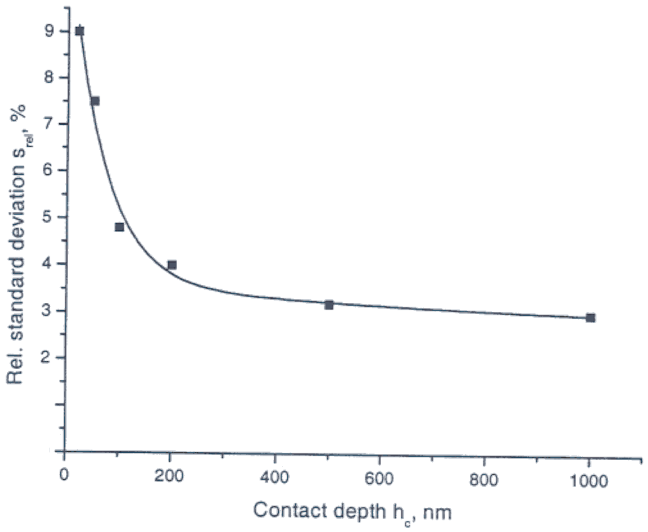


Fig. 3.5: Relative standard deviation of the mean indenter area s_{rel} as function of the contact depth h_c

Fig. 3.6 depicts the influence of the pixel distance on the area deviation and Fig. 3.7 theinfluence of the tip radius of the SFM tip on the area deviation.

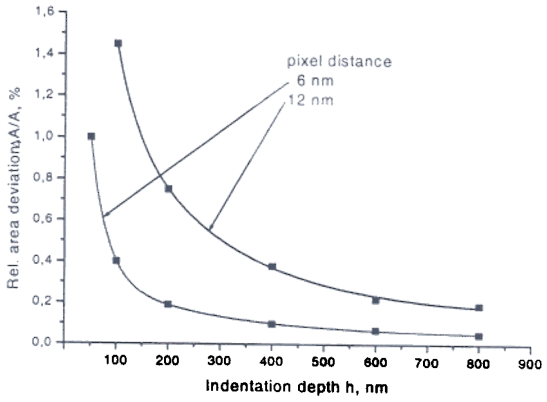


Fig. 3.6: Area deviation due to pixel distance as function of the indentation depth h

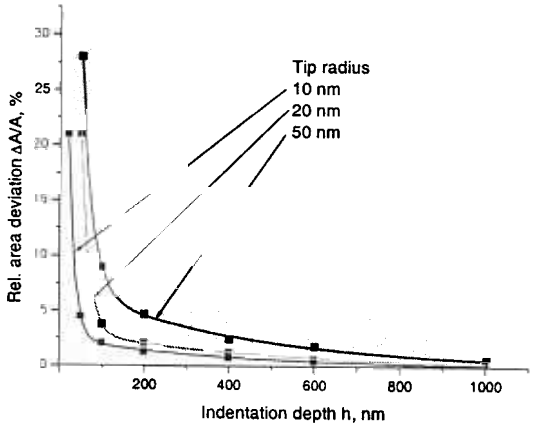


Fig. 3.7: The area deviation due to the tip radius of the SFM tip is function of the indentation depth h from the tip of a perfect Berkovich indenter.

The uncertainty due to pixellation can be reduced by reducing the pixel distance. However, the finite size of the SFM tip radius acts to dilate the measured shape by an amount that is a function of the probe radius and the local gradient of the indenter For horizontal surfaces the

correction is zero and for vertical edges, the dilation is equal to the SFM tip radius. Transition from a flat facet to a rounded end properly requires a progressively reducing correction for this error [5]. The blunter the indenter, the less the error is at low depths.
Ultimately, one gets for the expanded uncertainty U_A of the indenter area:

$$U_A = 2\sqrt{s_{rel}^2 + f_{pd}^2 + f_{tr}^2} \qquad (2)$$

As an example the area function of the investigated Berkovich indenter would have a relative uncertainty of U_A = 25 % at 20 nm; this value decreases to U_A = 6 % at h_c = 1000 nm.
In rough approximation the uncertainty of the indenter area can be expressed by s_{rel}. Therefore in Fig. 3.8 the uncertainties of the area of a Berkovich and of a ball-shaped indenter are compared with each other in the form of the function s_{rel} = f(h).

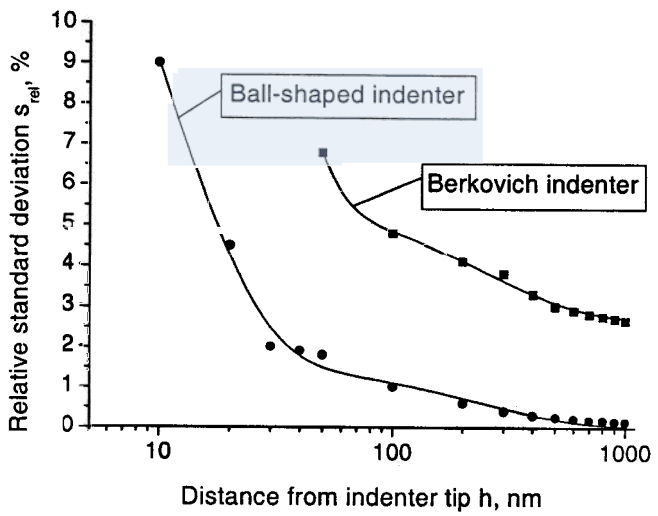


Fig. 3.8: Comparison of the uncertainty of the area functions of a Berkovich and a ball-are compared with each other in the form of the function s_{rel} = f(h).

Fig. 3.8 clearly reveals that the uncertainty of the area function for the ball-shaped indenter is about 4 to 15 times smaller than the uncertainty of the Berkovich indenter's area function. The reason of this result is that the scan of a sharp tip is has a much higher uncertainty than the scan of a steady ball surface.

3.2.1.4 Comparison of area functions of indenters determined with SFM and with reference materials

Comparison of the indenter area function determined with the SFM was made with that determined by the indirect method using reference materials according to the method developed by Oliver and Pharr [6] in a modified version.
The indirect method for the determination of the tip shape consists in carrying out indentation measurements with different test forces into a well characterized reference material and in the determination of the contact area on the assumption that the Young's modulus is constant and does not depend on the indentation depth. Here, the universal connection between the

stiffness S and the contact area A_c is used, for which independently from the indenter geometry is valid [7]:

$$S = \beta \cdot \frac{2}{\sqrt{\pi}} \cdot E_r \cdot \sqrt{A_c} \tag{3}$$

The correction factor β considers the deviation of the pyramids from the rotation symmetry which with good approximation can be assumed as 1. The contact stiffness is calculated from the slope of the test force decreasing curve at the point of the maximum test force. With this aim the upper 60 % - 80 % of the test force decreasing curve are fitted with the function

$$F = C(h - h_0)^m \tag{4}$$

(C, m, h_0 are fit parameters) and the first derivative is formed. The desired quantities contact depth h_c and square root of the contact area (a) then follow from the formulas:

$$h_c = h_{max} - \varepsilon \frac{F}{S} \tag{5}$$

$$a = \sqrt{A_c} = \frac{\sqrt{\pi}}{2E_r(1/S - C_f)} \tag{6}$$

The factor $\varepsilon = 0.75$ was used in equation (5) [6]

The selection of suitable reference materials is essential for accuracy of the indirect method. The reference materials must be homogeneous and, as far as possible, isotropic materials with a depth-independent Young's modulus, whose elastic constants are exactly known. Therefore amorphous bulk materials and glasses are often used. Almost ideally plastic materials (e.g. metals) are often not suited because they show the so called 'pile-up' effect, where the displaced material piles up above the original surface. This effectively increases the contact area A_c but, the shape of the pile-up cannot be determined from the test force – indentation depth – curve itself, for this one needs the imaging of the surface with an SFM. If the pile-up is not considered, the true contact area can be evaluated up to 50 % too small [8]. Also the opposite effect of the sink-in at the border of the contact area leads to a false evaluation of the contact area. Materials that undergo a pressure induced phase transition, like Si single crystals, are also not suited. Furthermore, in these cases, one cannot assume constant elastic properties. Another error source is crack propagation during the indentation, which happens for brittle materials, especially at larger test forces. Cracks change the contact stiffness and lead to errors in the area calculation.

Investigations were carried out on three different materials: Fused silica, optical glass BK 7 and sapphire (0001) single crystal. The elastic parameters of the materials are given in Table 3.2.

Table 3.2 Elastic constants of the used reference materials

Material	Young's modulus/GPa	Poisson ratio
Fused silica	72.9 ± 0.8	0.159
BK7 glass	81.9 ± 0.9	0.203
Sapphire (0001) single crystal	403	0.234

If the same area function is determined from measurements on materials with different Young's modulus, the indirect method can be evaluated as reliable.
For the following investigations measurements in the test force range from 0.3 mN until 300 mN each with 10 measurements for each used test force were carried out. From the 10 single measurements for each test force were calculated average value curves with which according to the above described method the stiffness was determined. The frame compliance of the indentation measuring device UMIS-2000 used for this investigation amounted to $C_f \approx 0.2$ nm/mN.

The area calculation showed that the determined areas for the both materials fused silica and sapphire (0001) differed significantly.
The first possibility is that this was due to an inexactly determined frame compliance. This becomes more significant as both the test force and the Young's modulus of the reference material increase. But, simply altering the compliance of the device cannot get agreement of the area functions from both materials. For better agreement corrections on the model by Oliver and Pharr [6] are necessary, whose effect is presented in Fig. 3.9.

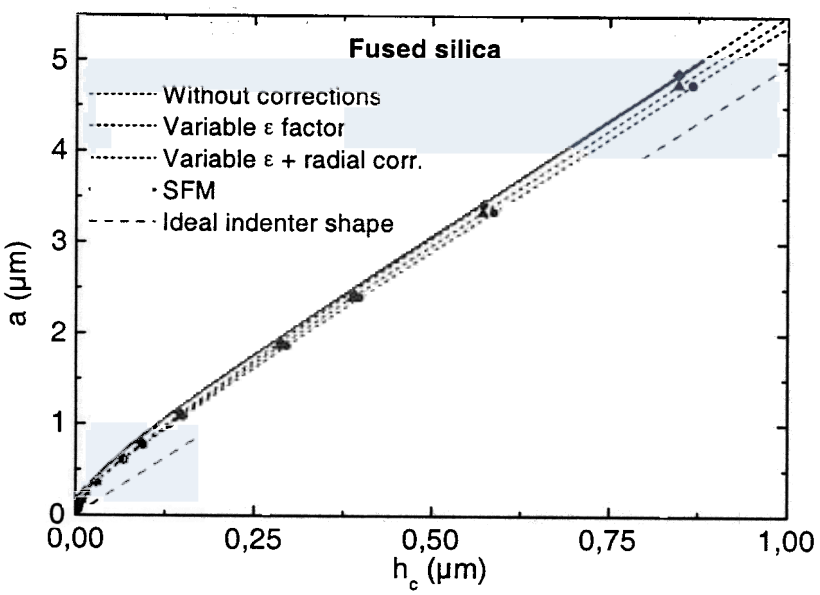


Fig. 3.9: The influence of different corrections on the area function determined with fused silica compared with the area function determined with the AFM.

Here, the area function determined on fused silica is compared with the directly measured AFM area function. A first correction refers to the ε factor of 0.75. According to the elasticity theory it is valid only for an exponent m of the test force decreasing curve of 1.5. But for fused silica m = 1.2 was determined, whereas m for sapphire is near to 1.5. The correct ε factor for fused silica is 0.79. As can be seen in Fig. 3.9, this correction is still not sufficient. A second correction considers the radial elastic deformation within the surface plane, which is a maximum exactly at the border of the contact area. This follows from a comprehensive application of elasticity theory but, up to now, it has not been considered because of its small effect. The projected contact area under test force due to the radial deformation is slightly smaller than after unloading. But the relative change of the edge length for fused silica is especially large at 2.7 %, clearly larger than on other materials, where it is mostly below 1 %. For sapphire it amounts to 1.1 %. The larger the ratio between hardness and Young's modulus the larger is the correction. Using both corrections, the agreement between the area functions from the direct and the indirect method is very good. The average deviation on fused silica is only 6 % in the range up to 300 nm und less than 2 % in the range above this depth. For sapphire this deviation is still clearly smaller. Thus, the results are within the estimated uncertainty of measurement of the SFM measurement. Fig. 3.10 finally shows the comparison of the area function from the direct method with the area functions determined with fused silica, BK 7 glass and sapphire.

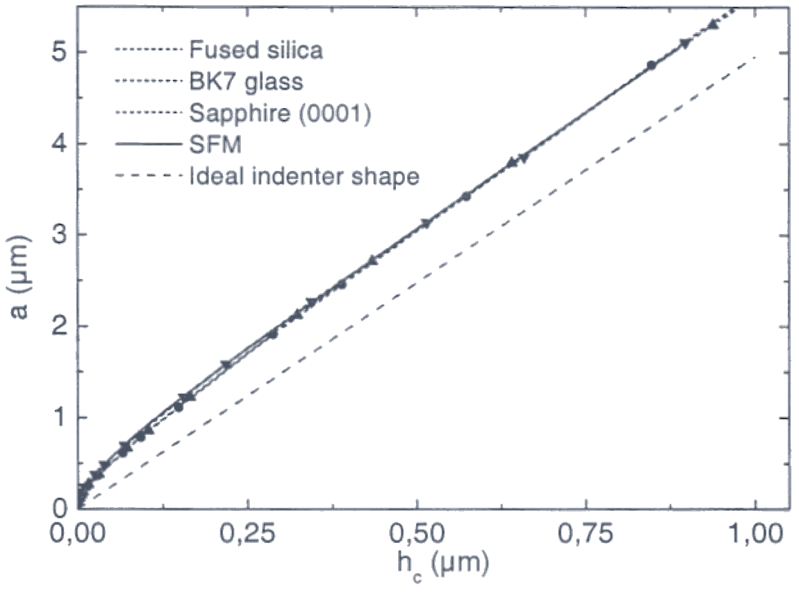


Fig. 3.10: Comparison of the AFM area function with the area functions determined with three different reference materials using the corrections to Oliver and Pharr.

The result does not depend on the reference material. The deviations for the glasses in the depth range up to 0.3 µm can be attributed to sink-in effects. Here, further investigations for the improvement of the accuracy still are necessary.

3.2.2 Measuring deviation of the depth measuring system

For calibration of the depth measuring system of the nanoindentation instrument laser interferometers with high resolution and small uncertainty of measurement are normally used. The laser interferometer delivers traceability to the unit of length directly via the laser wavelength. Fig. 3.11 shows a setup for the calibration of the depth measuring system using a multi- pass Jamin-interferometer.

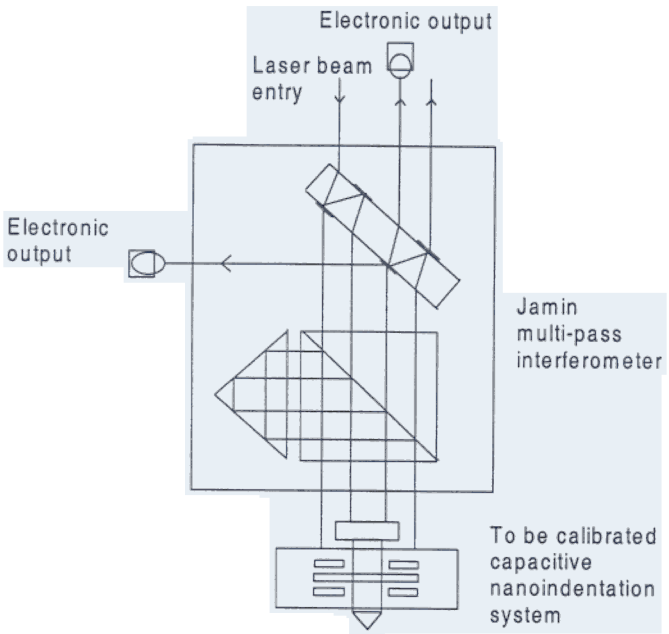


Fig. 3. g system using a multi-pass Jamin-interfe

In the g system using a plane mirror laser interfe ı) was developed.
A coı capacitive measuring system from Queen of this laser interferometer is U ≤ 1 nm. At present a thorough investigation of this laser interferometer with the X-ray interferometer at PTB is underway.

3.2.3 Compliance of the nanoindentation instrument

3.2.3.1 Determination of the frame compliance with the SFM area function

In the method proposed by Doerner and Nix [9] and Oliver and Pharr [6], the frame compliance is determined by observation of the intercept of a plot of total compliance, C_t, versus $1/\sqrt{A_c}$, where A_c is the contact area, for a series of indents at different loads. The

method follows by modelling the instrument and specimen as two springs in series, in which case

$$C_t = C_f + C_s \tag{7}$$

where C_f and C_s are the compliance of the instrument frame and the specimen, respectively. Since the specimen compliance is given by the inverse of the contact stiffness, S, equ. (7) can be rewritten as:

$$C_t = C_f + \frac{\sqrt{\pi}}{2}\frac{1}{E_r\sqrt{A_c}} \tag{8}$$

Oliver and Pharr used aluminium was used as a reference material because of its low hardness, allowing stiff contacts that yield data close to the intercept.
In the method presented here, only indents at a high load (as high as practically achievable with the instrument) are used. A simple, iterative procedure is adopted, assuming the elastic properties of the reference material. The procedure is schematised below:

raw indentation data of material with known elastic properties

determine C_t and h_c, and calculate A_c

calculate the frame compliance using

$$C_f = C_t - C_s = C_t - \frac{\sqrt{\pi}}{2}\frac{1}{E_r\sqrt{A_c}} \tag{9}$$

correct indentation data for the frame compliance

repeat until convergence

Tungsten was used as the reference material, because it is an elastically isotropic, homogeneous material, and it is less prone to handling damage compared to Aluminium. Moreover it has a high modulus and allows sufficient plastic deformation (high A_c), yielding better estimates of the frame compliance (right-hand side of equ. (9) is small, i.e. for stiff contacts). Twelve indents at a high maximum load of 100 mN were used.

In a nano-test it is important for the accuracy of this method that the area function (at distances relatively far from the indenter tip) is well known, because the result is very sensitive to that input. Indeed, when using the indenter area function obtained by SFM, a frame compliance value of 0.46 ± 0.032 (one σ) nm/mN was found, whereas when the theoretical Berkovich area function was used ($A_c = 24{,}5h_c^2$), the frame compliance became 0.37 ± 0.03 nm/mN, i.e. a difference of 20 %. In the method proposed by Doerner and Nix [9] and Oliver and Pharr [6] however, uncertainties in the area function play an even greater role since it must be known over a range of distances from the indenter tip, since different loads are used.

3.2.3.2 Determination of frame compliance and area function with two different reference materials

This method is essentially the same as the combined iterative method proposed by Oliver and Pharr, but the alternative method to determine the frame compliance, as explained in section 3.2.3.1, is used. The frame compliance is thus determined using W(100) as reference material, while the indenter area function is derived from indents in fused silica, allowing accurate stiffness measurements at shallow depths, which in turn allows measurement of the area function near the indenter tip. Indentation loads ranged from 10 mN to 180 mN. The area was calculated from the indentation data, knowing the frame compliance, by rearranging equ. (8)

$$A = \frac{\pi}{4}\frac{1}{E_r^2\left(C_t - C_f\right)^2}$$

The data were fitted to the following function, which proved to perform adequately

$$A = a\left(\frac{h-b}{h_{max}}\right)^c$$

where a, b and c are fitting parameters.
After only two combined iterations, the determined area function was very close to that determined by SFM (measured in NPL), as shown in Fig. 3.12.

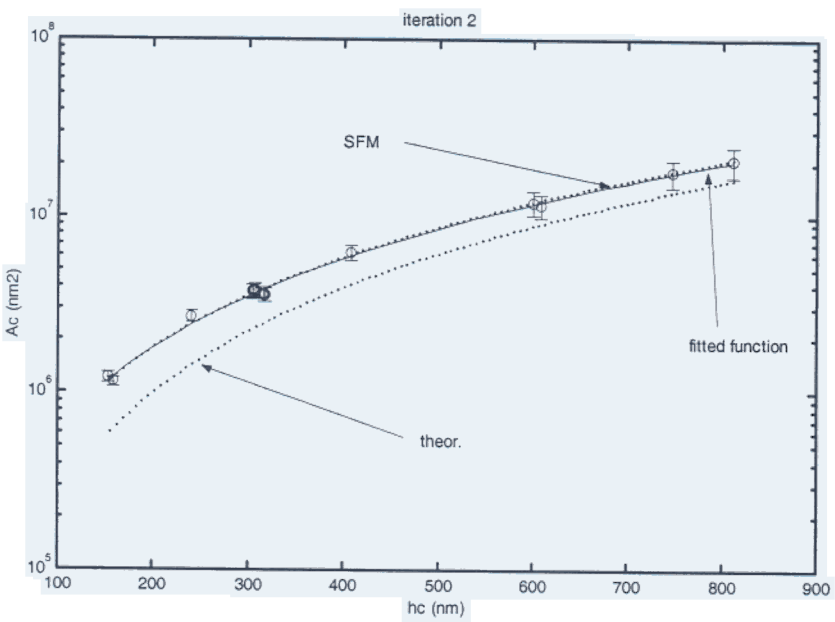


Fig. 3.12: Area functions of a Berkovich indenter determined by SFM and indentation technique

The error bars are 2 times the standard deviation in length (at each side), and take into account the statistical scatter of the indentation results as well as the uncertainty in the frame compliance value. The theoretical Berkovich area function is also shown, and it is clear that the area function of the indenter under investigation deviated significantly from the perfect

geometry. For example, the area function far from the indenter tip (h_c > 566 nm), as determined by SFM, was $\sqrt{A} = 5.3h_c + 287$ nm.

The frame compliance given by this combined iterative procedure was 0.47 ± 0.047 nm/mN, which corresponds to that when using the area function determined by SFM, within the error margins.

These results clearly demonstrate that the combined iterative method is able to yield reliable values of frame compliance as well as valid estimates of the indenter area function. The method does, however, require considerable experimental effort. It would be desirable, therefore, that indenters for nanoindentation are certified for area function by SFM.

3.2.4 Measuring deviation of the force measuring system

For the calibration of the measuring deviation of the force measuring system in a nanoindentation instrument generally balances or weights are used. As the depth deflection of common electronic balances is too large, for this purpose electronic balances with depth compensation have been used successfully. The achievable uncertainty of calibration is estimated as U ≈ 0.1 mg which corresponds to 1 µN. If weights are used for the force calibration, they are directly hanged on the indenter. The corresponding uncertainty is estimated as 10 µN.

Another possibility for the force calibration is the use of cantilevers made from Silicon where the force is traced back to the geometry quantity „deflection of the cantilever".

The development of calibration methods for test forces F < 1 µN is the aim of the recently submitted EU-project proposal 'NANOFORCE.'

3.3 Summarization of measurement uncertainties

Considering the example of the Martens Hardness *HM* the uncertainty of this measuring method can be estimated under consideration of the following error influences:

1) measuring deviation of the force measuring system ΔF
2) measuring deviation of the length measuring system Δh
3) relative uncertainty of the indenter's area function $\Delta A/A$
4) deviation at the zero point determination for the depth measurement Δh_o
5) mechanical deformation of the measuring device Δh_m

Under the precondition of relative measuring deviations and an assumed rectangular distribution (pessimistic estimation) of the measuring deviations the combined standard uncertainty is

$$u_c = \sqrt{\frac{1}{3}\sum_i \left(\frac{\Delta HU}{HU}\right)^2}$$

and the expanded uncertainty:

$$U = ku_c$$

In Table 3.3 the calculation of the measurement uncertainty is summarized.

Table 3.3: Procedure for the estimation of the uncertainty of the Martens Hardness HM

Error influence	Rel.measuring deviation $\Delta HM/HM_i$	Limit value of rel. meas. Deviation	Assumed error distribution	Contribution to variance (with assumed error distribution) $1/3(\Delta HM/HM)_i^2$
1	$\Delta F/F$	1 µN	Rectang.	0.00000027
2	$-2\Delta h/h$	1 nm	Rectang.	0.00000133
3	$\Delta A/A$	3.11 % at h = 1000 nm	Rectang.	0.00032240
4	$-2\Delta h_o/h$ (h = 1000 nm)	1 nm	Rectang.	0.00000133
5	$-2\Delta h_m/h$ (h = 1000 nm)	1 nm	Rectang.	0.00000133
Square of combined standard uncertainty u_c^2				0.00032666
Expanded uncertainty U (k=2)				**0.0361**

The expanded relative uncertainty of the Martens hardness for h = 1000 nm in this example is estimated as U = 3.6 %.

In order to get the dependency of the uncertainty on the indentation depth one has to carry out the calculation shown above for various indentation depths h. Here, the following assumptions were taken: Use of a Berkovich indenter. The uncertainty of force calibration is u = 1 µN, and the forces were calculated for HM = 4000 N/mm^2. For the uncertainties of the depth measuring system, of the zero point determination and of the determination of the mechanical deformation (stiffness resp. compliance) were estimated u = 1 nm. The result of this evaluation is shown in Fig. 3.13.

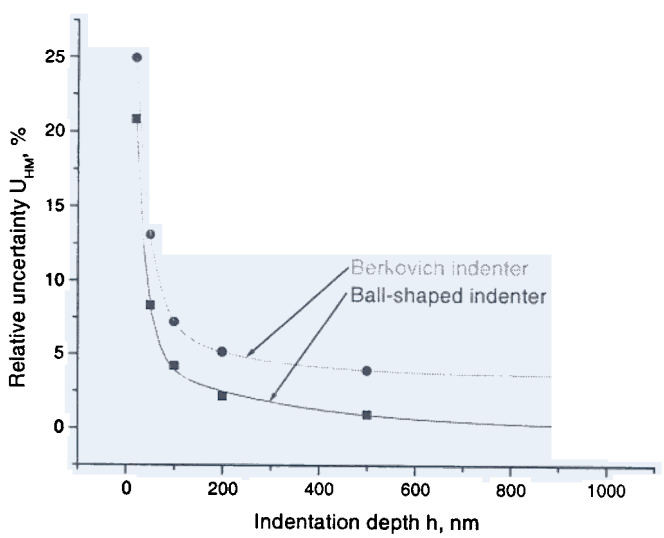


Fig. 3.13: Relative uncertainty of Martens hardness HM as function of depth h

The result in Fig. 3.13 clarifies that for uncorrected AFM data at small indentation depths h = 20 nm for a sharp Berkovich indenter, a relatively high expanded uncertainty U = 25 % has to be considered, which until an indentation depth h = 1000 nm steadily decreases to U = 4 %. On the other side, the ball-shaped indenter delivers a smaller uncertainty. The high uncertainty at small indentation depths can be reduced if one uses ball-shaped indenters and develops calibration methods for the indentation depth, the zero point determination and for the compliance with an uncertainty U < 1 nm.

References

[1] M. Bienias, S. Gao, K. Hasche, R. Seemann, K. Thiele: A metrological Scanning Force Microscope used for coating thickness and other topographical measurements, Appl. Phys. A 66, S837 – S842 (1998)

[2] G. Jäger: Laser-Based Measurement to Nanometer Scale Accuracy, Proc. Laser metrology 1999, 5.38 – 5.47, Florianopolis, Brazil, October 1999

[3] K. Hasche, K. Herrmann, W. Mirandé, F. Pohlenz, R. Seemann: Development of Scanning Force Microscopy with subnanometric capability, Proc. Quantitative Microscopy 2000, Semmering, Austria, January 2000, 219 – 225

[4] K. Herrmann, N.M.Jennett, W. Wegener, J. Meneve, K. Hasche, R. Seemann: Progress in determination of the area function of indenters used for nanoindentation, Thin Solid Films 377 – 378 (2000) 394 – 400

[5] N.M. Jennett, G. Shafirstein, S.R.J. Saunders: Comparison of indenter tip measurement using calibrated AFM and indentation into Fused silica, Symposium Hardness Testing in Theory and Practice, Düsseldorf, 23.-24. 11. 1995, VDI-Berichte 1194, 201 – 210

[6] W.C. Oliver, G.M. Pharr: An Improved Technique for Determining Hardness and Elastic Modulus Using Load and Displacement Sensing Indentation Experiment, J. Mater. Res., 7 (1992) 6, 1564 – 1583

[7] G.M. Pharr, W.C. Oliver, F.R. Brotzen: On the generality of the relationship among contact stiffness, contact area, and elastic modulus during indentation, J. Mater. Res. 7 (1992) 613

[8] A. Bolshakov, G.M. Pharr: Influences of pileup on the measurement of mechanical properties by load and depth sensing indentation techniques, J. Mater. Res. 13 (1998) 1049

[9] M.F. Doerner, W.D. Nix: A Method for Interpreting the Data from Depth Sensing Indentation Instruments, J. mater. Res., 1, 601 – 609 (1986)

[10] Bushby and Jennett: "Determining the area function of spherical indenters for nanoindentation. Proc MRS Symp Q, Boston Fall 2000 (in press)

4 AFM images

4.1 Introduction

The following figures show direct observations of indents produced using a Berkovich indenter on specimens of aluminium coated BK7 glass and alumina coated nickel. The sample examined are listed in the following table:

Table 4.1 Specimens examined using AFM after nanoindentation.

Code	Coating Material	Substrate Material	Nominal Thickness (nm)
HS1	Alumina	Nickel	200
HS2	Alumina	Nickel	800
HS3	Alumina	Nickel	2000
SH1	Aluminium	BK7 glass	310
SH2	Aluminium	BK7 glass	1050
SH3	Aluminium	BK7 glass	3400

HS - hard on soft (Alumina on Nickel)
SH - soft on hard (Aluminium on BK7 glass)
Number 1 is the thinnest layer and 3 the thickest.

The investigations were conducted using a Quesant AFM (Nomad type) installed beside the indenter column within the UMIS-2000 instrument. Images have been obtained of the surface and line scans along the lines that are marked in the images, are shown below each image. The line scans show the residual depth as a function of the position within the indent to an accuracy of approximately 10%.

4.2 Results

AFM images of the Alumina on Nickel and the Aluminium on BK7 glass are shown in Figures 4.1- 4.15. A summary of the features observed in each of these images is shown below in tables 4.2 and 4.3. In the hard coatings cracking and sinking-in that are observed whereas in the soft coatings pile-up is observed. Cracking is most common in thin hard coatings whereas sinking-in is more significant in the thicker coatings. Pile-up is the main feature of the soft aluminium coatings. Pile-up is most noticeable in the thinner coatings and at high indentation loads.

4.3 Summary

AFM examination of an indentation is extremely useful for interpreting nanoindentation results. The results show that pile-up is a common feature in the soft aluminium coatings, whereas sinking-in and cracking are more common in the hard alumina coatings.

Table 4.2 Results obtained from the Alumina on Nickel specimens.

	50nm Indentation	100nm Indentation
HS1	Cracking across the face of the indentation.	Cracking across the face of the indentation.
HS2	Sink-in can be observed but no cracking.	Circular cracks can be observed around the indent.
HS3	Sinking-in can be seen.	Sinking-in can be seen.

Table 4.3 Results obtained from the Aluminium on BK7 glass specimens.

	3nm Indentation	10nm Indentation	50nm Indentation
SH1	70 nm of pile-up	120 nm of pile-up	350 nm of pile-up
SH2	Shallow indent with no significant pile-up	50 nm of pile-up.	400 nm of pile-up.
SH3	Shallow indent with no significant pile-up	No significant pile-up	100 nm of pile-up.

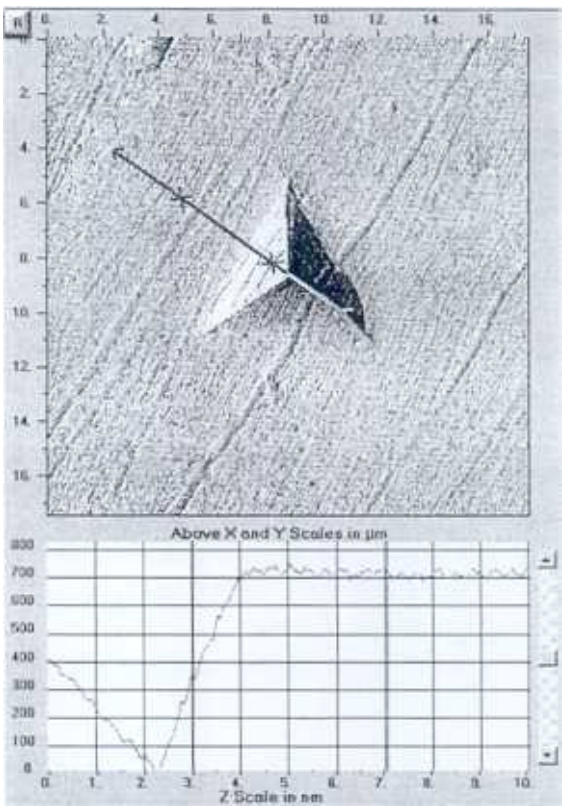


Fig. 4.1: Berkovich indent into HS1, 50mN

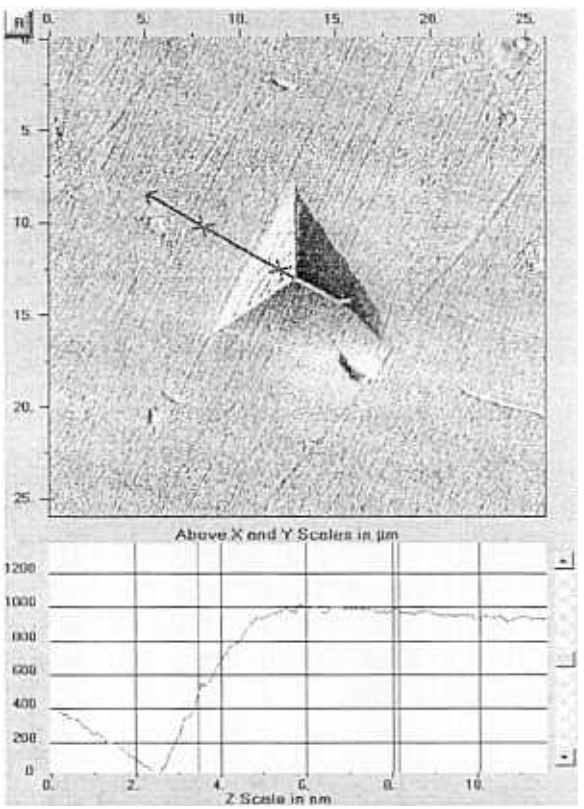


Fig.4.2: Berkovich indent into HS1, 100mN

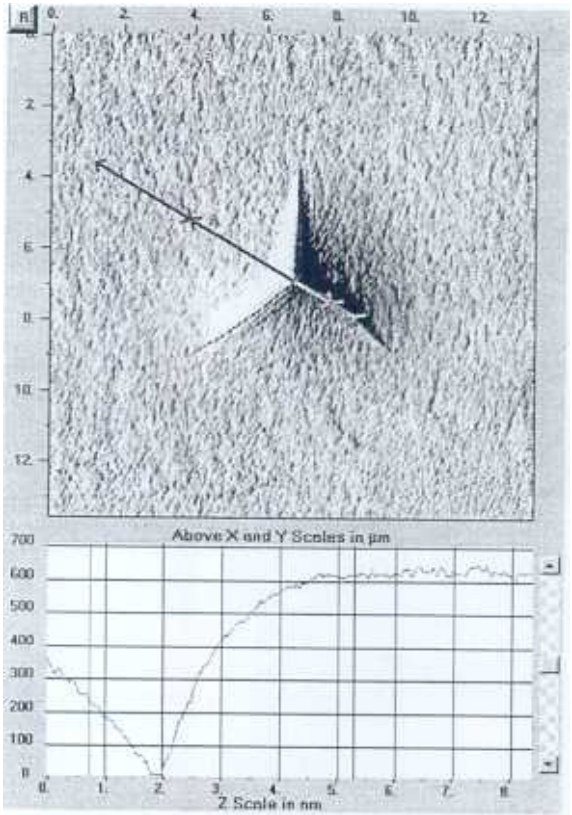


Fig. 4.3: Berkovich indent into HS2, 50mN

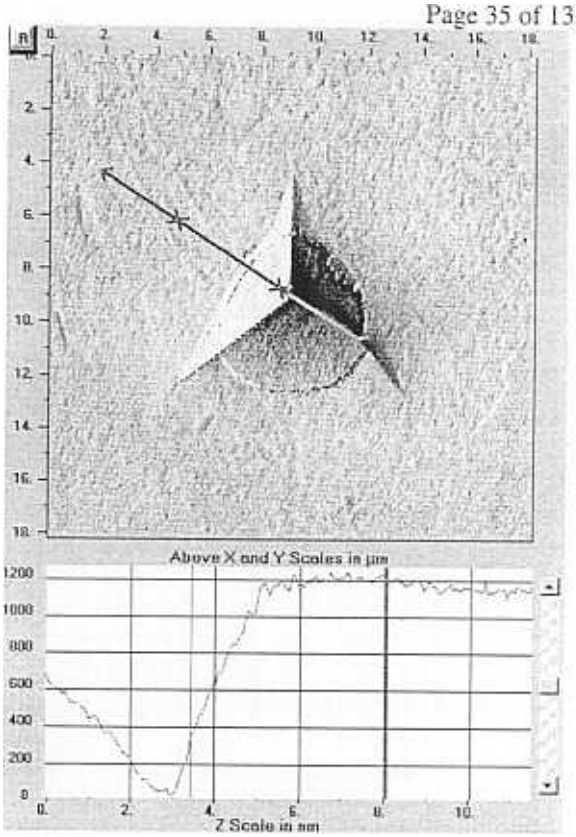


Fig.4.4: Berkovich indent into HS2, 100mN

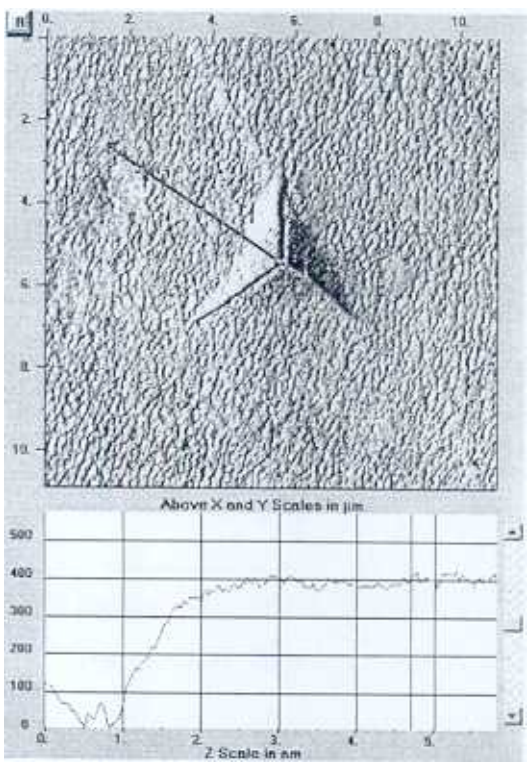


Fig. 4.5 Berkovich indent in HS3, 50mN

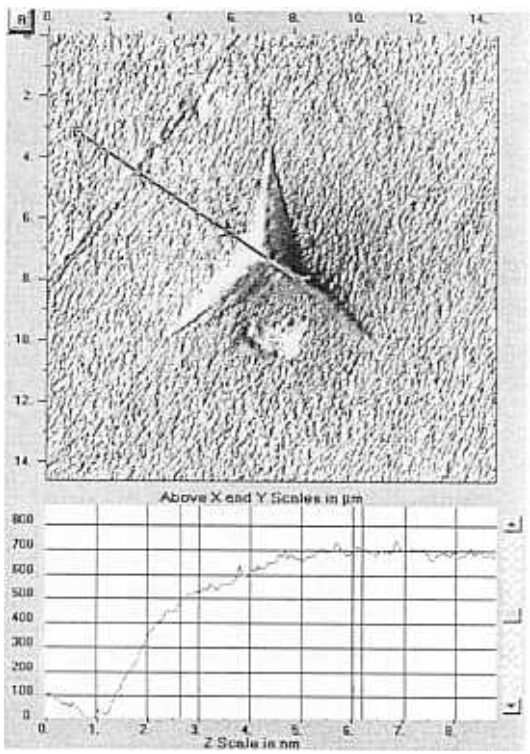


Fig. 4.6 Berkovich indent in HS3, 100mN

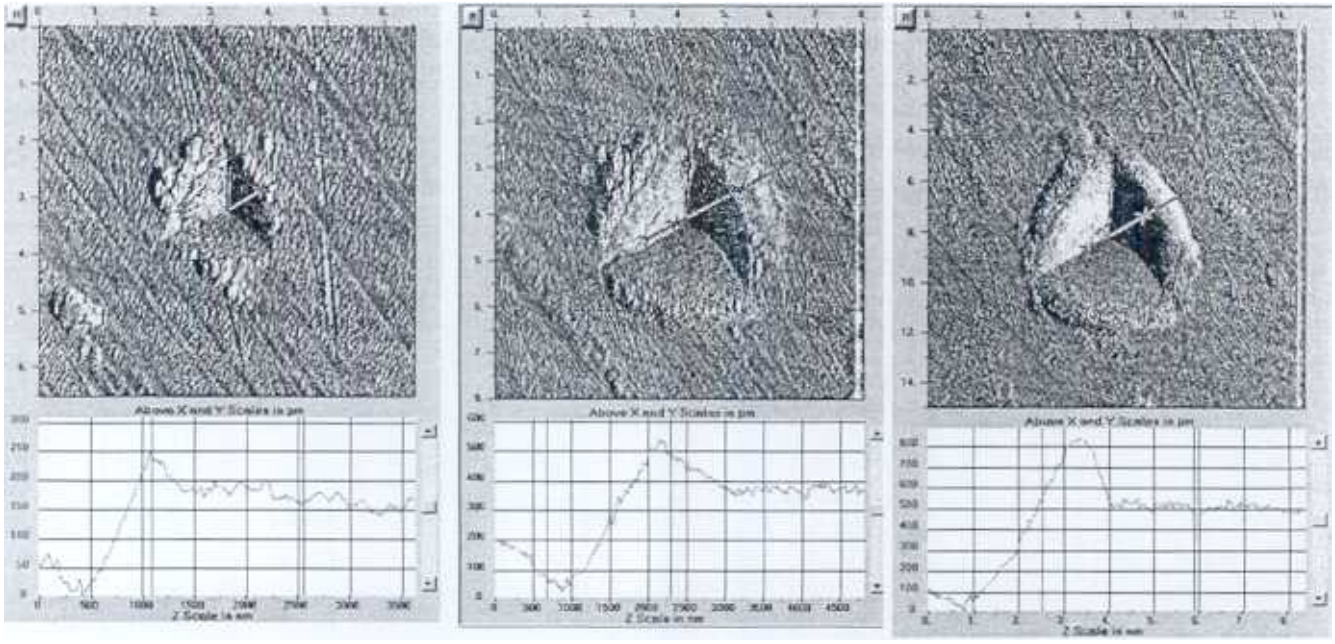


Fig. 4.7, 4.8, 4.9: Berkovich indent into SH1, 3mN, 10mN, and 50mN, respectively.

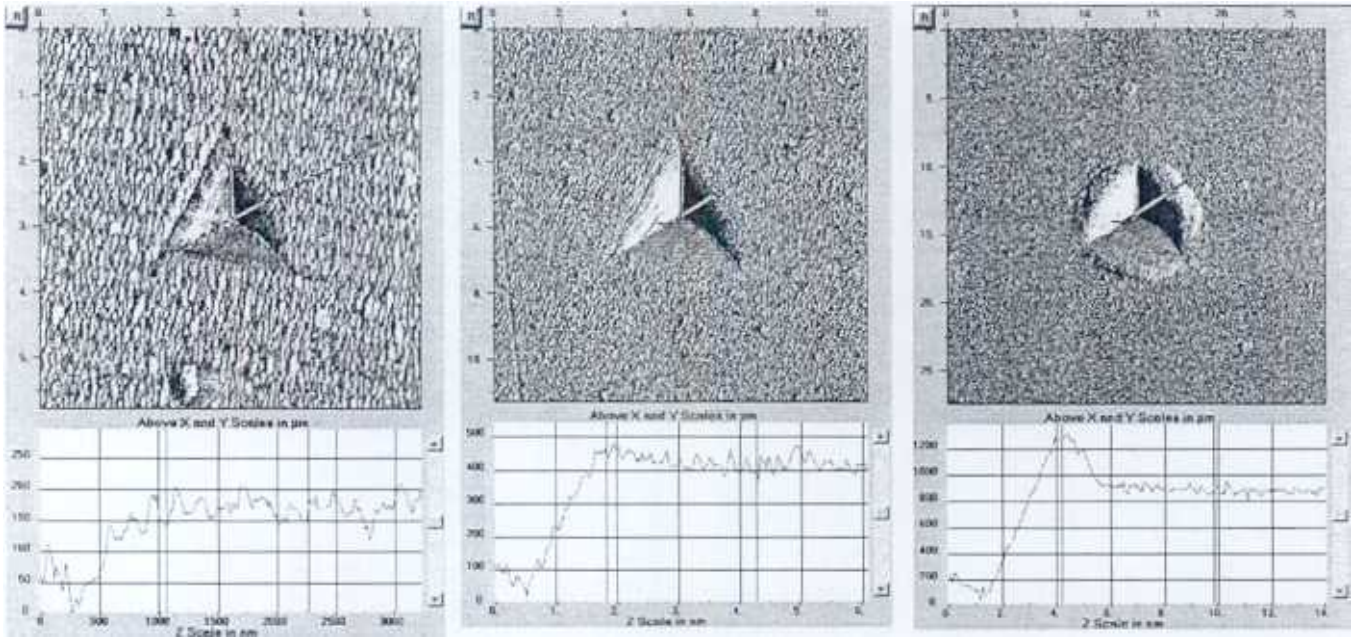


Fig. 4.10, 4.11, 4.12: Berkovich indent into SH2, 3mN,10mN and 50mN, respectively.

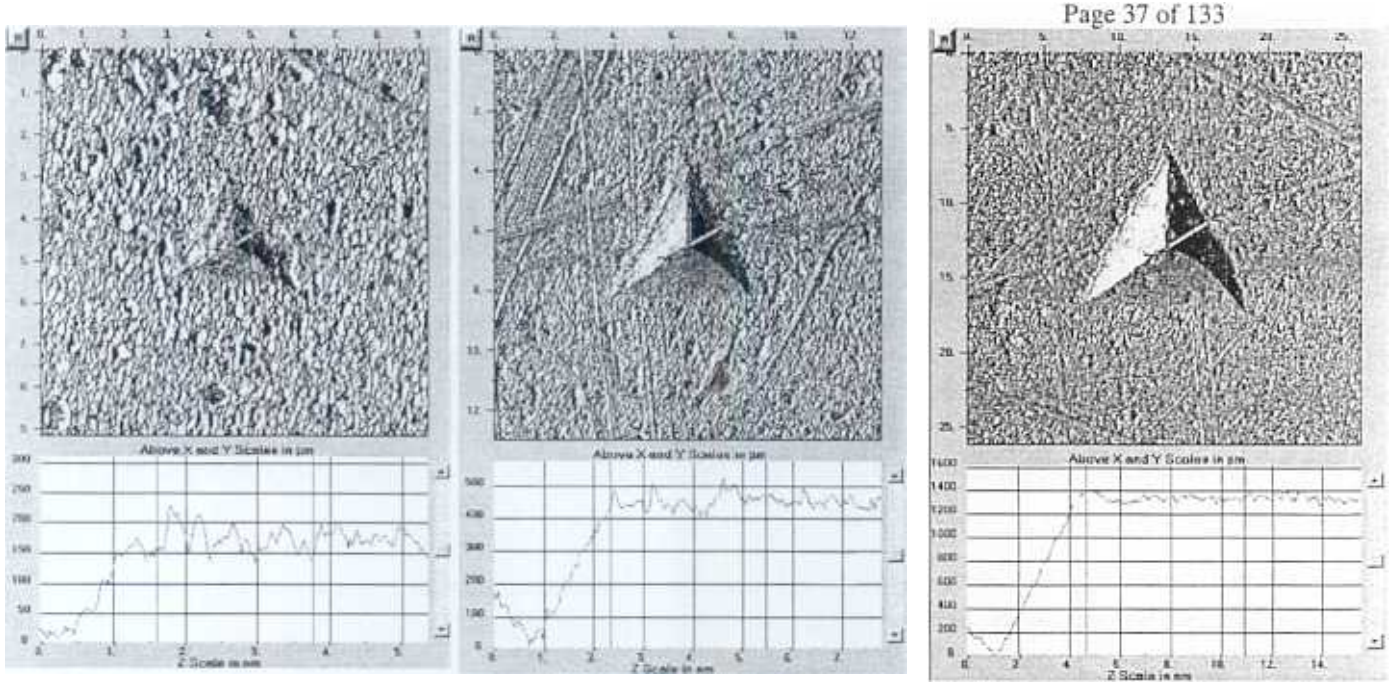


Fig. 4.13, 4.14, 4.15 Berkovich indent into SH3, 3mN, 10mN, 50mN, respectively.

5 Intercomparison of indentation experiments

5.1 Objectives and approach

The objectives of the intercomparison task were to :

1. provide a means of comparing results of indentation experiments from the different laboratories in the consortium, using different instruments and indenter geometries and on all the research coating types and thicknesses;

2. look for relations between indentation measured values as a function of coating type and thickness and with those of the properties of the substrates and coatings determined in WP1;

3. identify experimental anomalies associated with particular coatings or indenter geometries;

4. compare the results of the modelling task with experimentally determined values for a specific case;

5. identify regimes whereby the properties of the coating can be determined from the indentation data and hence provide the basis for developing an indentation protocol for the Round Robin task and, subsequently, for the draft standard;

The intercomparison task would therefore provide key results contributing to many of the work packages, (e.g. WP 2.9, WP 3.2, WP 4.3, WP 6.2 and others).

The approach taken was to compare values for specimen hardness and elastic modulus calculated from indentation results, for all coating types and thickness. The calculation of results was based on:

- a best estimate for instrument frame compliance, C_f, determined in WP4.1,
- a best estimate for indenter area function, A(h), based on direct measurement by AFM or nearest equivalent WP5.1
- a correction for thermal drift from a hold period at contact or 90% unloading, WP4.8
- a calculation of hardness and modulus from the unloading slope using the Oliver and Pharr method.

A pro-forma spreadsheet was produced to facilitate the collection of results from the different partners and provide an archive of all the experimental results.

5.2 Presentation of results

The parameters measured by indentation into coatings are always a combined response of both coating and substrate. Therefore, the values of hardness and modulus are plotted as a function of normalised coating thickness. This approach allows comparison of results for coatings of the same material but different thickness.

For elastic modulus, the appropriate parameter for intercomparison is reduced modulus of the specimen (i.e. the coating / substrate combination), E_{IT}*

$$E^*_{IT} = \frac{E_{IT}}{\left(1 - \nu^2\right)}$$

This value is the measured elastic response of the specimen, corrected for the elastic response of the indenter, E_i*. It is not appropriate to attempt to infer the elastic modulus of the coating E_c, even if the modulus and Poisson ratio of the substrate are known. It is not clear how the Poisson ratios of the coating and substrate affect the measured response since the relative contribution of the substrate increases with depth of penetration.

For hardness, the appropriate parameter for intercomparison is the specimen hardness, H_{IT}, i.e. the measured indentation hardness, a combination of the hardness response of the coating and substrate.

$$H_{IT} = \frac{F_{max}}{A_c}$$

The relative coating thickness may be normalised in a number of ways. For elastic modulus it is widely held that the most appropriate non-dimensional normalising parameter is the ratio of radius of the contact area to coating thickness, a / t_c. The coating and substrate can be thought of as two springs in series loaded over the area of contact. For indenters of different geometries (e.g. Berkovich, Vickers, spherical, cone etc) the radius of the contact area, a, is approximated by the radius of a circle having the same area as that in contact with the indenter,

$$a = \sqrt{\frac{A_c}{\pi}}$$

This value clearly has exact equivalence for a spherical or conical indenter but becomes increasingly less physically meaningful as the axisymmetry of the indenter reduces, i.e. Cone >Sphere >Berkovich >Vickers >Knoop.

The same parameter, a / t_c, can be used for the hardness results. However, since hardness is only defined for pointed indenters, the non-dimensional parameter h_c / t_c (ratio of contact depth to coating thickness) can also be used and gives a more sensitive measure of normalised coating thickness (since $h_c << a$). The relative contact area for different indenter geometries will then depend on the included angle of the indenters and so may be a source of scatter in the results from different indenter geometries.

The coating thickness, t_c, also needs to be known with high accuracy. Several methods of determining coating thickness were attempted (in WP1.2) to improve accuracy compared to the nominal values. The coating thickness measurements made by cross-sectional SEM and by Rutherford backscattering were in close agreement and were used for calculating all the results presented in this section. However, the actual coating thickness may vary locally between areas where the tests were performed and also between individual specimens. Thickness is predicted to vary from the measured values by over $\pm 5\%$ (due to deposition non-uniformity, particularly between samples) and this will significantly contribute to the scatter in the aggregation of results from different samples (additional to any calibration uncertainty between laboratories).

Results are presented for each coating type for elastic modulus and hardness in Figures 5.1a,b, 2a, 3a,b, 4a,b, 5a, 6a, 7a. Each data point represents the mean value from 10 repeated experiments (standard deviations from the mean are omitted in the interests of clarity but were recorded in the database). In some cases, the number of results included in the mean is less than 10. Partners were allowed to identify results for which they could recognise an experimental or calculation anomaly, which would justify rejection of the data, e.g. poor contact with the surface, discontinuity in the raw data etc.

In the figures, the following symbol conventions are used to indicate the indenter geometry:

× Cone
○ Sphere
Δ Berkovich
□ Vickers

◇ Indentation values for substrates obtained using both Berkovich and Vickers indenters.

_____ Solid line indicates a reduced nominal value of the substrate, e.g. E^*_s, or H_s,
- - - - - - Dashed line indicates a reduced nominal value of the coating, e.g. E^*_c, or H_c.
These values were determined by SAW methods in WP1.1 for elastic constants and by indentation into uncoated substrates for hardness.

In Figures 5.2b, 5b, 6b, 7b, different symbols to those given above may be used to represent the data. In these figures the symbols are described in the legend and captions.

In figures 5.8a-d, the elastic modulus and hardness data for the ductile coatings are presented as a 3D surface function of normalised coating thickness and loading rate.

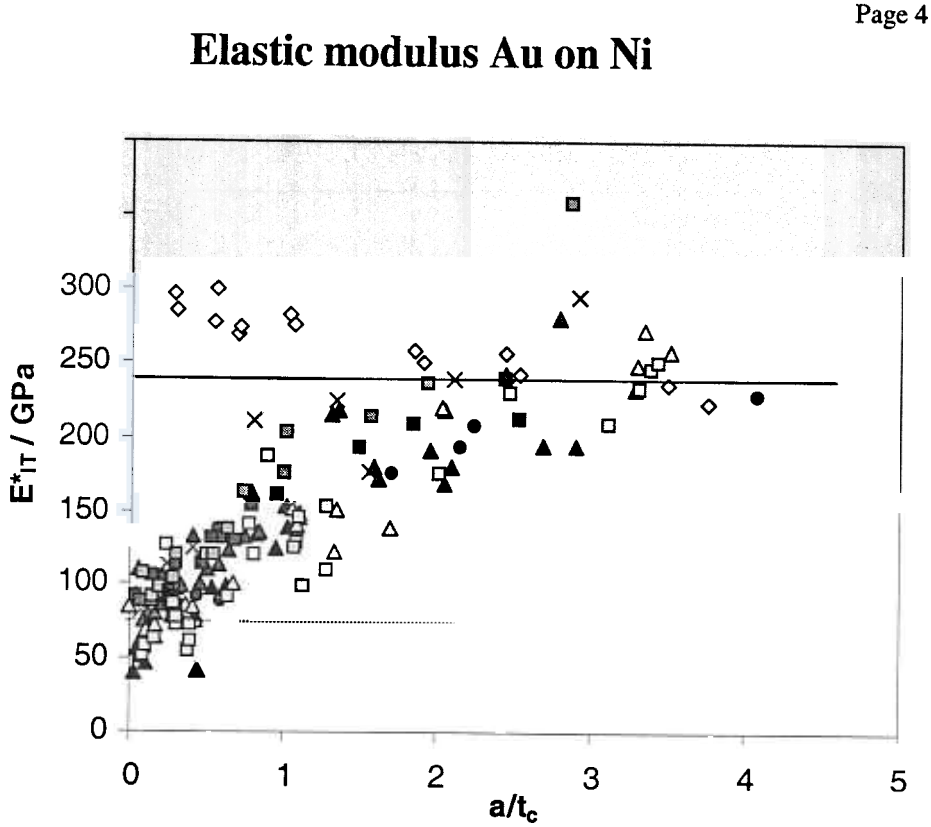


Figure 5.1a Indentation elastic modulus vs normalised coating thickness Au on Ni, all data.

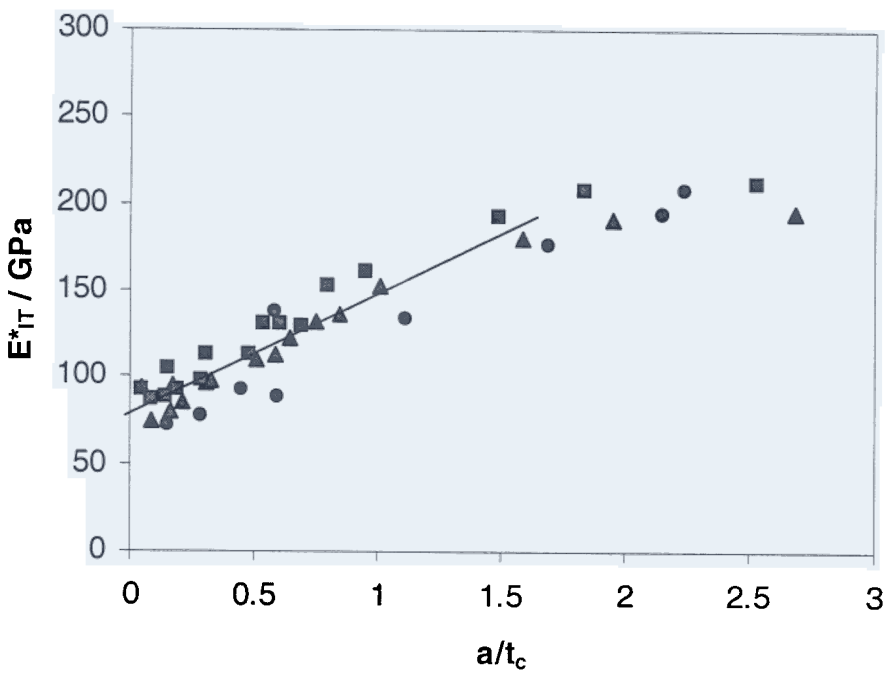


Figure 5.1b Indentation elastic modulus vs normalised coating thickness Au on Ni, selected data for spherical, Berkovich and Vickers geometries.

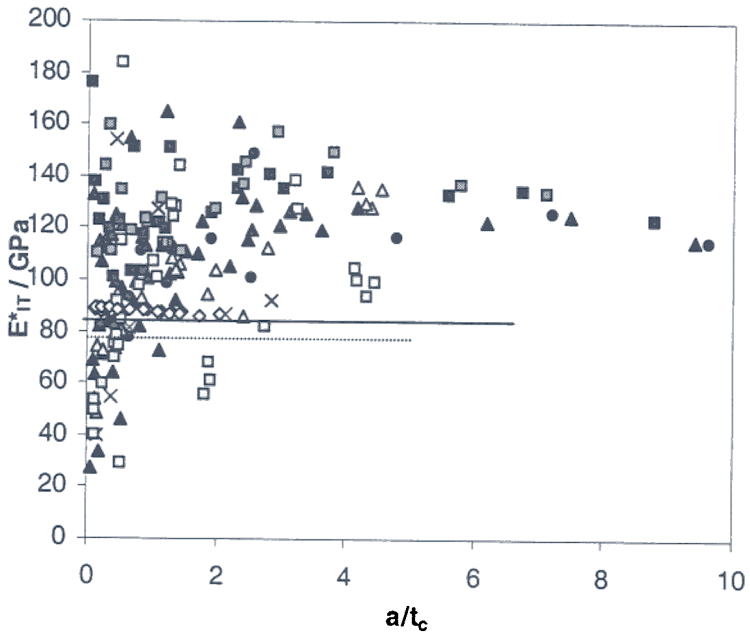


Figure 5.2a Indentation elastic modulus vs normalised coating thickness Al on BK7, all data.

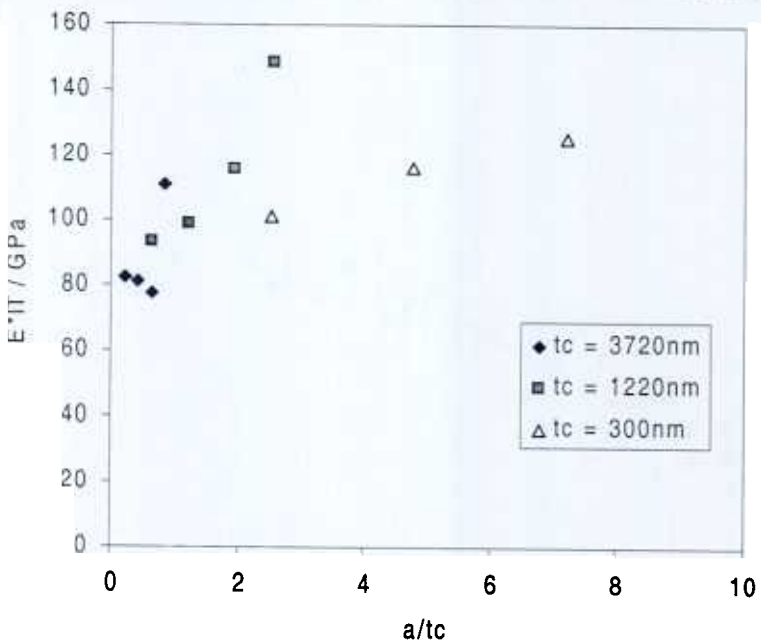


Figure 5.2b Indentation elastic modulus vs normalised coating thickness Al on BK7, selected data for spherical, Berkovich and Vickers geometries.

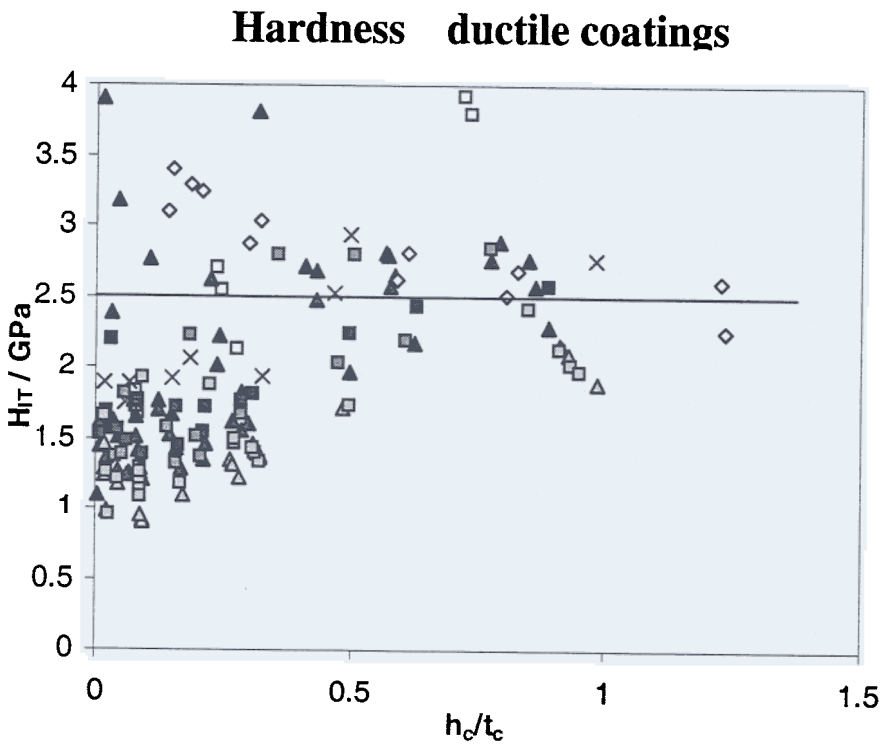


Figure 5.3a Indentation hardness vs normalised coating thickness Au on Ni, all data

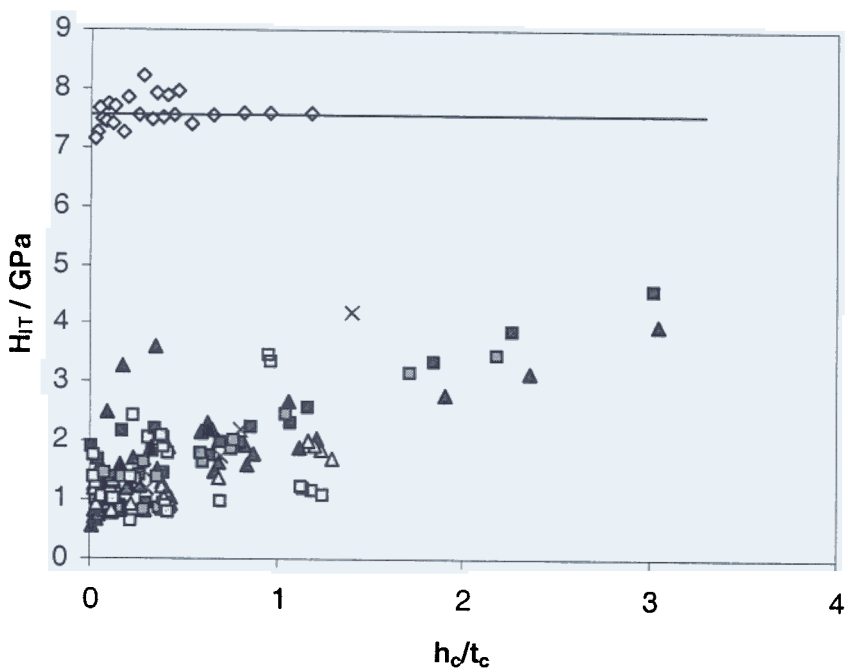


Figure 5.3b Indentation hardness vs normalised coating thickness Al on BK7, all data

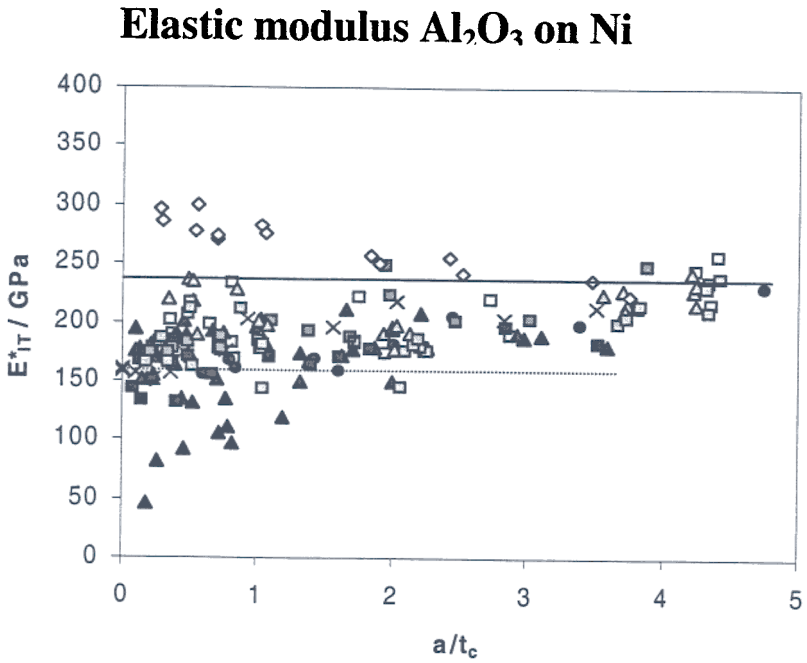


Figure 5.4a Indentation elastic modulus vs normalised coating thickness Al_2O_3 on Ni, all data

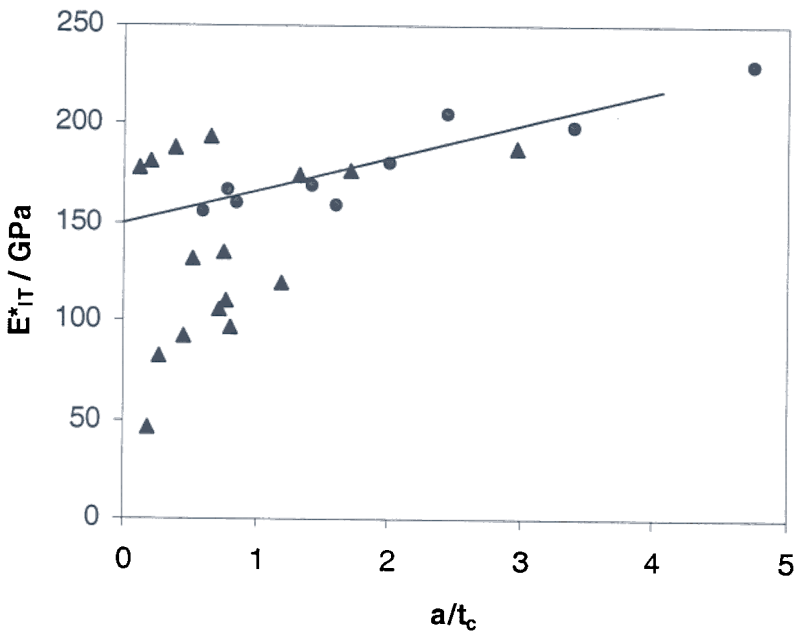


Figure 5.4b Indentation elastic modulus vs normalised coating thickness Al_2O_3 on Ni, selected data showing the delamination of one of the coatings.

Elastic modulus DLC on Steel

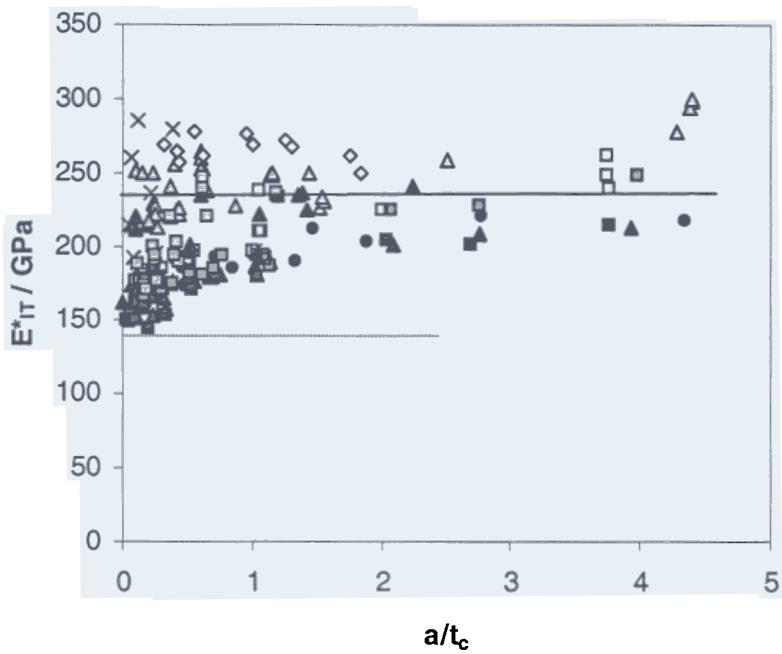


Figure 5.5a Indentation elastic modulus vs normalised coating thickness, DLC on Steel, all data

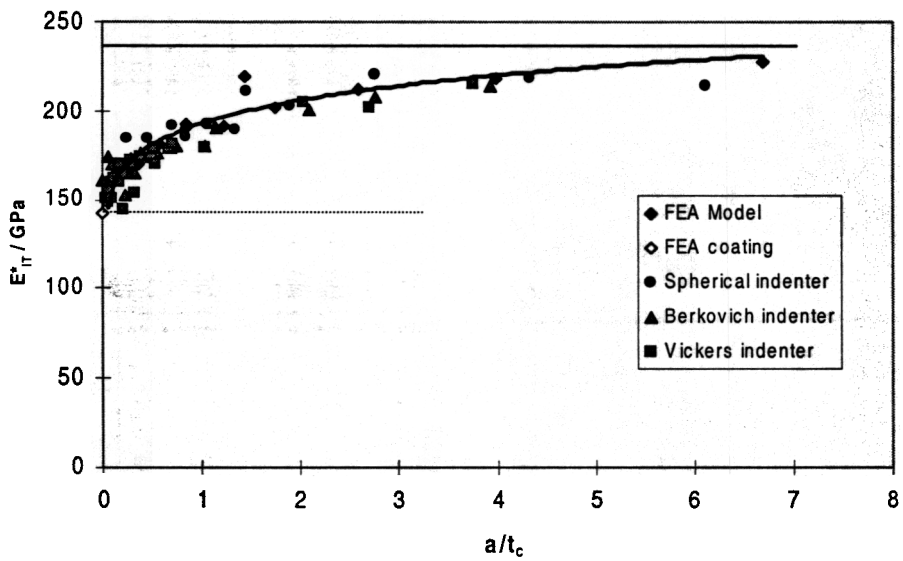


Figure 5.5b Indentation elastic modulus vs normalised coating thickness DLC on Steel, selected data plotted with values calculated from FEA simulation. Solid line is a non-linear fit to the FEA data.

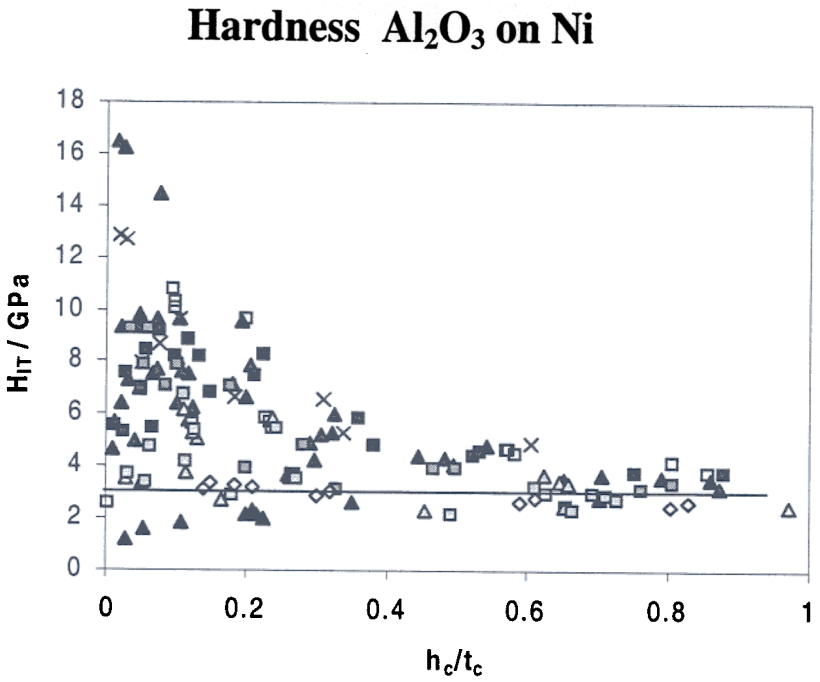


Figure 5.6a Indentation hardness vs normalised coating thickness Al_2O_3 on Ni, all data

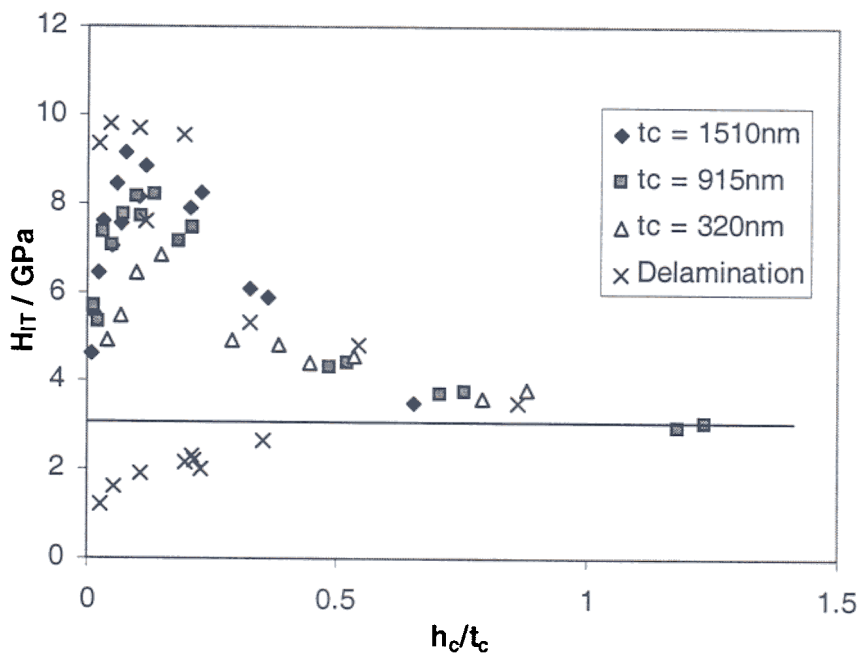


Figure 5.6b Indentation hardness vs normalised coating thickness Al_2O_3 on Ni, selected data showing the effect of substrate yield for the thinnest coating and coating delamination (crosses) for one of the coatings. Data from Berkovich and Vickers indenter geometries.

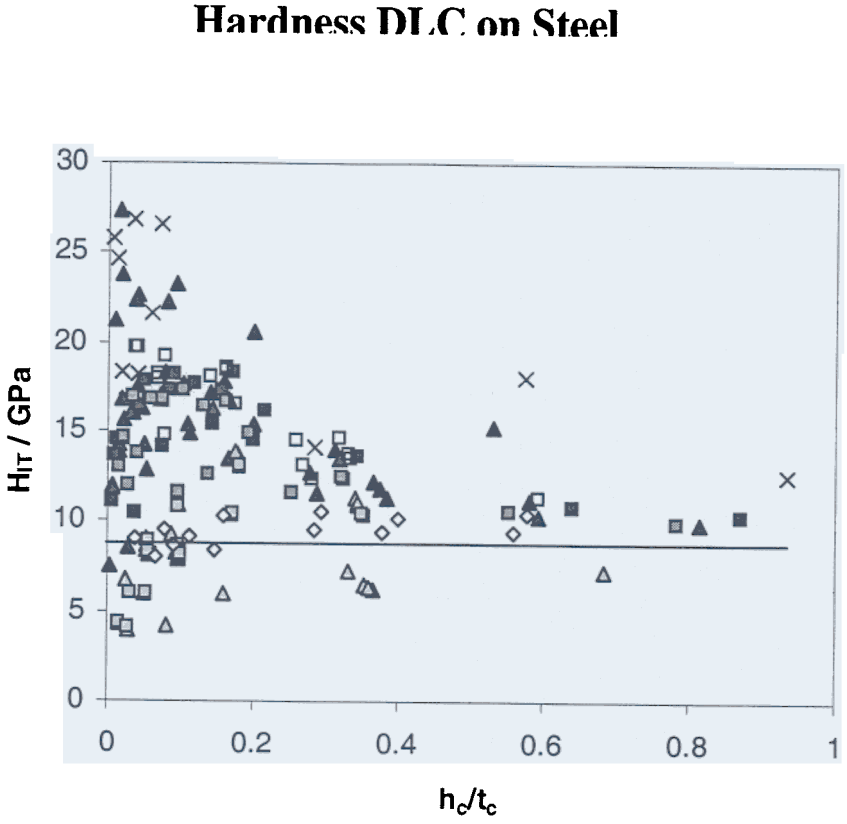


Figure 5.7a Indentation hardness vs normalised coating thickness DLC on Steel, all data

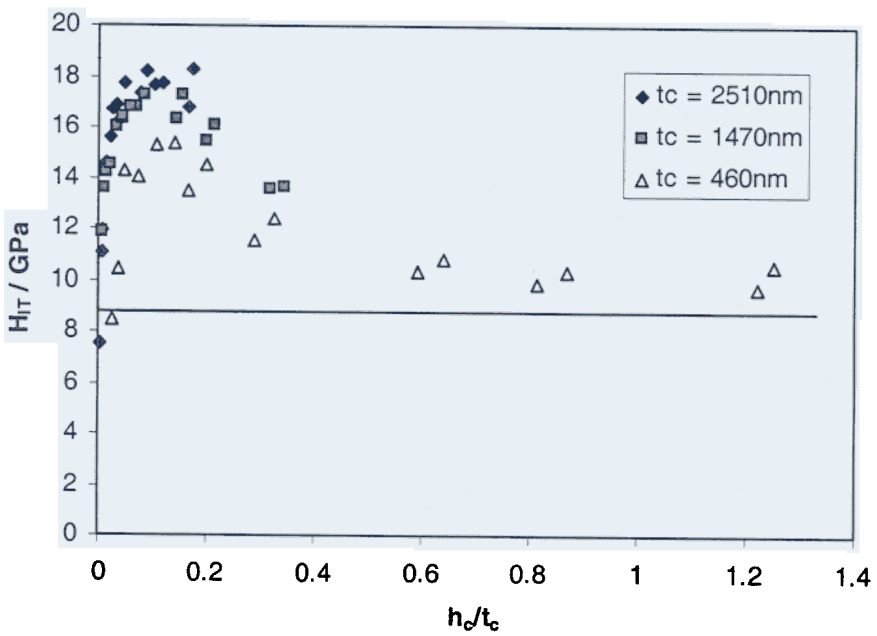


Figure 5.7b Indentation hardness vs normalised coating thickness DLC on Steel, selected data showing the effect of substrate yield for the thinnest. Data from Berkovich and Vickers indenter geometries.

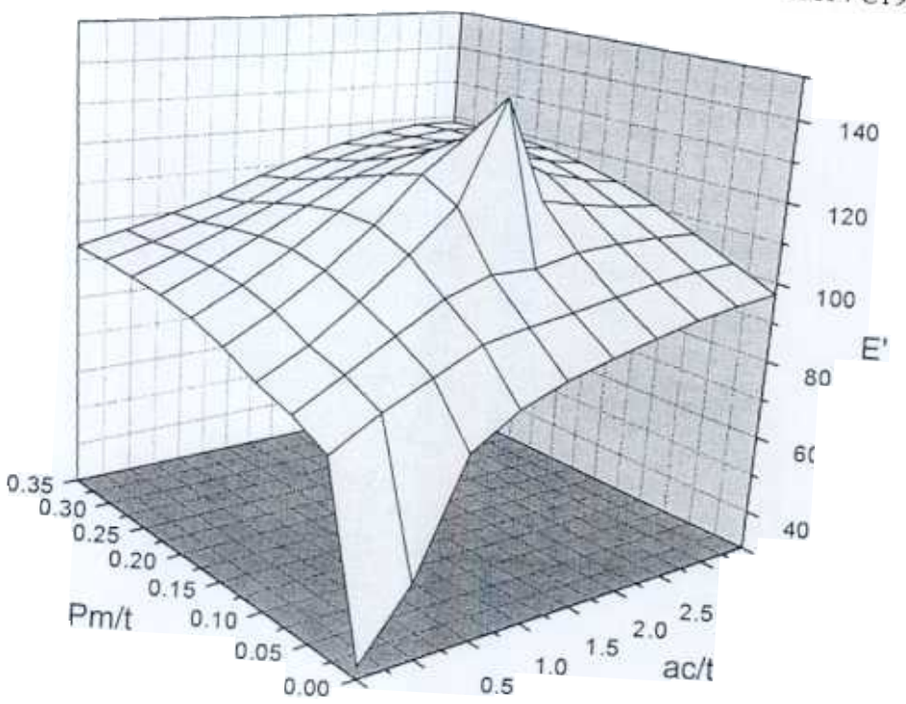


Figure 5. Indentation elastic modulus normalised coating thickness vs loading rate for on BK7

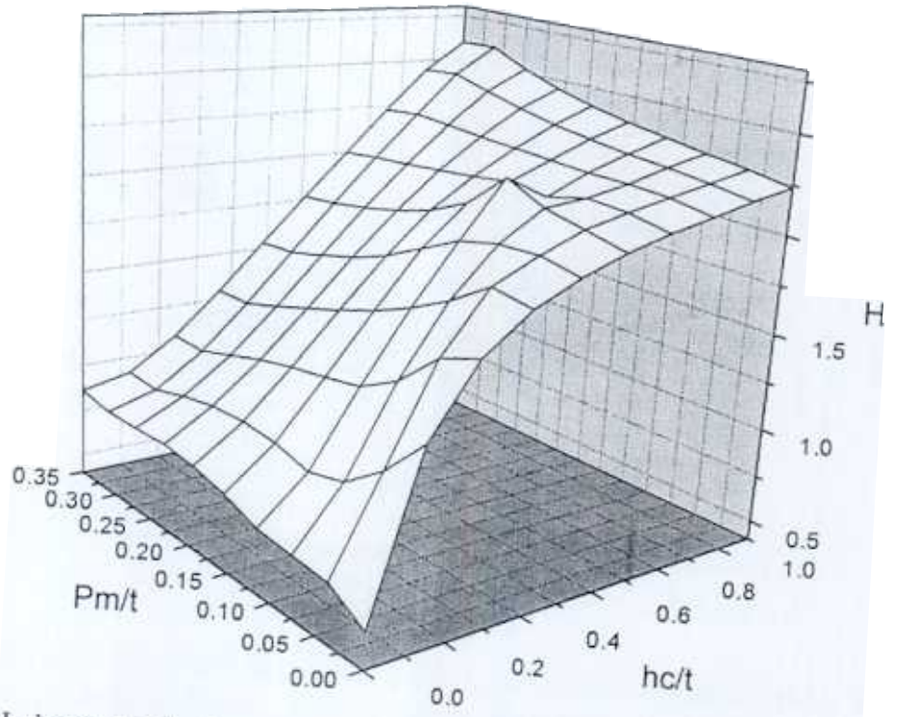


Figure 5.8b Indentation elastic modulus vs normalised coating thickness vs loading rate for Al on BK7.

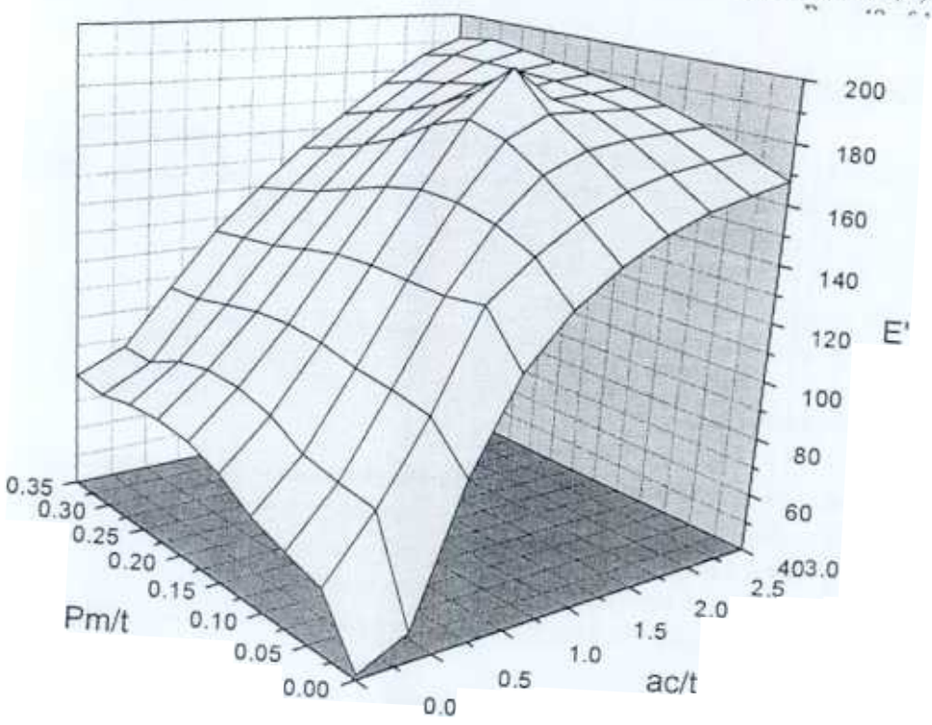


Figure 5.8c Indentation elastic modulus vs normalised coating thickness vs loading rate for Au on Ni.

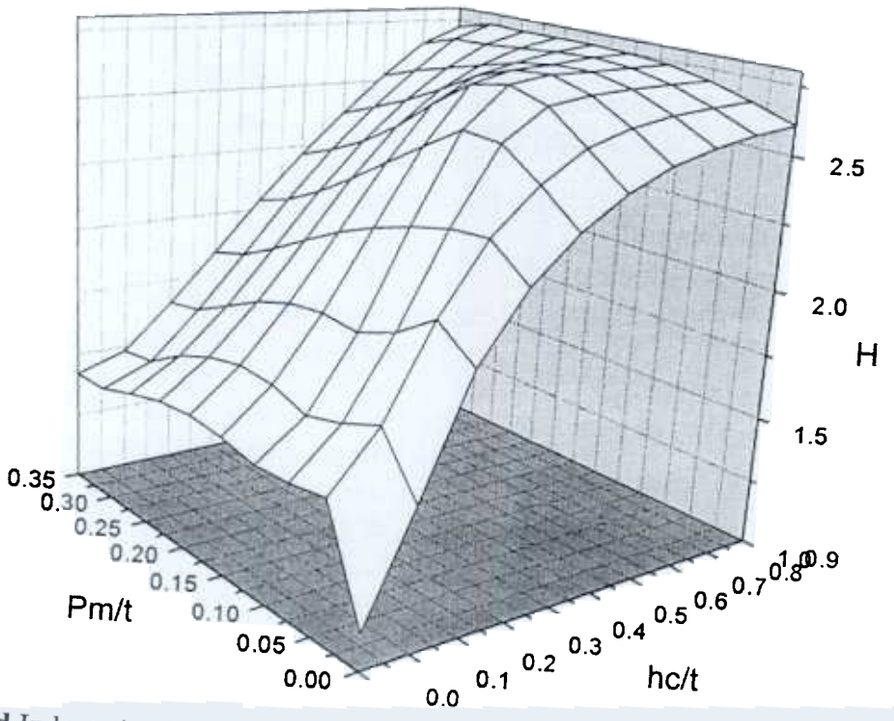


Figure 5.8d Indentation hardness vs normalised coating thickness vs loading rate for Au on Ni.

5.3 Discussion

The results can be discussed in two distinct categories that require different considerations to be taken into account, both in terms of interpreting the results and in defining suitable test parameters. These are:

1 ductile coatings on hard substrates
2 hard or brittle coatings on more ductile substrates

5.3.1 Ductile coatings

Figure 5.1 shows the effect of relative coating thickness on the indentation elastic modulus for Au on Ni. In the regime $a / t_c < 1.5$ a straight line gives a reasonable fit to the data and projects to a value close to the SAW measured coating value of $E^*_c = 74$ GPa. Figure 5.1b suggests that pile-up of material may affect the result. Pile-up is expected to be more severe for a sharper indenter and the data ranks in that order, i.e. spherical < Berkovich < Vickers.

Figure 5.2 shows that the aluminium coatings are strongly affected by creep since the measured values are up to a factor of 2 higher than either of the materials in the combination. The amount of creep increases with the thickness of the coating (as can be seen from the reduction in pile up with coating thickness in Figures 4.7-4.15) and this is apparent in Figure 5.2b where the actual coating thickness is identified. The apparent modulus is seen to increase at high forces (high a / t_c) for each coating thickness (see Figures 4.10-4.12). Clearly, the effects of creep must be considered in defining test protocols.

The hardness of the ductile coatings appears to increase linearly with h_c / t_c until the substrate hardness value is reached. Data in the regime $h_c / t_c < 1$ appears to conform to this rule of thumb.

5.3.2 Hard coatings

For the hard coatings studied, the measured indentation elastic modulus values lie, in general, between those of the coating and substrate, see Figures 5.4 & 5. However, Figure 5.4b shows that delamination of the coating can produce artificially low values of modulus since the compliance of the system has increased due to the presence of the crack. The cracking of the coating can also be seen in the hardness results in Figure 5.6b. For the regime $a / t_c < 2$ a straight line gives a reasonable fit to the data. However, for $a / t_c > 3$, it is clear the relation is not linear. In Figure 5.5b, experimental results from Spherical, Berkovich and Vickers indenter geometries are compared with elastic-plastic FEA results (generated in WP2). The modelled data is for a spherical indenter on DLC coatings with varying thickness and a reduced modulus, $E_c^* = 142.7$ GPa. A non-linear fit to the FEA data is plotted as the solid line. There is excellent agreement between the model and the experimental data, which confirms the non-linear relation. The precise nature of that relation is not clear, since it depends of the combination of elastic constants in the system and their combined contributions as a function of relative coating thickness. The determination of that relation

and its behaviour under various coating-substrate combinations is a subject for further work and is beyond the scope of INDICOAT.

The hardness of the hard (or brittle) coatings is more difficult to determine. Clearly at $h_c / t_c > 0.5$ the coating has fractured and the substrate property is measured. The hardness of the coating is only determined if the coating itself yields before the substrate. For the thicker coatings, yielding of the coating can be achieved with a sufficiently sharp indenter. For the thin coatings, yielding is initiated in the substrate before the coating yield point is reached and the coating hardness value is never achieved. FEA analysis of the Al_2O_3 coating on Ni has predicted the hardness of the system to within 0.2 GPa. Stress analysis of the coating system may be necessary to determine the sharpness of the indenter required to determine the coating hardness or if, indeed, the hardness of the coating can be determined at all.

For the ductile coatings a load rate effect is seen in the indentation measured values, Figure 5.8. However, the effect is relative small (< 10%) and it is not clear whether this is due to a material response (load rate dependency) or is a measurement effect due to creep of the material distorting the shape of the unloading curve. Evidence (from WP3.1) suggests that creep may have a major effect on the calculated values of E_{IT}* and H_{IT}, and that this may be more significant than a true material load rate dependency. The time until effective exhaustion of creep during a maximum load hold is clearly an important consideration for ductile coatings.

5.4 Conclusions

1 Test parameters for ductile and brittle coatings need to be considered separately. However, in both cases, an accurate measurement of coating thickness is essential for reproducible measurement of coating properties.

2. It is relatively easy to measure the hardness of ductile coatings or the elastic modulus of brittle coatings. It is more difficult to determine the hardness of brittle or hard coatings or the elastic modulus of ductile coatings.

3. For modulus measurement of ductile coatings a maximum hold period must be used that is sufficiently long to eliminate creep effects. Apparent rate sensitivity is often dominated by creep. A combination of a long hold at maximum load and a high removal rate of the test force is the best strategy for minimising the effect of creep on the measurement of contact compliance.

4. For ductile coatings a linear fit to indentation elastic modulus vs a / t_c gives a first approximation in the regime $a / t_c < 1.5$.

5. For ductile coatings a linear fit to indentation hardness vs h_c / t_c gives a first approximation in the regime $h_c / t_c < 1$, providing the hardness of the substrate is not reached.

6. For hard coatings a linear fit to indentation elastic modulus vs a / t_c gives a first approximation in the regime $a / t_c < 2$. However, in general, a non-linear relationship appears to apply and can be reproduced by FEA analysis. The exact nature of this non-linear relation is not known and so a linear fit over the restricted range indicated is a reasonable first approximation but is not applicable over a range wider than this.

7. The hardness of hard or brittle coatings can only be determined with a sharp (small tip radius) indenter that causes yielding within the coating. In general, this will only occur when $h_c / t_c < 0.5$. It is recommended that an elastic stress analysis of the coating/substrate system be undertaken (e.g. using 'Elastica' with a spherical indenter of a radius equivalent to the tip radius of the pointed indenter). This will determine which of the coating or substrate will yield first during indentation and if it is possible to determine the coating hardness at all. It is recommended that hardness values for the substrate be obtained for comparison, by testing if necessary. Delamination or fracture of the coating can be recognised by the hardness values obtained clustering at the substrate value, even at low h_c / t_c. Note, sharper indenters may cause fracture at lower loads than more blunt indenters.

6 Intercomparison results

6.1 Protocol

Industrial samples were obtained of three challenging coatings of unknown modulus and hardness. These were: 3000nm of MOST™ on steel, NPL ref JDQ, 5000nm of Au on a thin Steel pump diaphragm (NPL ref JDR); and 5000nm of Au on a steel strip (NPL ref JDS). The strips were purported to be witness specimens for the deposition of the Au on the Diaphragm samples. The roughness of the samples could be clearly seen to increase JDQ<JDR<JDS. The steel sheet was also extremely thin. Thus the exercise represented a near worst case scenario for the test protocol.

The full protocol forms an annex to this report. All participants were required to perform an indirect validation of their instruments using reference materials provided by the project. Results are summarised below and each instrument compared against a set of performance criteria based on those in ISO/DIS 14577 for calibrating machines and for indirect verification results, with additional classes to cover likely outcomes based on previous experience.

Compensating Errors in C_f and Ac can make the classification vary for each ref material therefore a double classification has been adopted in the order FS-W. Averaged results and classifications for all participants are summarised in the table below.

Table 6.1 Classification of indirect calibration of participant instruments.

Classification	Tolerance on reference values	Repeatability	Standard deviation of 10 results as % of ref. values
Grade 1	≤ +/-2%	A	≤ 2%
Grade 2	≤ +/-5%	B	≤ 5%
Grade 3	≤ +/-10%	C	≤ 10%
Grade 4	> +/-10%	D	> 10%

Table 6.2 Classification results for intercomparison.

Laboratory	FS 100 %dev	FS100 %cov	FS10 %dev	FS10 %cov	W100 %dev	W100 %cov	W10 %dev	W10 %cov	class
1 (FASTE)	-6.5	0.4	-6.2	0.6	-3.5	5.9	-9.3	3.3	3A-3B
1 INDICOAT	-4.0	0.38	-4.4	0.52	N/a	N/a	-5.3	4.4	2A-3B
3	-1.9	0.87	0.99	5.9	3.7	9.0	-0.07	9.3	1B-1C
4	(60mN) 3.9	0.68	4.3	0.96	-6.3	1.1	9.5	2.6	2A-3A
5	4.4	0.33	14.2	0.59	-20.7	1.2	10.4	4.9	3A-4B
7	-1.9	0.2	-2.7	0.5	-23.1	1.2	-4.6	4.7	2A-4B
8	3.9	1.9	0.7	0.9	12.7	8.3	13.1	5.1	2A-4C
9					-19.3	10.1	-61.0	2.6	un-4C
10	-3.8	1.1	-0.36	1.35	-3.3	2.0	-2.0	3.8	2A-2B

In addition, a pilot comparison was performed on all samples to be used. Figure 6.1 plots the results as a scatter plot for E and H .

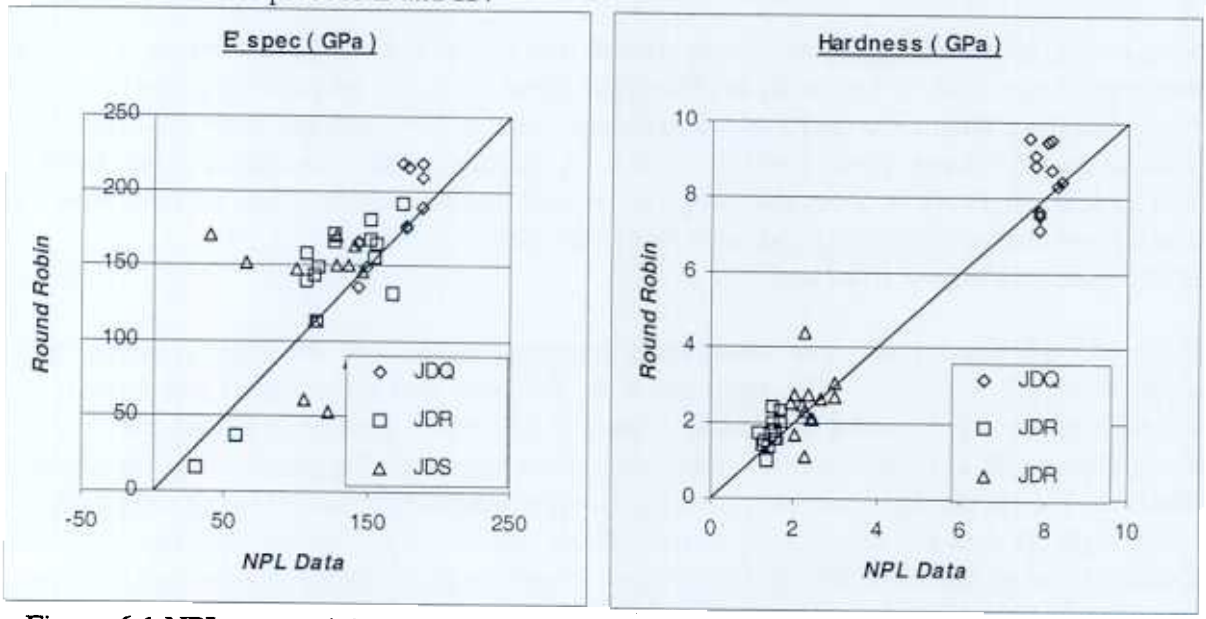


Figure 6.1 NPL vs. participant results for E* and H.

It can be clearly seen that some coatings have a variation in properties, which shows as a tendency for results to form a line gradient 1 showing that both NPL and the Participant agree that the properties vary. In other cases, e.g. JDQ hardness, there is a symmetrical distribution representing a uniformity in sample properties and is a measure of the reproducibility the measurements between laboratories. The roughest sample, JDS shows a marked scatter in

results, particularly for modulus. In Figure 6.2, the results for each sample are plotted individually to demonstrate where systematic calibration differences existed. In principle the subsequent intercomparison data can be normalised to take such type B uncertainty out of the comparison.

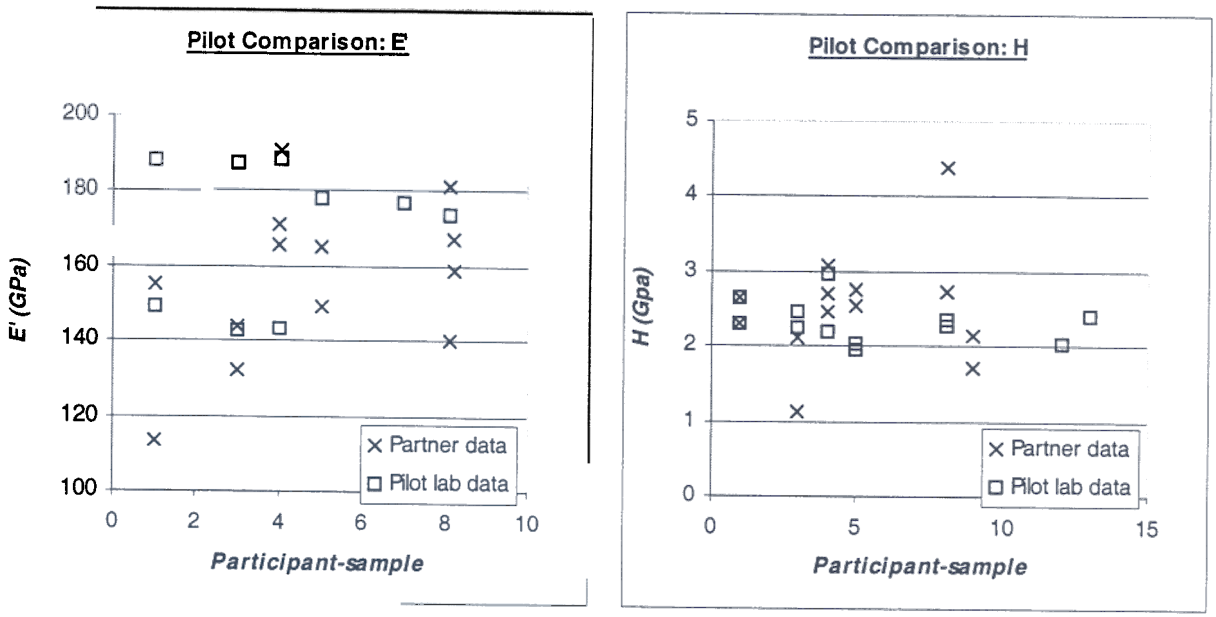
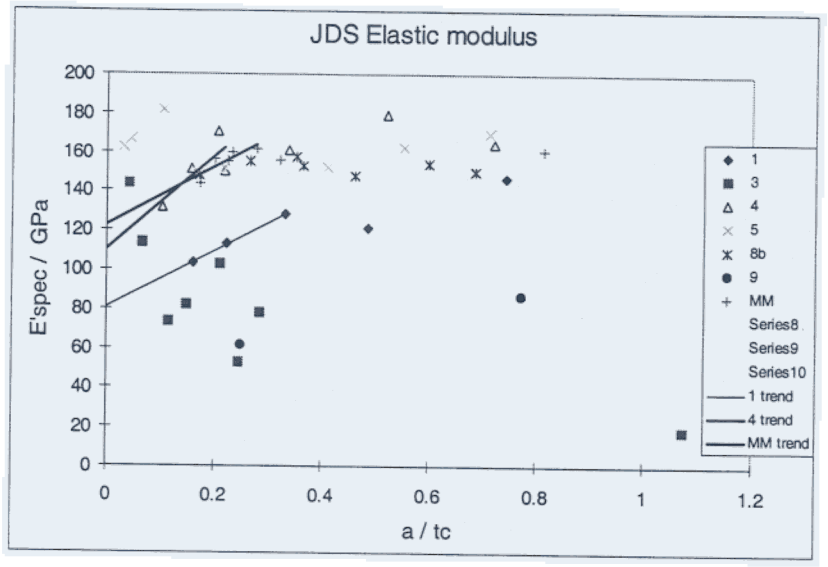
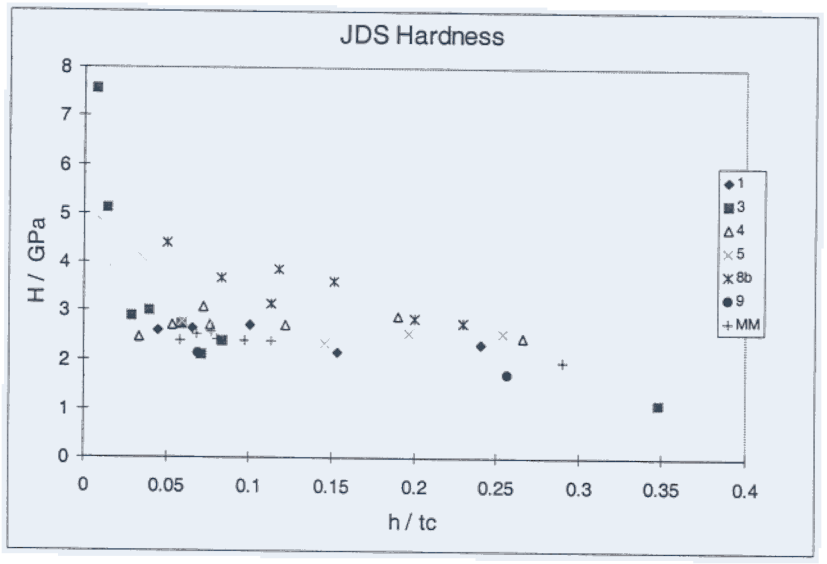


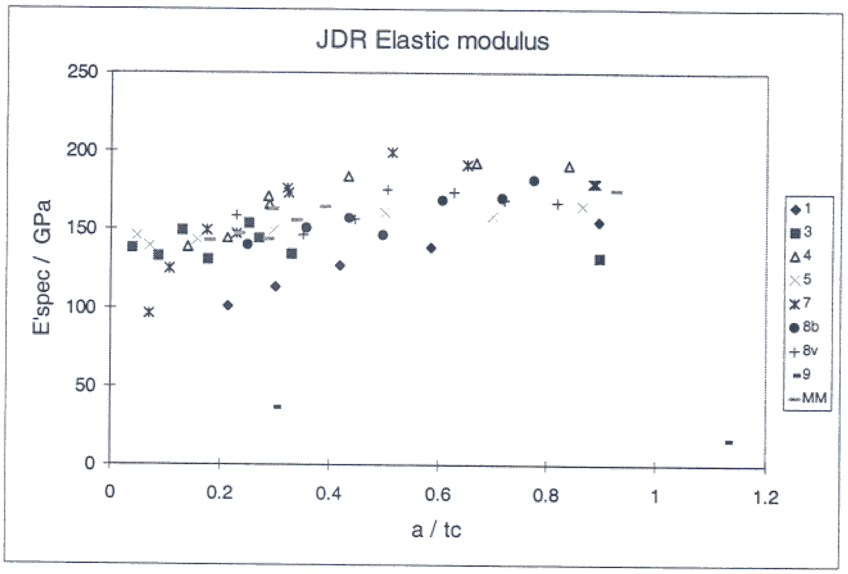
Figure 6.2 Sample by sample comparison against the pilot laboratory results.

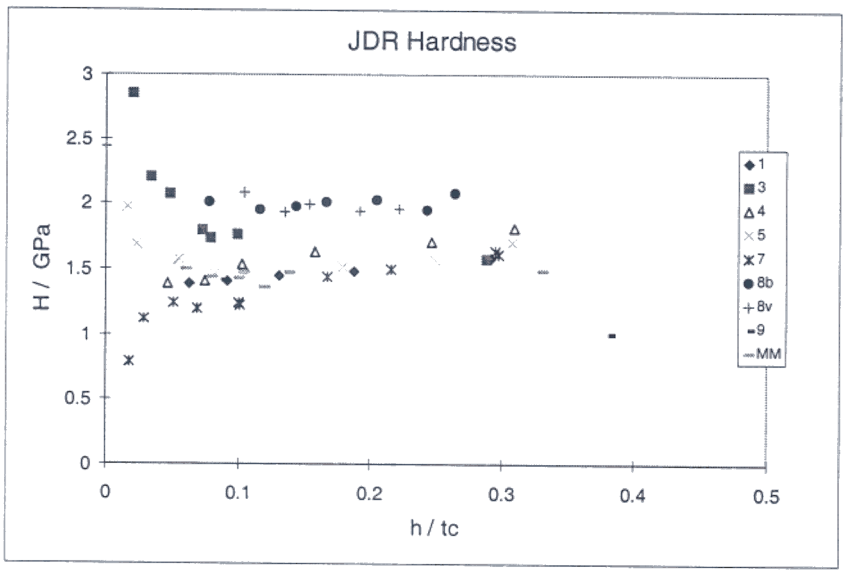
The essential step in the protocol was to require two sets of standard indentations into each sample and inspection of the results to inform the lab of the exact parameters to use to obtain appropriate data. This is the only method to obtain a relationship between force and a/t or hc/t for an unknown sample. Armed with these results, the labs were then instructed to obtain a set of at least 5 points in a suitable range of a/t and hc/t and estimate the coating reduced modulus and hardness by fitting a straight line to the data
and extrapolating to zero a/t or hc/t .

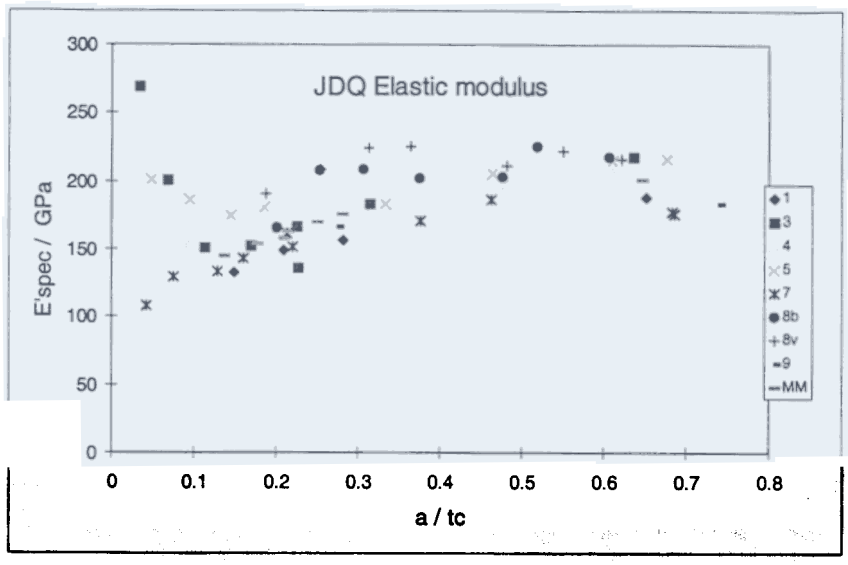
Figures 6.3-6.9 show that some laboratories struggled at the low indentation depths and produced unrealistic results. The main result is, however that the form of the plots is in reasonable agreement between laboratories. Often the response function is almost flat making the assignation of a value easy. In other cases, there is some dispersion but a reasonable consensus. Taking the worst sample it, from a measurement viewpoint, and excluding the low a/t and high a/t data for data sets with discernable trends - the reduced modulus may be estimated to be in the range 80-120 GPa. This is despite high surface roughness and without correction for systematic errors and without an accurate thickness calibration for any of the coatings. The expected E_{IT}* for gold is approx 100 GPa. The data for the component, JDR is better and there is a clear difference in the hardness of the two, nominally identical coatings.

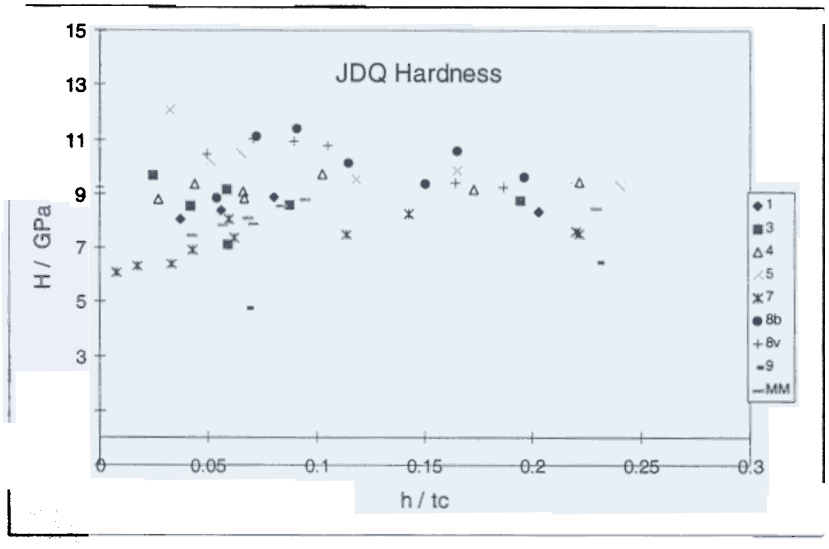

JDS Elastic modulus
E'spec / GPa
a / tc
0
20
40
60
80
100
120
140
160
180
200
0
0.2
0.4
0.6
0.8
1
1.2
1
3
4
5
8b
9
MM
Series8
Series9
Series10
1 trend
4 trend
MM trend


JDS Hardness
H / GPa
h / tc
0
1
2
3
4
5
6
7
8
0
0.05
0.1
0.15
0.2
0.25
0.3
0.35
0.4
1
3
4
5
8b
9
MM


JDR Elastic modulus
E'spec / GPa
250
200
150
100
50
0
0
0.2
0.4
0.6
0.8
1
1.2
a / tc
1
3
4
5
7
8b
8v
9
MM


JDR Hardness
H / GPa
3
2.5
2
1.5
1
0.5
0
0
0.1
0.2
0.3
0.4
0.5
h / tc
1
3
4
5
7
8b
8v
9
MM


JDQ Elastic modulus
E'spec / GPa
300
250
200
150
100
50
0
0
0.1
0.2
0.3
0.4
0.5
0.6
0.7
0.8
a / tc
1
3
4
5
7
8b
8v
9
MM


JDQ Hardness
H / GPa
15
13
11
9
7
5
3
0
0.05
0.1
0.15
0.2
0.25
0.3
h / tc
1
3
4
5
7
8b
8v
9
MM

7 Data Analysis

7.1 Hardness calculation

7.1.1 Comparison of different hardness definitions

For the hardness calculation the following hardness definitions were considered:

Indentation hardness H_{IT} acc. to ISO/CD 14577

1)
$$H_{IT} = \frac{F_{max}}{A_p} \approx \frac{F_{max}}{24.5 h_c^2}$$

with h_c = contact depth

$$h_c = h_{max} - \varepsilon(h_{max} - h_r)$$

valid for ideal Vickers indenter and modified Berkovich indenter
$\varepsilon = 0.75$ (value for pointed indenter)

2) Plastic hardness acc. to Doerner/Nix

$$H_{pl} = \frac{F_{max}}{A_n} \approx \frac{F_{max}}{24.5 h_c^2} \approx \frac{F_{max}}{24.5 h_r^2}$$

$$h_c = h_{max} - \varepsilon(h_{max} - h_r) = h_i$$

h_r = linear fit to top portion of unload curve.

$\varepsilon = 1.0$ (value for flat punch)

3) Modified indentation hardness $H_{IT(mod)}$

Modification under consideration of the radial displacement correction Δl

$$H_{IT\,mod} = \frac{F_{max}}{a^2}$$

with
$$a = \frac{\sqrt{\pi}}{2} \frac{1}{E_r} \frac{1}{1/S - C_f} (1 + \Delta l)$$

$$\frac{(1-2\nu)(1+\nu)}{2} \frac{F}{Ea^2} \cos(\arctan(\frac{h_0}{a}))$$

4) Martens hardness HM acc. to ISO/CD 14577

$$HIT = \frac{F_{max}}{A_s(h)} = \frac{F_{max}}{26.43 h^2}$$

5) Vickers hardness HV acc. to ISO 6507-1

$$HV = 0.1891 \cdot \frac{F}{d^2}$$

with d – arithmetic mean value of the two diagonals d_1 and d_2 of the indent
(F in N, d in mm)

Values of H_{IT}, H_{pl} and HM were measured with Fischerscope H100 and Berkovich indenters on the various samples according to the experimental plan of the project. The hardness values were corrected with the area function of the indenter. Moreover, the parameter h_{max}/ t_c (h_{max} = corrected value of maximum indentation depth, t_c = layer thickness) has been indicated.

As a general conclusion the values of Martens hardness HM in all cases are smaller than those of the indentation hardness H_{IT} and the plastic hardness H_{pl}. As this one has to consider that HM reflects both the elastic and plastic behaviour of the material and H_{IT} and H_{pl} exclusively the plastic behaviour. H_{pl} delivers still larger values than H_{IT}.

In table 7.1 the relationships H_{pl}/H_{IT} and HM/H_{IT} are summarized for the investigated coated samples.

Table 7.1
Relationships H_{pl}/H_{IT} and HM/H_{IT} for the investigated coated samples

Sample	H_{pl}/H_{IT}	HM/H_{IT}
IND 71 Au 0 nm on Ni	1.26 ... 1.91	0.90 ... 0.94
IND 58 Au 300 nm on Ni	1.24 ... 1.74	0.90 ... 0.94
IND 19 Au 1200 nm on Ni	1.21 ... 1.63	0.89 ... 0.93
IND 38 Au 5000 nm on Ni	1.22 ... 1.88	0.89 ... 0.94
IND 90 Al2O3 200 nm on Ni	1.28 ... 2.57	0.84 ... 0.93
IND 81 Al2O3 800 nm on Ni	1.41 ... 2.90	0.84 ... 0.94
IND 73 Al2O3 2000 nm on Ni	1.53 ... 3.56	0.85 ... 0.94
IND 11 Al 310 nm on BK7	1.25 ... 1.66	0.90 ... 0.93
IND 31 Al 1050 nm on BK7	1.19 ... 1.56	0.89 ... 0.93
IND 51 Al 3400 nm on BK7	1.20 ... 1.85	0.89 ... 0.94
IND 67 DLC 0 nm on M2	1.25 ... 2.85	0.85 ... 0.94
IND 12 DLC 200 nm on M2	1.28 ... 2.99	0.85 ... 0.95
IND53 DLC 1000 nm on M2	1.43 ... 2.94	0.85 ... 0.95
IND 29 DLC 2000 nm on M2	1.54 ... 3.03	0.83 ... 0.95

Table 7.1 reveals that the relationship H_{pl}/H_{IT} varies in a much larger range than the relationship HM/H_{IT}. The variance of these relationships obviously depends on the hardness of the coatings. The soft coatings Au and Al show a smaller variance than the hard coatings

Al_2O_3 and DLC. The relationship H_{pl}/H_{IT} significantly depends on the parameter h_{max}/ t_c which reflects the applied test force.
As a typical example Fig 7.1 depicts the relationships H_{pl}/H_{IT} and HM/H_{IT} as function of h_{max}/d for the sample IND JDE 31 (Al 1050 nm on BK7).

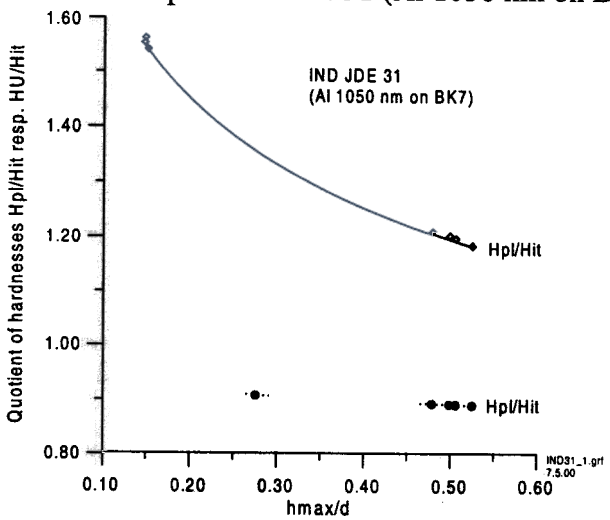


Fig. 7.1 Relationships H_{pl}/H_{IT} and HM/H_{IT} as function of h_{max}/ t_c for the sample IND JDE 31 (Al 1050 nm on BK7)

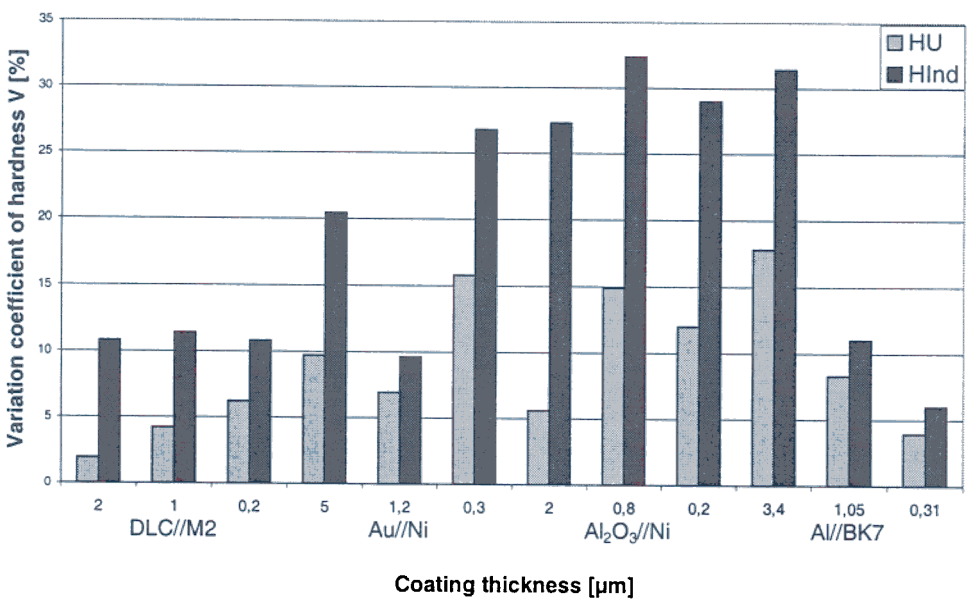


Fig. 7.2 Variation coefficients of the hardnesses H_{ind} (≡ H_{IT}) and HM for the investigated coated samples.

In all cases the variation coefficient of HM is smaller than that of H_{IT}. The cause is that HM depends only on the force increasing curve, whereas H_{IT} depends both on the force increasing and force decreasing curve.

7.1.2 Uncertainty estimation of the hardness measurement

On the example of the Martens Hardness HM the uncertainty of this measuring method can be estimated under consideration of the following error influences:

1) measuring deviation of the force measuring system ΔF
2) measuring deviation of the length measuring system Δh
3) relative uncertainty of the indenter's area function $\Delta A/A$
4) deviation at the zero point determination for the depth measurement Δh_o
5) mechanical deformation of the measuring device Δh_m

Under the precondition of relative measuring deviations and an assumed rectangular distribution (pessimistic estimation) of the measuring deviations the combined standard uncertainty is

$$u_c = \sqrt{\frac{1}{3}\sum_i \left(\frac{\Delta HU}{HU}\right)^2}$$

and the expanded uncertainty:

$$U = ku_c$$

In table 7.2 the calculation of the measurement uncertainty is summarized.

Table 7.2 Procedure for the estimation of the uncertainty of the Martens Hardness HM.

Error influence	Relative measuring deviation $\Delta HM/HM_i$	Limit value of rel. meas. dev.	Assumed error distribution	Contribution to variance (with assumed error distribution) $1/3(\Delta HM/HM)_i^2$
1	$\Delta F/F$	0.5 % F	Rectang.	0.00000833
2	$-2\Delta h/h$	0.5 % h	Rectang.	0.00003333
3	$\Delta A/A$	6 % at h = 1000 nm	Rectang.	0.00120000
4	$-2\Delta h_o/h$ (h = 3000 nm)	1 nm	Rectang.	0.00000015
5	$-2\Delta h_m/h$ (h = 3000 nm)	10 nm	Rectang.	0.00001481
square of combined standard uncertainty u_c^2				0.00125662
expanded uncertainty U (k=2)				0.0709

The expanded relative uncertainty of the Martens hardness for h = 1000 nm in this example is estimated as U = 7.1 %. In order to get the dependency of the uncertainty on the indentation depth one has to carry out the calculation shown above for various indentation depths h. Thermal drift has not been included as a separate uncertainty in the above analysis. On instruments where this is significant uncertainty a separate analysis would be appropriate.

7.2 Modulus calculation

Objective: recommendations of the preferred analysis method for determining E modulus for each coating type.

7.2.1 Experiment

We analysed results obtained with the NanoTest 600, using a Berkovich indenter. Experimental conditions: Maximum load p_{max}=10mN; maximum depth $h_{max} \approx$ 10% of layer thickness; load rate: 0.49 mN/s; 10s hold for creep; 60s hold at 10% of p_{max}. The coating types used were hard/hard (DLC/M2), soft/hard (Al/Bk7); soft/soft (Au/Ni). The type hard/soft (Al2O3/Ni) has not yet been studied since we received the sample too late.

7.2.2 Analysis and results

We applied two types of analysis:

- ***Oliver and Pharr*** ("O&Ph"): the power law $p(h)=a*(h-b)^m$ was fitted to different intervals
  of the unloading branch. Then successively
  $S = (dP/dh)$ at h_{max}, $h_s= \varepsilon*p_{max}/S$, $h_c=h_{max}-h_s$, $A_c=A(h_c)$ were calculated.

- ***Doerner and Nix*** ("D&N"): $p(h)=\alpha*h + \beta$ was fitted to different intervals of the unloading curve.
  Then h_p was determined from $p(h_p)=0$ and $A_c=A(h_p)$ calculated.

For both methods finally the E modulus was calculated from the reduced modulus $E_r = 0.5*S*\sqrt{(\pi/A_c)}$,
using the area function A(h) known from AFM measurements. The results are collected in Table 7.3.

Sample	fit region (% p_{max})	Oliver & Pharr E (GPa)	m	Doerner & Nix E (GPa)
Au30, 5µm	[illegible] *	90.1±5.6	2.4±0.5	65.1±2.3
	[illegible]	92.7±11	14±17	75.8±2.9
	[illegible]	81.7±13	[illegible]	81.6±6.1
	[illegible]	[illegible]	[illegible]	70.3±7.8
	[illegible]	[illegible]	2.1±0.4	65.8±2.5
	[illegible]	[illegible]	[illegible]	58.7±2.2
	20-100 *	128.8±2.3	1.8±0.3	80.5±2.5
	[illegible]	119.7±6.4	3.3±1.8	98.5±2.1
	[illegible]	100.7±8.5	[illegible]	99.6±2.5
		77.1±14	[illegible]	78.7±5.5
		121.5±2.8	2.6±0.4	83.9±2.4
		132.7±25.7	[illegible]	70.3±2.3
	20-100 *	214.9±12	1.8±0.1	265±26
	[illegible]	[illegible]	[illegible]	262.6±23
	[illegible]		[illegible]	263.8±22
	80-100		[illegible]	266.6±20
	30-90		1.7±0.2	260.9±25
	[illegible]		[illegible]	258.5±25

O&Ph: Creep distorts the unloading curve; its upper part should not be used in the analysis (see Fig.7.3a). The fit region 20%...80% of p_{max} is a possible choice although better choice of indentation cycle to reduce the effect of creep is perhaps preferable.

D&N : Less sensitive to creep; here the lower part of the unload curve is less useful (deviation from linearity too big). The fit region 67%...100% of p_{max} is a good choice.

For the case studied here, with the recommended choices the modulus values E(O&Ph) and E(D&N) agreed well.

soft/hard (Al/Bk7):

O&Ph: Since there is less creep, a higher upper limit of the fit region is possible (Fig.7.3b). Good fit region: 20%...100% of p_{max}.

D&N : Same situation as for soft/soft; the E result is smaller than that for O&Ph. Good fit region: 67%...100% of p_{max}

With the recommended choices E(D&N) differed from E(O&Ph) by -22%

hard/hard (DLC/M2 steel):

O&Ph: No creep, no sensitivity to upper fit limit (Fig.7.3c). The fit region may start at 20%...30% and end at 80%...100% of p_{max}.

D&N : No systematic influence of fit limits visible.

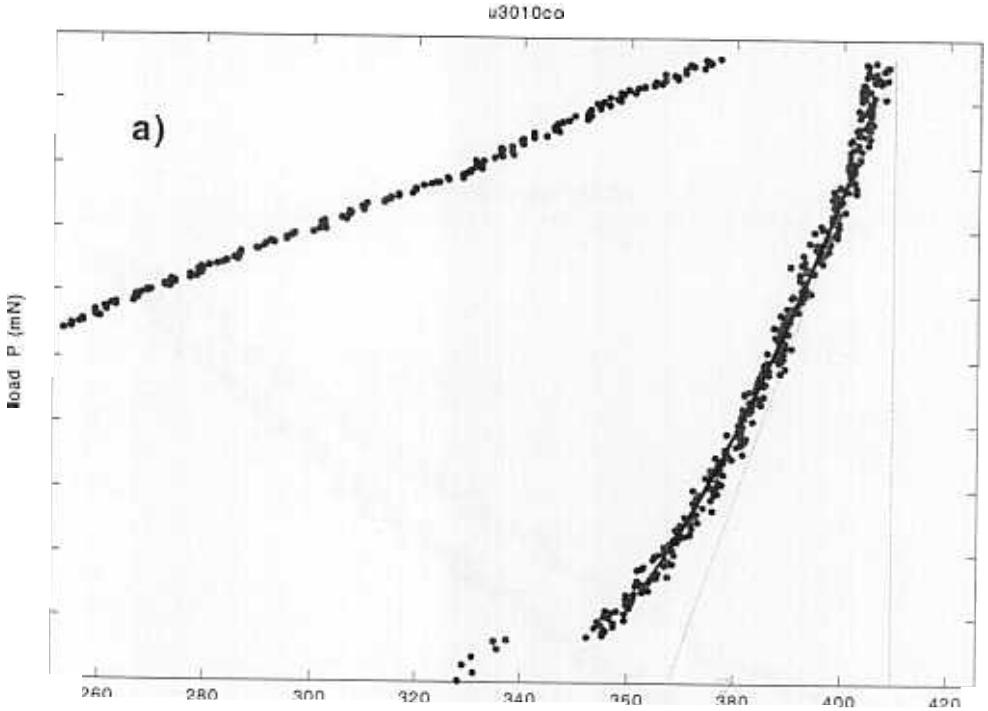
With the recommended choices E(D&N) differed from E(O&Ph) by +20%.

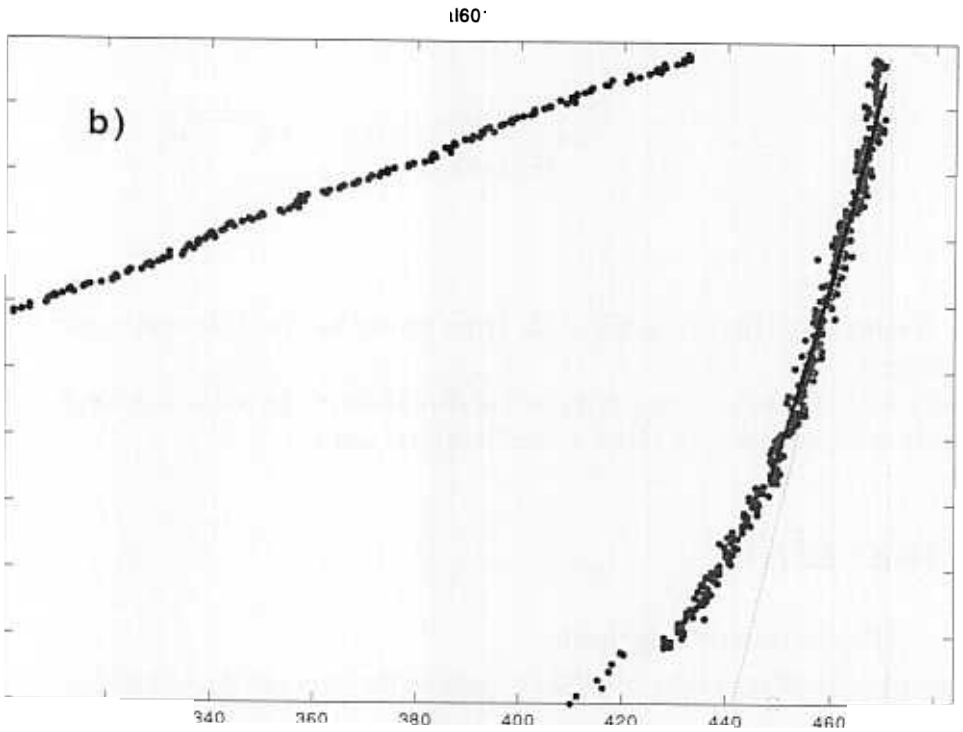
7.2.4 Conclusions

- If soft coatings are involved, one has to check carefully whether the unload curve is distorted by creep. Indications are the shape of the upper part of this curve or fit results with m > 2. In that case the upper limit of the fit region has to be lowered for the O&Ph analysis. (This difficulty can be reduced by using a higher unload rate during the measurement to reduce the effect of creep).
- For hard/hard the D&N analysis gives strongly deviating E-values; the more reliable O&Ph method should be used.
- Generally there is no reason to use the D&N analysis. Using computer programs O&Ph is as simply applicable as D&N.

Recommendations: see Table 7.4

coating type	O&Ph: fit limits (% of p_{max})	D&N: fit limits (% of p_{max})	% deviation of E(D&N) from E(O&Ph)
s/s	20 ... 80	67 ... 100	≈ 0
s/h	20 ... 100	"	≈ -22
h/h	20 ... 100	"	≈ +20


a)
load P (mN)
260
280
300
320
340
360
380
400
420


b)
340
360
380
400
420
440
460

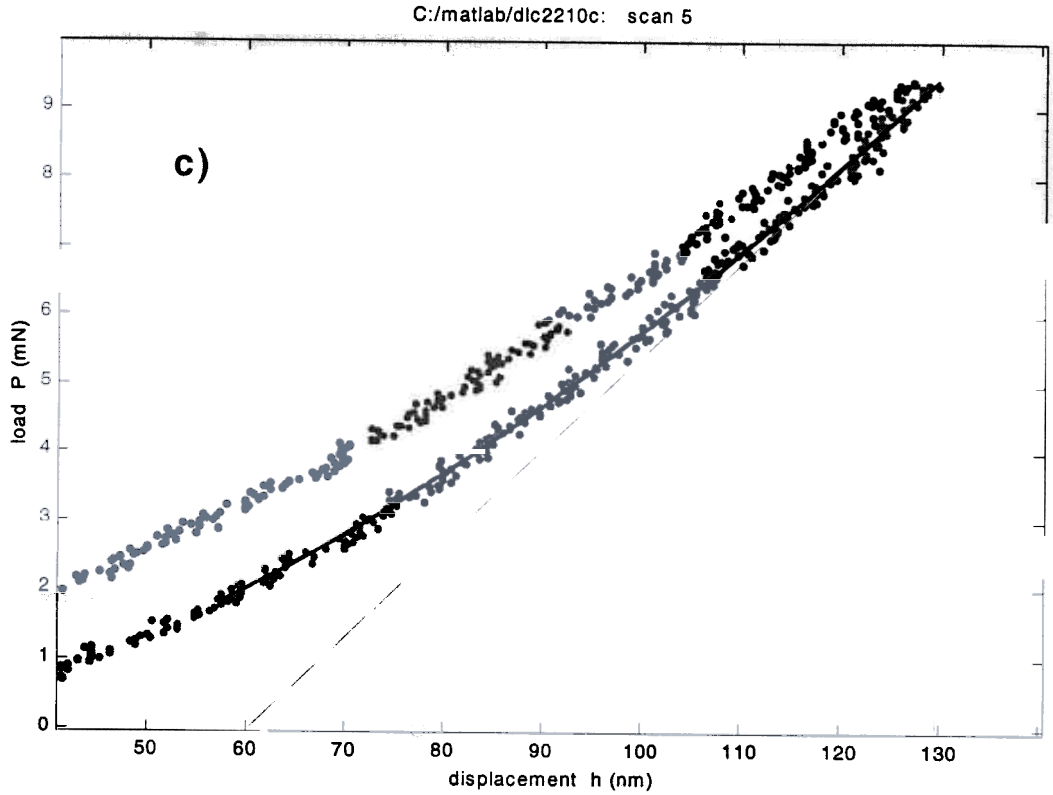


Fig.7.3: Examples of fits of the Oliver & Pharr power law for different coating/substrate combinations:
a) Au/Ni (soft/soft) with creep causing a big distortion of the unload curve; b) Al/Bk7 (soft/hard) with less creep; c) DLC (hard/hard): no creep.

8 MODELLING

8.1 Objectives and approach

The principal objectives of the modelling tasks in the Indicoat Project are :

to use models of indentation behaviour to estimate the properties of the coating material, especially Young's modulus, Poisson's ratio and hardness,

2. to demonstrate by computer modelling that the methodology to be adopted by indentation test methods of measurement are consistent with theoretical principles,

3. to investigate to what extent computer simulation of the nanoindentation behaviour of coatings is in accord with that found by measurement.

While much indentation in practice involves the use of 'sharp' 3D indenters, the modelling work has concentrated on the use of spherical indenters for three important reasons. Firstly, the axisymmetric nature of spherical indentations simplifies the analysis and enables more detailed finite element predictions to be obtained of good accuracy, and in reasonable times. Secondly, the simplified nature of the analysis enables a rigorous examination of the basic principles involved in the interpretation of load-penetration curves. Only if a satisfactory conclusion to axisymmetric modelling studies can be achieved does it make sense to embark on a rigorous examination of 3D indentation that will inevitably be highly elastic-plastic. Thirdly, as one important objective is to attempt an estimation of Young's modulus and Poisson's ratio from load-penetration curves, the use of a spherical indenter of relatively large diameter will delay the onset of plasticity, and lead to the possibility of using the initial elastic response as the basis of the methodology. For these reasons, and because of space limitations the information to be presented in this report concentrates of spherical indentation.

8.2 Elastic modelling

8.2.1 Introduction

The objective of work package WP2.2 is to carry out predictions of indentation behaviour (using semi-empirical, analytical and FEA methods) in order to select the most reliable method(s) that can be used to help with the interpretation of indentation tests in the elastic regime of deformation. All the methods studied except FEA are candidates for becoming the basis of testing standards. The involved nature of FEA methodology means that it is unlikely that FEA methods will be widely used in standards. Their major role in the project is to provide a reliable and accurate yardstick against which the performance of semi-analytical and analytical methods can be measured.

8.2.1.1 Material properties for elastic modelling

The coating systems to be considered in the inter-comparison exercise for elastic response were based on nominal values of coating and substrate properties, and they involved a hard coating of three nominal thicknesses applied to a soft substrate and vice versa.

Hard material

The properties of the selected hard material are assumed to be linear elastic, and are given by

Young's modulus = 200 GPa Poisson's ratio = 0.3

Soft material

The properties of the selected soft material for elastic deformations are:

Young's modulus = 70 GPa Poisson's ratio = 0.33

8.2.1.2 Geometry

Predictions have been made for indentation into coated systems for which the substrate material was assumed to be semi-infinite in extent. If only a finite volume could be modelled (as with FEA packages that do not have infinite elements) then the size was chosen to be large enough for the results to be independent of the substrate thickness and outer radius. The thicknesses of the coating were selected to be 0.2 μm , 0.8 μm and 2 μm. The coated systems were indented by a rigid spherical indenter having a radius of 10 μm.

8.2.2 Types of modelling

Three types of modelling methodology were included in the project, as follows. For each of the categories below, participants were asked to bring their preferred models to the project, and any others thought useful for inclusion in the inter-comparison exercise.

8.2.2.1 Analytical models

Analytical models regard the linear elastic indentation of a coated substrate as a classical mechanics problem where it is vital that the laws of continuum mechanics are obeyed, such as the equilibrium equations, stress-strain relations and compatibility equations. In addition it is vital that solutions should obey the correct boundary conditions. This is especially important for indentation problems where contact area varies with the applied load. Analytical models usually assume linear elastic behaviour, and axisymmetric stress and displacement fields, leading to non-linear load-deflection behaviour arising from the increase of contact area with load. Analytical methods may result in simple analytical formulae that have potential to be used to interpret the results of indentation experiments. Usually simple formulae will result only if some approximations are introduced when solving the classical elasticity equations.

Three types of analytical model have been considered. The first model (used by TUC) [1] develops a methodology that is based on the assumption that the pressure distribution over the contact area is Hertzian in form. The second model (used by VTT) [2] is based on the use of a Green's function technique where a continuous distribution of point forces acts over the contact area. The function defining the distribution of point forces is the unknown function that is solved by integral equation techniques. The third model (used by NPL) [3] is a hybrid technique that involves the use of analytical elasticity methods combined with simple FEA analysis for a flat ended rigid cylindrical punch. From such solutions it is possible to predict the indentation behaviour of any axisymmetric rigid indenter subject to either friction-free contact or to perfect adhesion (the latter case has not been considered here). The attraction of the NPL approach is that there is no need to take account of varying contact area when carrying out the FEA for a rigid cylindrical punch, and that predictions can easily be made for any coating thickness between 0.2 μm and 2 μm, and for *any* axisymmetric indenter geometry.

8.2.2.2 Finite element models

Finite element methods are thought to provide the most reliable and accurate predictions of the stress and displacement fields in the coating and substrate of an indented sample. The method is very likely to be the only technique that can adequately model non-linear

deformations arising from localised plasticity that occurs during indentation. For the inter-comparison of purely elastic deformations, the use of infinitesimal deformation theory was thought to be adequate. Three partners have carried out the FEA of the coating problems. KTH have used ANSYS to predict their results [4]. This FEA system does not have infinite elements and steps were taken by KTH to ensure that their results were independent of the model size. Both JRC and NPL used ABAQUS, together with the use of infinite elements, when carrying out FEA simulations of elastic indentation.

8.2.3 Results

A complete report presenting all the results gathered together from various partners has been written. There is space here only to present some results that are typical of those given in the detailed report.

8.2.3.1 Load/penetration curves

The results given in Figs. 8.1 & 8.2 indicate that for most cases there is very good agreement when the models are used to predict load-penetration.

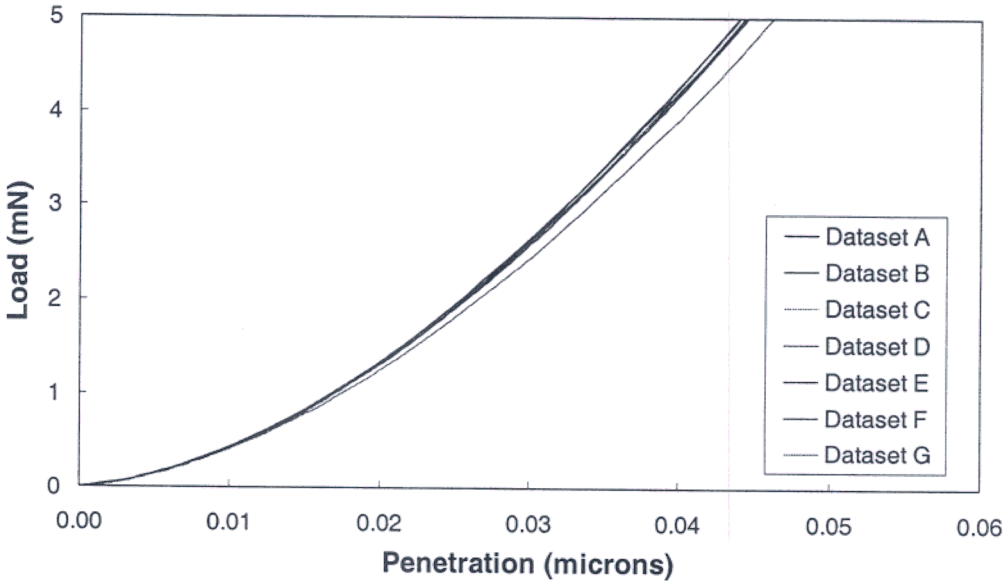


Fig. 8.1 : Comparison of all models: Soft coating (0.8 μm) on hard substrate.

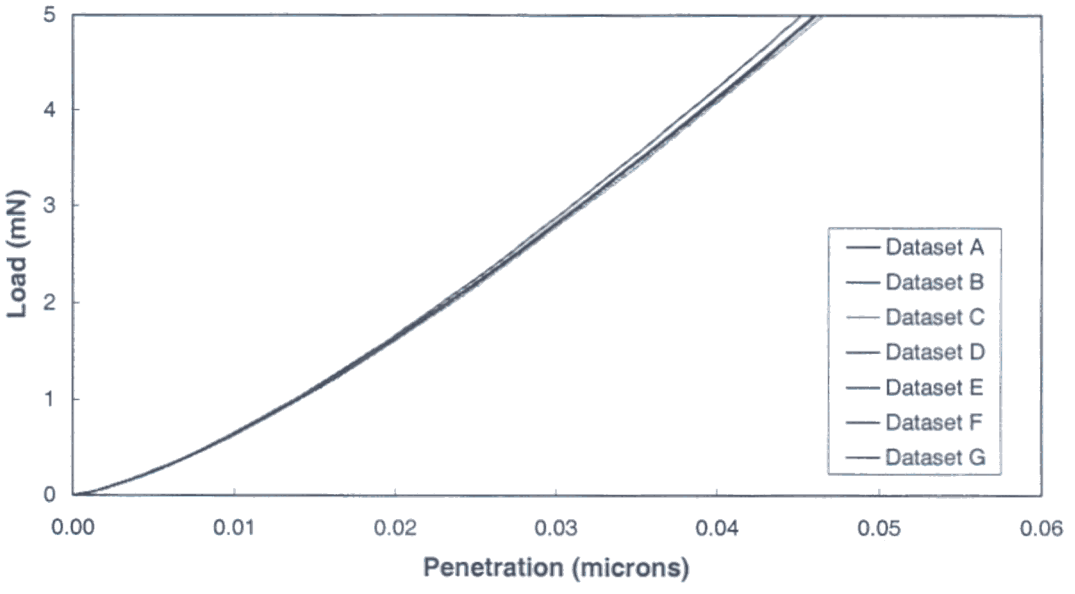


Fig. 8.2 : Comparison of all models: Hard coating (0.8 μm) on soft substrate.

8.2.3.2 Estimation of E_{IT}

For elastic deformations of a monolithic sample of material, the method of estimating the properties of the elastic constants is to use the following exact result (to be referred to as method 1) valid for any axisymmetric rigid indenter in the absence of friction

$$E_{IT}^{*} = \frac{1}{2}\sqrt{\frac{\pi}{A_p}}\left(\frac{dP}{dh}\right), \qquad (1)$$

where E_{IT}^{*} is the effective modulus measured in an indentation test, A_p is the projected contact area, P is the applied load and h is the corresponding penetration. This approach is also used for coated samples but for this case the value of E_{IT} is dependent upon the coating and substrate properties and the coating thickness.

For the Hertz solution, provided the contact radius is very much smaller than the indenter radius R, the value of E_{IT} is given by

$$E_{IT}^{*} = \frac{3P}{4h}\sqrt{\frac{\pi}{A_p}}, \qquad (2)$$

which is a very useful result that avoids having to estimate the derivative dP/dh from load-penetration curves (a procedure that is well known to introduce significant errors if the data is not smooth). The projected contact area (and contact radius) may be approximated by

$$A_p \equiv \pi a^2 = \pi Rh, \qquad (3)$$

which leads to the following expression for E_{IT} that is now independent of the contact area and does not require the estimation of the derivative dP/dh

$$E_{IT}^{*} = \frac{3P}{4h\sqrt{Rh}}. \qquad (4)$$

The result (4), and the approximation (3) for estimating the contact area and radius, will be referred to as method 2. It has been shown using the commercially available system 'Elastica', (developed by TUC), that when E_{IT} (estimated using (1)) is plotted as a function of t_c/a (the ratio of the coating thickness t_c and the contact radius a) a unique curve is obtained that is independent of indenter radius and coating thickness (see Figs.8.3 & 8.4). It has also been shown that the approximate method 2 based on (3) and (4) produces results that are in close agreement with the accurate predictions (see Figs.8.3 & 8.4). It should also be noted that the open symbols predicted by the approximate method 2 are based on the relations (3) and (4) that characterise indentation into homogeneous materials. The values of E_{IT} given by this approximation correspond to the effective reduced modulus of the coating and substrate when they are regarded as being smeared into an equivalent homogeneous medium having properties that will reproduce to a good approximation the load - penetration curves for penetration into the actual coating and substrate system.

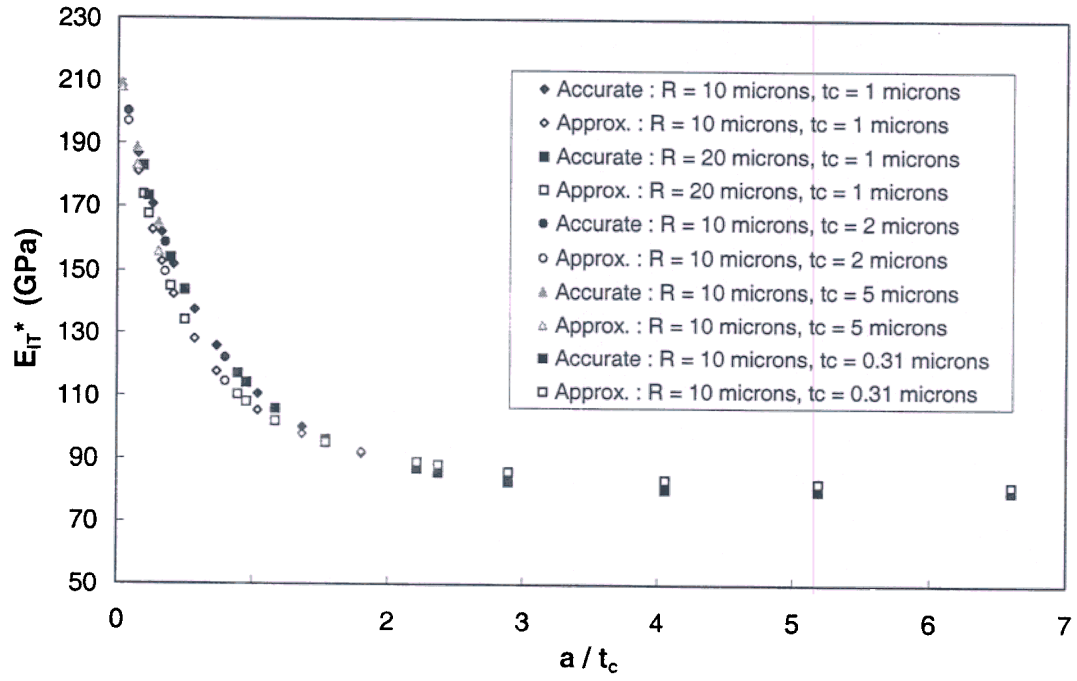


Fig.8.3 : 'Elastica' estimates of E_{IT} for a hard coating on a soft substrate by a rigid spherical indenter.

For the case of the hard coating of thickness 0.31 μm applied to the soft substrate, Fig.8.5 shows the dependence of E_{IT}^* / E_{IT}^{c*} on the ratio t_c/a where E_{IT}^{c*} is the indentation modulus for the coating. The results labelled 'FEA (flat circular punch)' were derived during the development of the hybrid solution technique [5]. The results labelled 'Hybrid-method' have been obtained by applying (1) to the load-penetration data generated by the hybrid model for a spherical indenter of radius 10 μm. It is seen that they correspond almost exactly to the FEA results for a flat circular punch. This is to be expected as, for the case of elastic deformations,

the results when plotted as shown in Fig.8.5 should not depend on the geometry of the axisymmetric indenter. As another example of the geometry independence for axisymmetric indenters, it should be noted that the value of E^*_{IT} should be independent of the radius of the spherical indenter for all values of t_c/a: a property has been confirmed using the hybrid model. This result implies that there is no effect of the shape and elasticity of the indenter, provided that the penetration is measured from the free surface. Experimentally such measurements are not usually possible with the result that corrections to account for the elasticity of the indenter are needed only to compensate for the contribution of the indenter to the penetration measurement. The results labelled 'FEA (sphere) – method 1' are for a rigid spherical indenter of radius 10 μm obtained using the accurate relation (1) for E^*_{IT}, which can only be implemented approximately due to inaccuracies in the estimation of dP/dh, and of the contact area. The corresponding results obtained using the approximate, but easy to use, relations (3) and (4) are denoted by 'FEA (sphere) – method 2'.

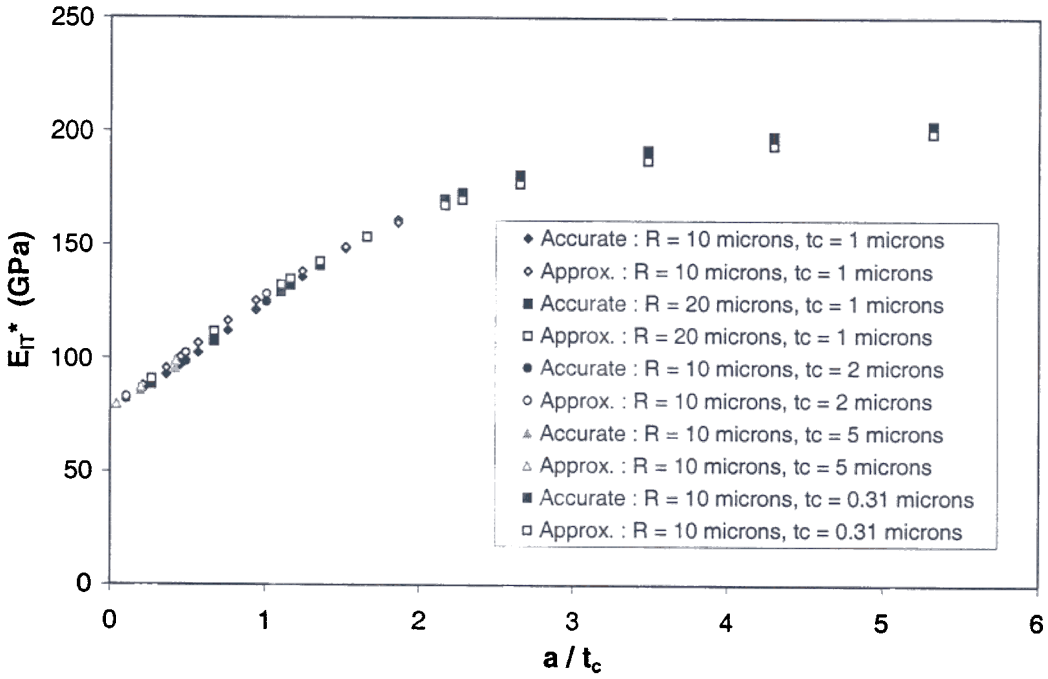


Fig. 8.4 : 'Elastica' estimates of E_{IT} for a soft coating on a hard substrate by a rigid spherical indenter.

From the results presented in Fig.8.5 it is clear that the methodology of the hybrid model is providing very consistent results for the case of elastic deformations as the same values of E^*_{IT} are predicted when using both spherical indenters (of any radius consistent with elastic deformations) and a flat circular punch. This verifies the 'theorem' that all axisymmetrical indenters with monotonic increasing contact radii, which may be described by the hybrid model, should give results lying on the same curve. In addition, the approximate method of estimating E^*_{IT} based on method 2 above leads to results that are in very good agreement with those obtained using the accurate method 1 except for large values of a/t_c which occur when

the coating is very thin or the load is large (where plasticity would also be encountered). The 'Elastica' prediction is also in good agreement although the predicted values appear lower than the other results at large values of a/t_c. The differences are not however, cause for any concern as they are probably due to the solution technique that assumes a specific form for the pressure distribution under the indenter. 'Elastica' has the benefit that it can be used easily for many coating systems (and coating thicknesses) whereas the hybrid model requires the FEA of a flat rigid circular punch for each material system considered.

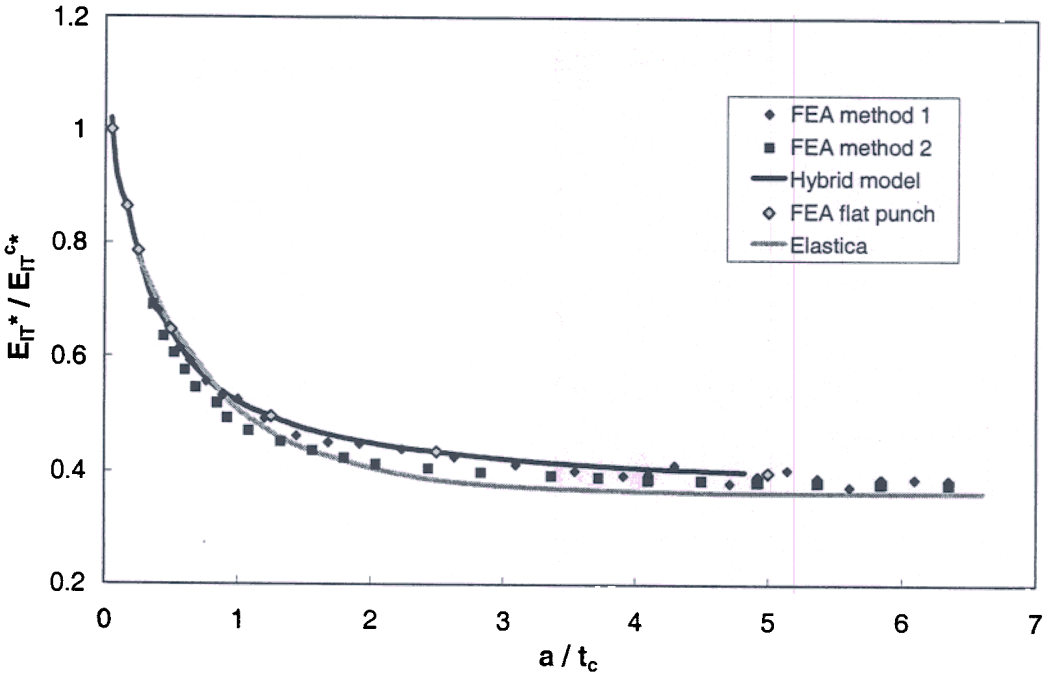


Fig.8.5 : Elastic estimates of E^*_{IT} for a hard coating of thickness 0.31 μm on a soft substrate by rigid indenters.

Figs.8.6 & 8.7 show the results of comparing the predictions of FEA carried out by KTH with the NPL hybrid model (and an approximation), and with the Gao et al model [6] for the case of the hard coating on the soft substrate and vice versa. It is seen that the trends of the FEA results for spherical indenters are, on the whole, in good agreement with the FEA results for the flat circular punch, and the hybrid model. The FEA results for spherical indentation, for the case of a hard coating on a soft substrate, do show a high degree of scatter that arises from the difficulties of estimating the contact area. This problem does not arise for the flat punch data which produce much smoother data. For the case of a soft coating applied to a hard substrate the FEA results for spherical indenters show some scatter and the data agrees very well with the flat punch and hybrid model results. The results of using the Gao et al model do not follow the FEA data nor the hybrid model where the discrepancy is more marked for the case of a soft coating applied to a hard substrate.

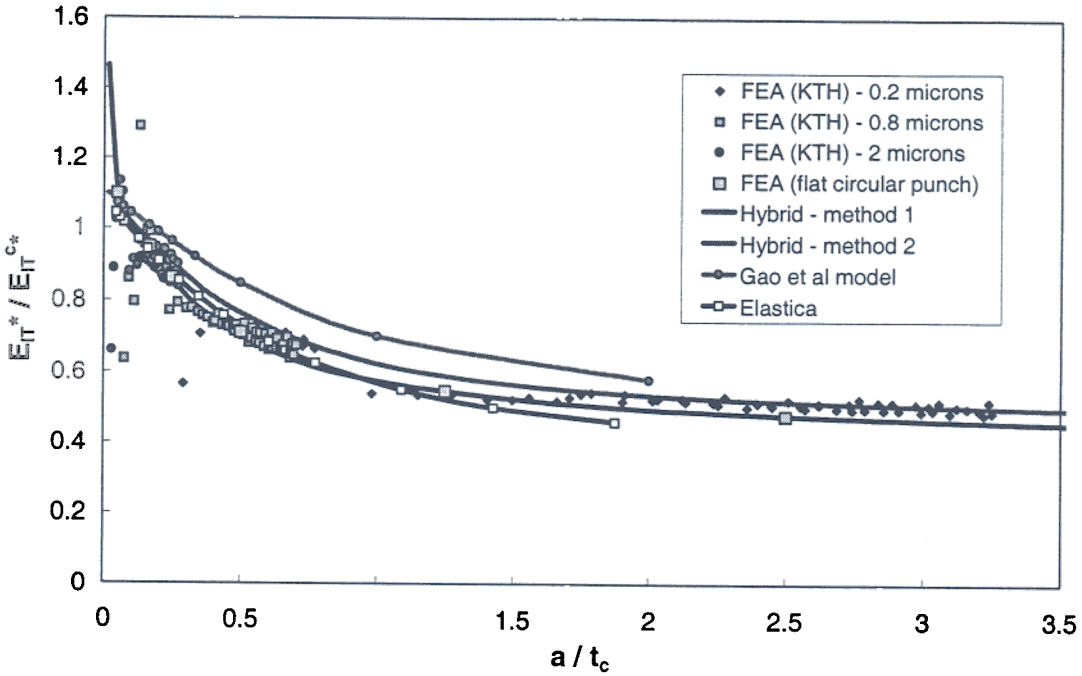


Fig.8.6 : Comparison of elastic estimates of E_{IT} for hard coatings on a soft substrate by rigid indenters.

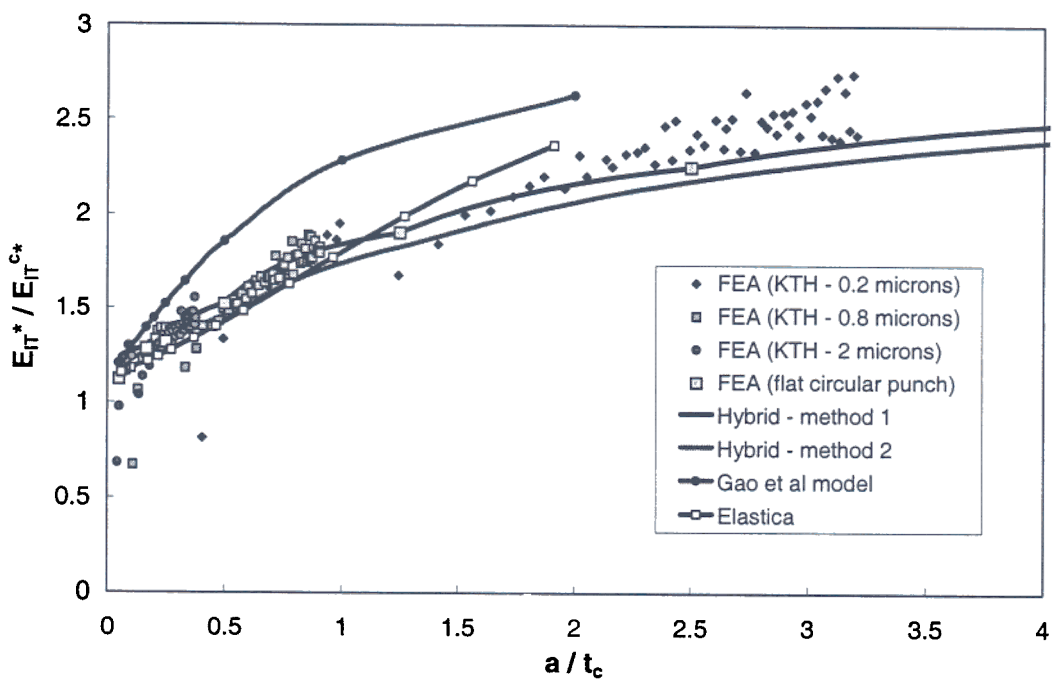


Fig.8.7 : Comparison of elastic estimates of E^*_{IT} for soft coatings on a hard substrate by rigid indenters.

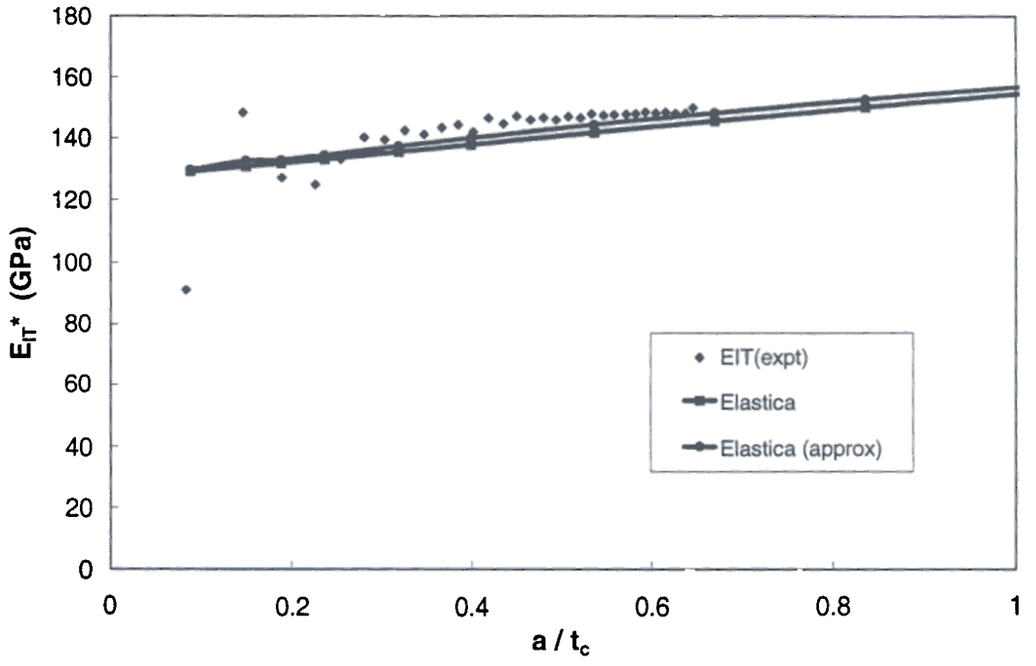


Fig.8.8 : Comparison of experimental results with elastic estimates of E^*_{IT} for a 2 μm DLC coating on M2 toolsteel substrate indented by a rigid spherical indenter of radius 9.5 μm.

In Fig.8.8 is shown the result of comparing 'Elastica' predictions for E^*_{IT} for the case of a 2 μm DLC coating applied to an M2 toolsteel substrate using a spherical indenter of radius 9.5 μm. For the 'Elastica' predictions the indenter has been assumed to be made of diamond rather than being rigid. It is seen that for values of t_c/a in the range $0 \leq t_c / a \leq 5$ there is good agreement between predictions and experimental results. For larger values of t_c/a the experimental data exhibit large variability arising when the applied loads are small.

8.2.4 Conclusions from elastic modelling investigation

1. There is generally good agreement between predictions of load-penetration behaviour based on analytical modelling and the corresponding FEA results for all thicknesses considered, and for both hard coatings on soft substrates and soft coatings on hard substrates. This means that any of the prediction techniques can be used with confidence when predicting the elastic response of the indentation of coating and substrate.
2. The effects of friction, at the low load levels considered for elastic responses, are small.
3. When estimating the indentation modulus E^*_{IT} very good agreement between the FEA analyses, 'Elastica' and the hybrid model is achieved for a wide range of properties, coating thicknesses and axisymmetric indenters (spheres of various radii and flat circular punches). 'Elastica' offers a very practical and convenient way of predicting E_{IT} for coated systems.

4. When estimating E_{IT}^{*} for a coated system it is found that the predictions obtained based on the use of FEA, 'Elastica' and the hybrid model differ from those of the Gao et al model [6] except when $t_c / a \rightarrow 0$ and $t_c / a \rightarrow \infty$. The discrepancy between the Gao et al model and the hybrid model is thought to arise from a basic inaccuracy of the Gao et al model.
5. The validity of the Gao et al model [6] at large values of t_c / a means that it should be possible to unravel both E and Poisson's ratio from the results of indentation tests by making use of thick coatings and applying low loads. This approach is consistent with the use of large indenter radii and low loads that avoid plasticity so that the results of elastic modelling are applicable. The 'Elastica' model can be used to estimate coating Young's modulus only if the coating Poisson's ratio is already known, and vice versa.

8.3 2D elastic/plastic FE solutions

8.3.1 Introduction

The objective of this work package is to investigate the effects of plasticity on the indentation of coated samples by a spherical indenter. The only feasible method of modelling plasticity is to make use of FEA simulations of behaviour. Key issues are: i) intercomparison of predictions by partners using FEA, ii) the interpretation of the data in order to extract elastic properties such as Young's modulus and Poisson's ratio of the coating, and iii) the effects of coating/substrate combinations on hardness.

8.3.1.2 Material properties

When modelling the elastic response of coatings and substrates, it is assumed that the materials are isotropic so that their elastic properties are fully characterised by values of the Young's modulus E and Poisson's ratio ν such that the elastic strain ε_{ij}^{E} is the following linear function of the stress tensor σ_{ij}

$$\varepsilon_{ij}^{E} = \frac{1}{E}\left[(1+\nu)\sigma_{ij} - \nu\sigma_{kk}\delta_{ij} \right] \tag{5}$$

When modelling the inelastic response of a metallic phase, it is assumed that the accumulated effective plastic strain $\bar{\varepsilon}_P$ during monotonic loading is related to the effective stress $\bar{\sigma}$ as follows :

$$\bar{\varepsilon}_P = \varepsilon_0 \left(\frac{\bar{\sigma}}{\sigma_Y} - 1 \right) \quad \text{for } \sigma \geq \sigma_Y , \qquad \text{otherwise } \bar{\varepsilon}_P = 0 \tag{6}$$

Here σ_Y denotes the uniaxial yield stress and the effective stress $\bar{\sigma}$ is defined by

$$\bar{\sigma} = \sqrt{\frac{3}{2}\,\hat{\sigma}_{ij}\,\hat{\sigma}_{ij}} \ , \tag{7}$$

where $\hat{\sigma}_{ij}$ is the deviatoric stress defined by

$$\hat{\sigma}_{ij} = \sigma_{ij} - \frac{1}{3}\,\sigma_{kk}\,\delta_{ij} \ . \tag{8}$$

The quantity $\bar{\varepsilon}_P$ is the accumulated effective plastic strain during monotonic loading calculated from the incremental relation

8.3.1.4 Indenter tip geometry

Spherical indenters have been considered having a radius of 10 μm. Where conical, Berkovich and other sharp indenters are investigated, it was suggested that the indenter tip could be taken as a sphere having radius 1 μm. Model predictions were, in the first instance, carried out for a rigid indenter. Elastic/plastic solutions used finite deformation theory.

8.3.1.5 Maximum loads

The maximum loads for each FEA simulation correspond to one of the maximum loads specified by the INDICOAT Experimental Matrix which are given in Table 1. For FEA simulations the loading stage was always followed by an unloading stage to zero load.

Maximum Load [mN]							No. Expts. per thickness
0.1	0.3	1.0	3.0	10.0	30.0	100.0	
(Soft)							2
	(Soft)	Soft		(All)			8
		All					4
		Soft	All	All		Hard	12
				All			4
		(Soft)		All	Hard	Hard	10
						Hard	2
		(Soft)		(All)		Hard	8

"Soft" = Soft coatings only "Hard" = Hard coatings only "All" = All coatings

Table 1 : Maximum loads use for modelling and experiments

8.3.2 Results of 2D elastic-plastic analyses

In Fig.8.9 is shown one example of FEA predictions of load-penetration behaviour for a 10 μm radius spherical indenter into a 2.1 μm DLC coatings on an M2 steel substrate (a hard-on-hard combination). Results indicate that the predictions of JRC, KTH and NPL are in good agreement.

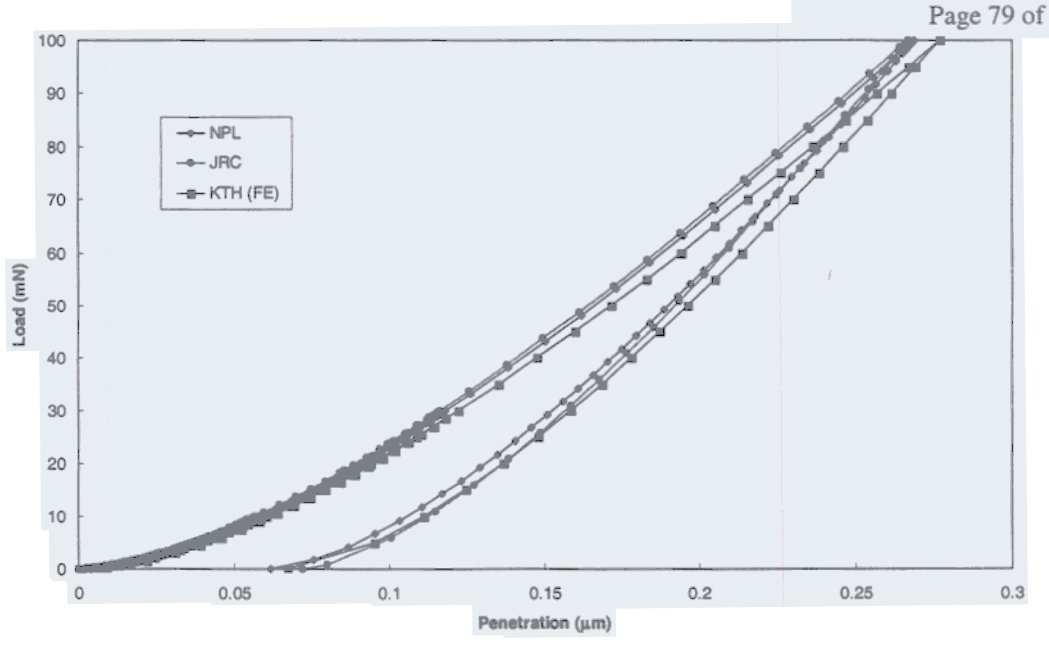


Fig.8.9 : 2.1µm DLC coating on an M2 toolsteel substrate

The load-penetration results of the elastic-plastic FEA predictions for various coating systems and maximum loads (including unloading to zero load) have been analysed in exactly the same way as would experimental data. This was achieved by modifying the software used at NPL to analyse experimental load-penetration data. The methodology for interpreting the results corresponds to that developed by Oliver and Pharr [7] providing an estimate of the reduced elastic modulus $E_{IT}^* = E / (1 - \nu^2)$. The fact that the Oliver and Pharr method involves estimating the gradient of the unloading part of the load-penetration data means that the unloading predictions by FEA should be as accurate as possible. As the NPL FEA results were readily available for analysis, they have been used as the basis of the following analysis. It is emphasised that when estimating the gradient of the unloading curve the procedure followed was to fit a curve to the simulation data and then to differentiate the fitted curve in order to estimate the gradient of the data. Table 2 shows the results for three coating thicknesses where DLC has been deposited on an M2 steel substrate. The Oliver and Pharr method estimate of E_{IT} is again much greater than the coating value with the difference increasing as the maximum load is increased. All the results in Table 2.4.4 lie between the values of E_{IT} for coating and substrate: 142.708 GPa and 240.856 GPa respectively although this was not always the case. The result (bold italics) for the case of a maximum load of 3 mN and coating thickness 2.1 µm does not follow the trend of the other results. This result has been checked and no explanation for this phenomenon has been found.

Coating thickness (microns)	Max. load (mN)	E^*_{IT} for coating (GPa)	E^*_{IT} Oliver & Pharr	Unloading Hardness (GPa)	Contact radius (microns)
0.28	1	142.71	191.272	2.65	0.3463
	3	142.71	201.342	3.99	0.4894
	10	142.71	211.729	6.05	0.7256
	30	142.71	218.619	7.68	1.1149
	100	142.71	227.905	9.04	1.8763
1.3	1	142.71	171.604	2.66	0.3374
	3	142.71	174.712	3.75	0.5046
	10	142.71	181.390	5.64	0.7516
	30	142.71	192.366	8.05	1.0894
	100	142.71	219.382	9.14	1.8664
2.1	1	142.71	169.534	2.55	0.3531
	3	142.71	***166.505***	3.70	0.5083
	10	142.71	170.535	5.49	0.7617
	30	142.71	177.428	7.92	1.0978
	100	142.71	190.983	10.16	1.7698

Coating $E_c = 137$ GPa, $\nu_c = 0.2$. Substrate : $E_s = 220.6$ GPa, $\nu_s = 0.29$

Table 2 : DLC coating on a M2 steel substrate.

In order to check the Oliver and Pharr methodology for the case of indentation into a homogeneous material, predictions and analysis have been carried out for the case of nickel. Table 3 shows that the Oliver and Pharr predictions over-estimate the E^*_{IT} value, with the over-estimate increasing with the maximum load applied before unloading. This is the same trend that was observed for indentation into coated samples, and is thought to arise because of the significant effects of plastic deformation.

Max. load (mN)	E^*_{IT} for nickel (GPa)	E^*_{IT} Oliver&Pharr (GPa)	Unloading Hardness (GPa)	Contact radius (microns)
1	243.38976	252.689	1.66	0.43841470
100	243.38976	299.225	2.80	3.37362870

Substrate : $E_s = 220$ GPa, $\nu_s = 0.306$

Table 3 : Homogeneous nickel substrate.

8.3.3 Hardness results

The FEA simulations were for a spherical indenter. Although H_{IT} may be calculated for the results according to the definition:

$$H_{IT} = P / A_p \qquad (12)$$

where P is the applied load and A_p is the contact area. The values obtained will be a function of indentation depth.

8.3.4 Direct comparison of NPL and KTH predictions of E^*_{IT} and H_{IT}

In order to investigate further the integrity of the elastic-plastic FEA results, when attempting to predict values for the effective modulus E^*_{IT} and the hardness H_{IT}, the results from NPL (almost identical to those of JRC) and KTH have been compared. Following the approach of KTH, the results for E^*_{IT} and H_{IT} are plotted against penetration depth/coating thickness. The NPL results were on the whole numerically larger than the KTH results, and this is in part due to differing definitions of the contact area A_c used by the two institutions. NPL has used the same methodology as would be used by the Oliver & Pharr method of analysing experimental data. KTH have used the contact area predicted directly by the FEA. A correction procedure for contact area has been applied to the effective modulus and hardness results for a gold coating on a nickel substrate. The effect on hardness of modifying the contact area is shown in Fig.8.10, where it is seen that the KTH and NPL results cluster together after the correction has been made. The corresponding correction to the effective modulus is shown in Fig.8.11 where again it is seen that there is much better agreement between the KTH and NPL results when using the same definition of contact area.

The main conclusion is that the FEA models of elastic-plastic indentation obtained do not simulate unloading responses that are well described by the Oliver and Pharr analysis. However, different FEA models agree once a common definition of contact area is used.

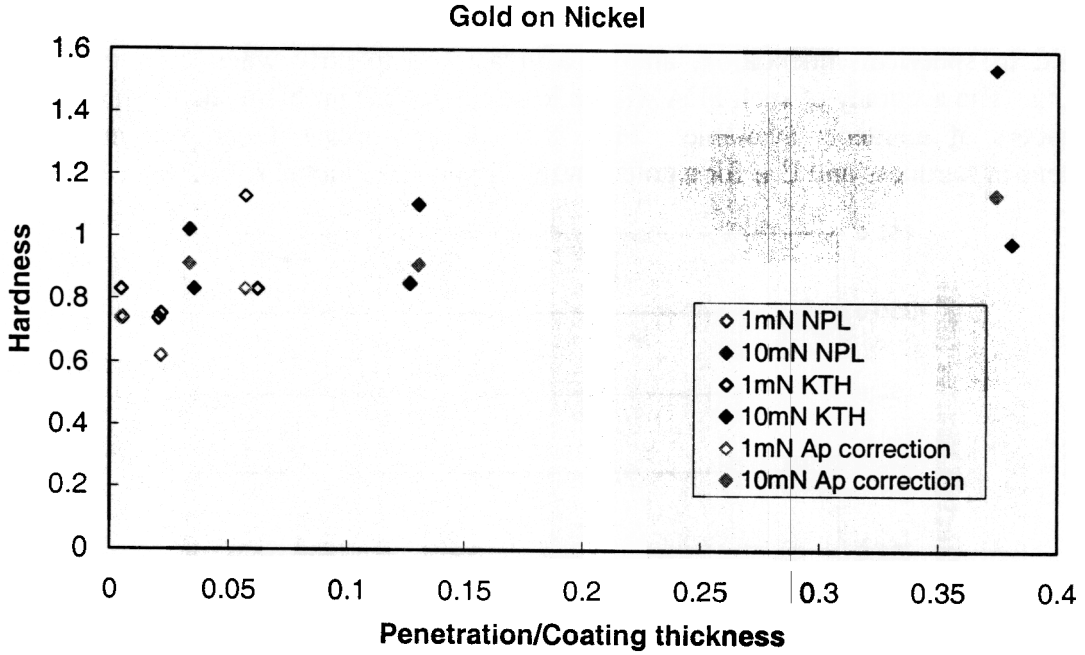


Fig.8.10 : Predicted values of H for the gold on nickel system by NPL and KTH, and the 'corrected' NPL values.

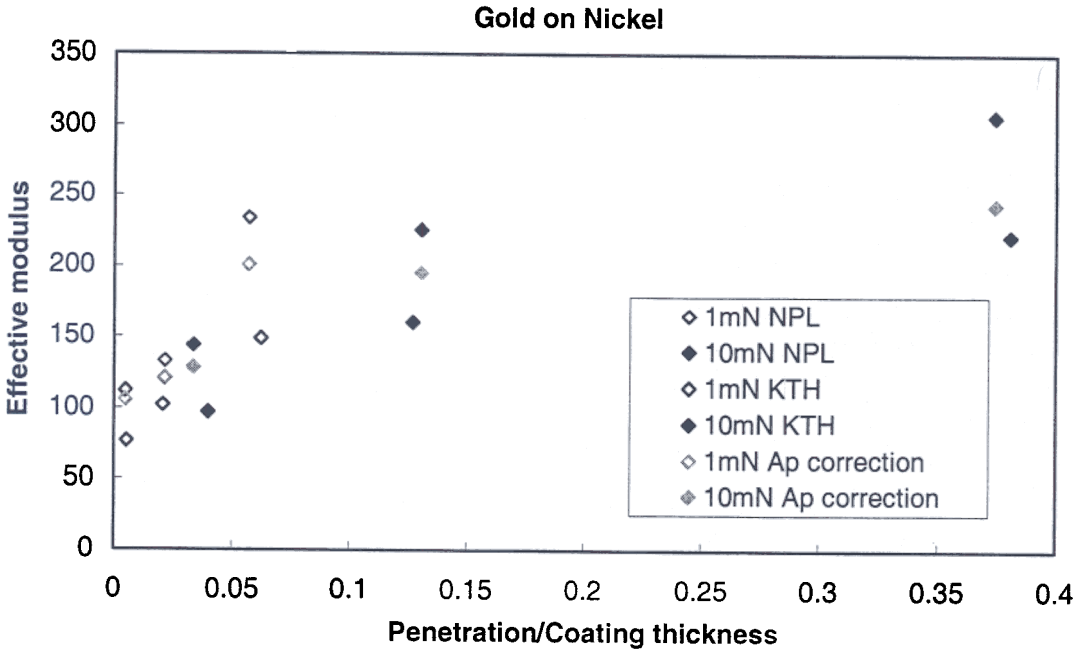


Fig.8.11 : Predicted values of E_{IT}^{*} for the gold on nickel system by NPL and KTH, and the 'corrected' NPL values. $E_{IT}^{c*} = 97.59\ GPa$, $E_{IT}^{s*} = 242.73\ GPa$

3D indentation

In practice, it is non-axisymmetric indenters that are most often used to measure load-penetration response of coated systems, leading on to a greater degree of plasticity when compared to spherical indentation, and to a greater complexity when carrying out FEA modelling. The accuracy of such FEA will be less than for 2D problems due to limitations on the numbers of elements available. Figs. 8.12 & 8.13 show a comparison (KTH) of predictions of hardness and E^{*}_{IT} for a gold coating applied to a nickel substrate.

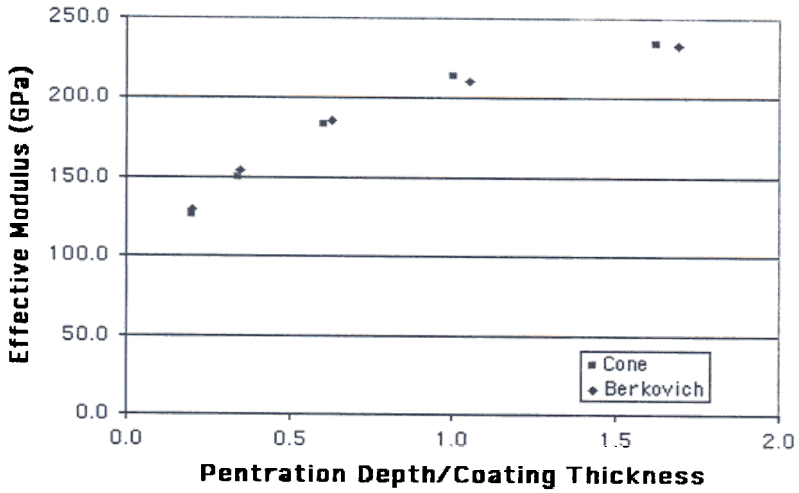


Fig.8.12 : Relationship between effective modulus and ratio of penetration to coating thickness for a gold coating on a nickel substrate.

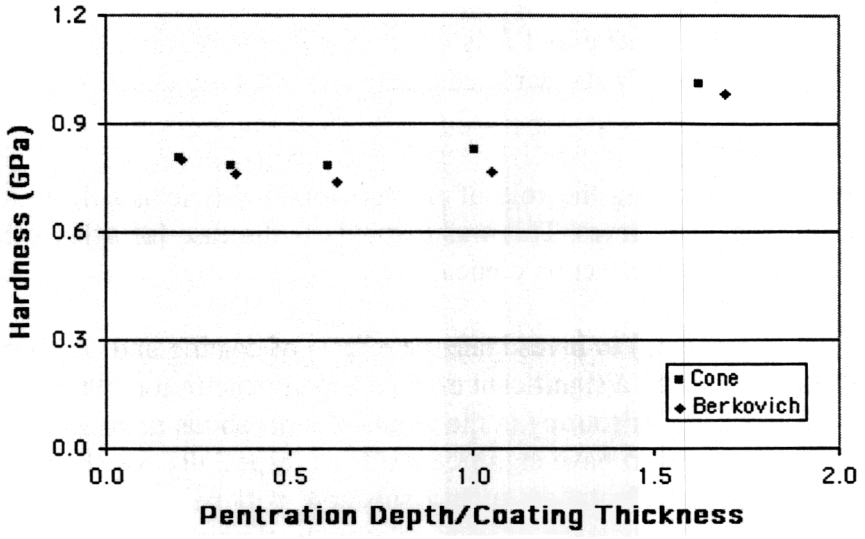


Fig. 8.13 : Relationship between hardness and ratio of penetration to coating thickness for a gold coating applied to a nickel substrate.

8.3.5 Conclusions regarding elastic-plastic modelling

1. Use of the Oliver and Pharr method to estimate the value of E^*_{IT} for a coating from unloading load-penetration data generated by FEA, generally does not return the input values of the model.
2. More accurate predictions arise when using elastic analysis methods on purely elastic deformations. This suggests that large radius spherical indenters should be used within the elastic limit when obtaining experimental modulus data.
3. The Gao et al analysis for the elastic penetration of a coated substrate by a flat cylindrical indenter has been shown to be too inaccurate for use in the procedure to extract values of Young's modulus and Poisson's ratio from two values of E^*_{IT} obtained from the same coating/substrate system.
4. The elastic-plastic results of load-penetration during loading and unloading for spherical indenters, analysed on the basis of Hertz theory, lead to remarkable linear plots when load is plotted as a function of $h^{3/2}$ and $(h-h_o)^{3/2}$. The approximate method of analysis to predict E^*_{IT} (method 2) has been shown to be very sensitive technique for indicating significant differences in FEA predictions which appear to be very close when observing load penetration behaviour.
5. Comparison of the three-dimensional Berkovich model and the two-dimensional cone model of various coating systems has shown that there is a relatively small difference (<10%) between the results from the two models. The results for the effective modulus and hardness indicate very similar results for both the conical and Berkovich indenters.
6. Reliable predictions of both 2D and 3D FEA models are possible only if the appropriate elastic-plastic material properties are known. The identification of this data is

exceedingly difficult to achieve and it is concluded that FEA modelling will not in the near future be the basis of any standardised method of measuring coating properties.

8.3.6 Other conclusions

1. Modelling work investigating the role of friction found that it usually has a negligible effect on load-penetration curves. This was particularly the case for spherical indentation. Friction will have a greater effect on conical indenter geometries, affecting hardness more than E^*_{IT}.
2. Modelling (elastic case only) to investigate the effects of coating and substrate anisotropy has shown that there will be a significant effect on load-penetration behaviour. Substrate anisotropy, resulting from anisotropy in the grains of amorphous microstructures were not modelled but are expected to have significant effects, especially for sharp indenters. At large distances from the indentation such a substrate will behave isotropically. When investigating the effect of indenter rotation relative to the axes of material orientation, there is little effect when the coating is nearly isotropic in the plane of the coating, and highly anisotropic in a direction normal to the free surface. There is a strong effect if the coating is anisotropic in the plane of the coating.
3. Modelling to investigate the roughness of the coating surface has concluded that there are two limiting situations. When the 'wavelength' of the coating surface roughness (modelled as axisymmetric) is much greater than the indenter tip radius, the load-penetration response is determined by the local coating surface curvature, but when the wavelength is much less than the tip radius, the effect is similar to having an additional low modulus coating. In the case where the wavelength is comparable with the tip radius, the load-penetration curve may only be found by detailed simulation.

References

1. N Schwartzer, F. Richter & G Hecht, 'Elastic field in a coated half-space under Hertzian pressure distribution', Surface and Coatings Technology , **114**, (1999), 292-304.
2. D Stone, J. Mater. Res., **13**, (1998), 3207-3213.
3. R.A. Hunt, C. Pierse & L. N. McCartney, 'A theoretical approach to the indentation of layered materials', NPL Report CMMT(A)71, October 1998.
4. Z. Xu & D. J. Rowcliffe, 'Comparison of FEA and semi-empirical model for indentation in coatings', Report on work for WP 2.2, 1999.
5. L N McCartney, 'Indentation for a coated half-space', Technical note, May 1999.
6. H Gao, C-H Chui & J Lee, 'Elastic contact versus indentation modelling of multi-layered materials', Int. J. Solids Structures, **29**, (1992), 2471-2492.
7. W C Oliver and G M Pharr, 'An improved technique for determining hardness and elastic modulus using load and displacement indentation experiments', J Materials Research, **7**, (1992), 1564-1583.

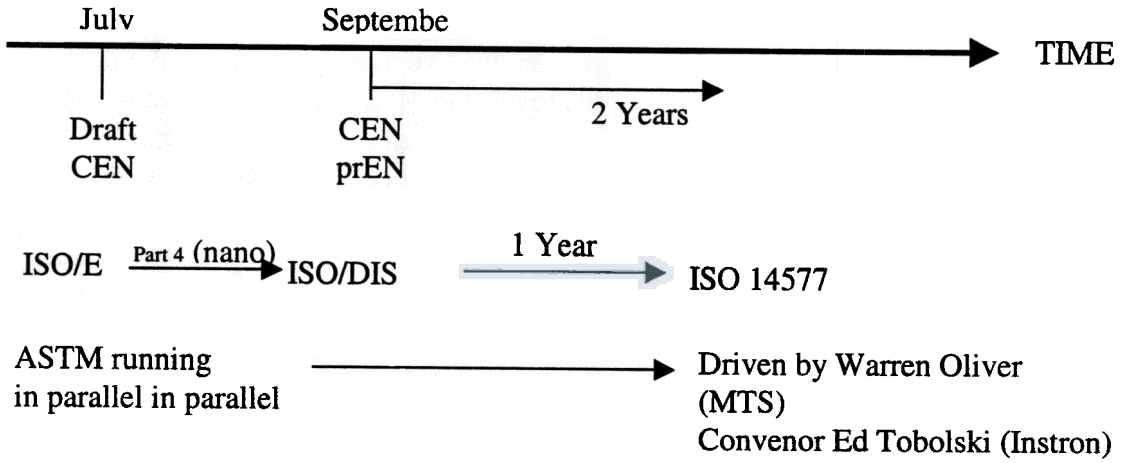
Technology Implementation Plan

Standardisation

Work Item (WI) 152 "Determination of Hardness and Young's Modulus by Depth Sensing Indentation" on European Standards Committee CEN TC184 WG5 has been thoroughly revised by incorporating the results and ideas from the INDICOAT project (May 2001). Further input will be provided by NPL and TUC to produce a technically correct version by July 2001. After that, final editorial changes can be made to meet the next deadline stage 49 (public enquiry) which is on the 31 October 2001.

Furthermore, it was discussed during the final project meeting of INDICOAT, that the CEN document will be wholly complementary to the ISO/DIS 14577-1.2,-2.2,-3.2: Metallic materials - Instrumented indentation test for hardness and materials parameters – Part 1: test Method, Part 2: Verification and calibration of testing machines, Part 3: Calibration of reference blocks, which deals with the entire range of macro- to micro- to nanoindentation experiments for bulk materials. Therefore, it is very likely that the Standards Committee ISO TC164 SC3, with NPL and PTB as INDICOAT representatives, which is preparing this Standard will use the CEN document to supplement the ISO Standard. This will be discussed at their next meeting in September 2001, when the final version of the CEN document will be available.

A timeline illustrating the standardisation procedure is shown below:



The following people will be used as contacts for dissemination of the Indicoat results:

A. Cavaleiro		CEN TC184/WG5
J. Meneve	ISO/TC107/SC2	CEN TC184/WG5
N.Jennett / S. Saunders	ISO/TC164/SC3	CEN TC184/WG5
K.Herrmann	ISO/TC107/SC2	CEN TC262
B.Bellaton	ISO/TC164/SC3	ASTM(G8)

Scientific dissemination

INDICOAT partners will benefit, from a scientific viewpoint, by an increased understanding of depth sensing indentation processes, which will be reflected in an increased number of scientific publications in the subject field, often written in collaboration with other Indicoat partners.

One paper that is already published is:

- K. Hermann, N.M. Jennett, W. Wegener, J. Meneve, K. Hasche and R. Seemann, 'Progress in determination of the area function of indenters used for nanoindentation', Thin Solid Films, 377-378 (2000) 394.

Two other presentations/publications that are underway are:

K. Herrmann, N. M. Jennett , J. Meneve, F. Pohlenz, 'Elaboration of a standard on testing of thin coatings with the nanoindentation method'.

J. Meneve , T. Chudoba , W. Wegener, S. Kuypers, N. Gibson and N. Jennett, 'Uncertainties in determining the zero of the depth scale in nanoindentation experiments using an initial contact load prior to indentation'.

Both will be presented at the 2nd European Symposium on Nanomechanical Testing in Hückelhoven, Germany, 25 – 27 September 2001.

Contract research

INDICOAT partners have also gained considerable confidence in measuring the mechanical properties of coatings which will assist greatly in providing measurement services to EU companies. The additional know-how obtained in the INDICOAT project will lead to a more efficient carrying out of depth sensing indentation measurements and processing of the data. For example, to date a time-consuming normalisation procedure was used to deal with indenter tip uncertainties. Instead, it will now use the two reference material method to determine the area function of our indenters. Moreover, the Matlab® codes developed in the project will facilitate the post facto processing of the data. As a consequence, it is expected that the volume of DSI measurements serviced to industry will increase by at least 30% in the next 2 years. This will also lead to a more reliable quality of the products of our customers.

Other exploration aspects

- The commercialisation of the developed computer codes, (VITO, NPL), is another possible exploitation route of the INDICOAT project. This was discussed at the INDICOAT final project meeting, however, and it is thought improbable that manufacturers of nanoindentation instruments would be interested as these usually develop their own codes tailored to the requirements of their instrument and company style. Offering the codes independently to users of nanoindentation would be an alternative but this would require the continuous support to such users if the code would be offered on a commercial basis, which in turn would require a very high customer interest which is considered doubtful in view of the still rather small world of nanoindentation. A shareware version, e.g. to support standardisation, is believed to be not successful since users probably would question the quality of the code, especially when there is no support. Furthermore there is the issue of incompatibility with the data

format of different instruments. Hence this is still considered to be a possible exploitation route but it is at present unclear how it can be achieved.

VITO, NPL and PTB are participating in the new project DESIRED (Contract G6RD-CT2000-00418), that assesses the feasibility of reference materials for the nanoindentation method. The new knowledge in the field of nanoindentation gained in the INDICOAT project represents an added value as to the increased chances for a successful completion of the DESIRED project.

Appendix 1 List of Publications

K. Hermann, N.M. Jennett, W. Wegener, J. Meneve, K. Hasche and R. Seemann, 'Progress in determination of the area function of indenters used for nanoindentation', Thin Solid Films, 377-378 (2000) 394

K. Herrmann, N. M. Jennett , J. Meneve, F. Pohlenz, 'Elaboration of a standard on testing of thin coatings with the nanoindentation method', 2nd European Symposium on Nanomechanical Testing in Hückelhoven, Germany, 25 – 27 September 2001.

J. Meneve , T. Chudoba , W. Wegener, S. Kuypers, N. Gibson and N. Jennett, 'Uncertainties in determining the zero of the depth scale in nanoindentation experiments using an initial contact load prior to indentation', 2nd European Symposium on Nanomechanical Testing in Hückelhoven, Germany, 25 – 27 September 2001.

N Jennett, "Depth Sensing Indentation of Thin Hard Film", Proc. of Materials Research Society PA, USA Spring 1998.

A J Bushby, N M Jennett, "Determining the area function of spherical indenters for nanoindentation", Conference proceedings: Proceedings of MRS Symposium Q, Boston Fall 2000.

D. Summa, P.N.Gibson, N. Jennett, R. Vitali and C. Lenardi, "FE simulations of nanoindentation measurements on thin films using perfect and blunt Berkovich tips", ABAQUS Users' Conference, 2001.

K. Herrmann, N. M. Jennett , S. R. J. Saunders, J. Meneve, F. Pohlenz "Development of a standard on hardness and Young's modulus testing of thin coatings by nanoindentation" Abstract for 2nd European Symposium on nanomechanical testing in Hückelhoven, 25 – 27, September, 2001

K. Hasche, K. Herrmann, W. Mirandé, R. Seemann, Th. Ahbe, H. Büchner: Technisches Messen "About Several Calibrated Scanning Force Microscopes in the PTB" (in German) 67 (2000) 7 – 8, 306 – 312

K. Herrmann, R. Seemann, F. Pohlenz "Metrological Problems during Hardness Measurements of Thin Layers" (in German), Materialprüfung 42 (2000) 7 – 8, 287 – 291

K. Herrmann, K. Hasche, F. Pohlenz, R. Seemann "Accuracy raise of micro- and nanohardness measurements by determination of the indenter geometry with a scanning force microscope" Proc. 4th Seminar on Quantitative Microscopy QM 2000, January 12th - 14th, 2000, Semmering, Austria, PTB-F-39, Braunschweig, January 2000, 132 – 138

Appendix 2 Guidelines for Use of the Test Method

Advanced technical ceramics - Methods of test for ceramic coatings - Part X: Determination of hardness and Young's modulus by depth sensing Instrumented indentation testing
(WI 152)

1 SCOPE

1.1 This part of the draft ENV describes a method of measuring hardness and Young's modulus of ceramic coatings by means of depth sensing indentation testing (DSIIIT) using instruments capable of measuring force and displacement as a function of time during the indentation process. This class of instruments includes instruments previously known as "Depth Sensing Indenters, DSI" and/or "Mechanical Microprobes."

1.2 The method is limited to the examination of single layers when the indentation is carried out normal to the test piece surface, but graded and multi-layer coatings may also be measured in cross-section if the thickness of the individual layers or gradations is greater than the spatial resolution of the indentation process. The latter is dependent upon instrument design and is determined by the displacement sensitivity and the precision of location of the indents.

1.3 ISO 14577 Parts 1-3 are being drafted which cover DSIIIT (instrumented indentation testing) for the entire range from macro through micro to nano indentation experiments for bulk materials. The procedures detailed in Annex A complement those in the ISO standards, but place more emphasis on the nano/micro range applicable to thin coatings.

2 REFERENCES

This European pre-standard incorporates by dated or undated reference, provisions from other publications. These normative references are cited at appropriate places in the text and the publications are listed thereafter. For dated references, subsequent amendments to or revisions of any of these publications apply to this European pre-standard only when incorporated in it by amendment or revision. For dated and undated references, the latest edition of the publication referred to applies.

EN ISO 17025: General criteria for operation of testing laboratories.

ENV 623-4: Advanced technical ceramics - Monolithic ceramics - General and textural properties - Part 4: Determination of surface roughness.

ENV 843-4 Advanced technical ceramics - Monolithic ceramics - Mechanical properties

at room temperature, Part 4: Vickers, Knoop and Rockwell superficial hardness.

ASTM D-1474 Indentation Hardness of Organic Coatings

BS 5411 Pt 6 Metallic and Related Coatings, Part 6 Vickers and Knoop Microhardness Tests

ASTM B578-87 Microhardness Testing of Electroplated Coatings (reapproved 1993)

ISO/DIS 14577-1 Instrumented Indentation Test for Hardness and Materials Parameters - Part 1: Test Method

ISO/DIS 14577-2 Instrumented Indentation Test for Hardness and Materials Parameters - Part 2: Verification and Calibration of Test Machines

ISO/DIS 14577-3 Instrumented Indentation Test for Hardness and Materials Parameters - Part 3: Calibration of Reference Blocks

ISO Guide to the Expression of Uncertainty in Measurement (GUM)

3 DEFINITIONS

See Annex A

4 SIGNIFICANCE AND USE

4.1 Instrumented indentation (e.g. using depth sensing instrumented instruments) is becoming an increasingly widespread method of investigating surface properties of bulk as well as coated materials. Unfortunately currently no standard currently exists to define usage of the method for bulk materials, so that the definitions, operating principles and calibration of the instruments used is described in Annex A. An ISO standard 14577 Parts 1-3 is being drafted which when complete may be suitable for this purpose.

4.2 The hardness and Young's modulus of a coating are critical factors determining the performance of the product. Indeed many coatings are specifically developed to provide wear resistance that is usually conferred by their high hardness. Also measurement of coating hardness is often used as a quality control check. Young's modulus becomes important when calculation of the stress in a coating is required in the design of coated components. For example, the extent to which coated components can withstand external applied loads is an important property in the application of any coated system.

4.3 While it is relatively straightforward to determine the hardness and Young's modulus of bulk materials using depth sensing instrumented indentation, However, when measurements are made normal to the coated surface, depending on the load applied and the

thickness of the coating, the substrate properties can alter the result. Therefore, the purpose of this ENV, is to provide guidelines for conditions where there is no significant influence of the substrate, and, where such influence is detected, to suggest possible analytical methods to enable the coating properties to be extracted from the composite measurement. In some cases where the coatings are thick enough, the coating property can be determined directly from measurements on a cross-section.

4.4 It must also be borne in mind that coatings can display a high degree of anisotropy, and thus the orientation of the indenter within the plane and the direction of indentation (plan or cross-section) can potentially significantly alter the experimentally observed value of hardness and or modulus.

5 PRINCIPLE

5.1 Depth sensing Instrumented indentation allows the direct measurement of hardness and Young's modulus from indentation experiments where the indentation process is continuously monitored with respect to force and displacement and time. The experiments may be performed under force or displacement control. A schematic diagram of typical equipment is shown in Figure 1. The principles of these instruments are described in detail in Annex A, section A2.

6 TEST PARAMETERS

6.1 The specific test parameters include:

a) loading rate of force increase
b) unloading rate of force decrease
c) maximum force
d) maximum displacement
e) hold times referenced to the load force displacement cycle
f) indenter geometry and indenter area function
g) instrument frame compliance (stiffness)
h) distance between indents

6.2 The coating/substrate specific parameters include:

a) substrate hardness, Young's modulus and Poisson's ratio
b) coating thickness
c) surface roughness
d) adhesion of the coating to the substrate
e) coefficient of friction between coating and indenter

NOTE 1: Hardness and Young's modulus values may be affected by adhesion see Annex B, references B1-B5.

NOTE 2: Modelling suggests that friction between the coating and the indenter has a

negligible effect [*insert reference Final report* EU-SMT project Determination of Hardness and Modulus of Thin Films and Coatings by Nanoindentation (INDICOAT), contract no. SMT4-CT98-2249].

6.3 All the above test parameters shall be kept constant if a direct comparison is made between two or more test pieces. It should be noted that variation in test piece parameters other than Hardness or Modulus may affect measurement of these quantities. It is possible that if the indentation depth is a sufficiently small fraction of the coating thickness, (e.g.< 10% for hardness or < 3-5% for modulus measurement) it may not be necessary to keep it constant for a direct comparison. The exact limits depend on the ratio of properties of coating and substrate. It is recommended that methods for normalising results to determine coating properties from coatings of different thickness be used if coating thickness is unknown or is varying.

7 INSTRUMENTATION

A variety of depth sensing Instrumented indentation instrument types suitable for coating property measurement is available commercially. which These are capable of have exerting maximum forces ranges varying between ranging from about 20 mN (Hysitron) and to 1000 2000 mN; most of these can operate in either displacement or force control modes, but with force control being is the more common mode of usage. Many laboratory built instruments are also in operation. A feature of suitable instruments is that it they must be possible capable of to traceably traceable measurement of force and displacement as a function of time throughout the load and unloading cycle. The operation and calibration procedures are described in Annex A, section A3.

8 SPECIMEN PREPARATION

8.1 For reasons given below, provided the surface roughness criteria in 8.2.1 can be satisfied the best surface preparation is to do nothing other than to remove contaminants such as dust, fingerprints and preservative oils etc., as described in 8.3.1.

8.2 Surface roughness

Indentation into rough surfaces will lead to increased scatter in the results with decreasing indentation depth. Clearly when the roughness value, R_a , approaches the same value as the indentation depth the contact area will vary greatly from indent to indent depending on its position relative to peaks and valleys at the surface. Thus it is recommended that the final surface finish shall be as smooth as available experience and facilities permit. Recommended R_a value shall be one tenth 5% of the maximum penetration depth achieved whenever possible.

NOTE 1: It has been shown that for a Berkovich indenter when the angle that the surface presents to the axis of indentation is greater than 7 ° significant errors result - see Annex B, reference B7.

NOTE 2: While R_a has been recommended as the a practical and easily understood roughness parameter, it should be borne in mind that this is an average and thus single peaks and valleys may be greater than this as defined by the R_z value. However,, although the likelihood of encountering the maximum peak, for example, on the surface is small. so that the Ra value is preferred. Modelling to investigate the roughness of the coating surface has concluded that there are two limiting situations for any Ra value. When the 'wavelength' of the roughness (in the plane of the coating surface) is much greater than the indenter tip radius, the force-penetration response is determined by the local coating surface curvature, but when the wavelength is much less than the tip radius, asperity contact occurs and the effect is similar to having an additional lower modulus coating on the surface.

NOTE 3: In cases where coatings are used in the as-received condition, nevertheless, random defects occur such as nodular growths or scratches and where an optical system is included in the DSIIIT instrument, it is recommended that "flat" areas away from these defects are selected for measurement.

8.3 Polishing

It should be appreciated that mechanical polishing of surfaces may result in a change of the residual stress state of the surface and consequently the measured hardness. For ceramics this is less of a concern than for metals although surface damage may occur. Grinding and polishing shall be carried out such that any stress induced by the previous stage has is been removed by the subsequent stage and the final stage shall be with a grade of polishing medium appropriate to the displacement scale being used in the property determination test.

NOTE 1: Many ceramic coatings replicate the surface finish of the substrate. If it is acceptable to do so, the surface preparation problems can be overcome reduced by ensuring that the substrate has an appropriate surface finish, thus eliminating the need to prepare the surface of the coating. In some cases, however, changing the substrate surface roughness may affect other coating properties so that therefore care should be taken when using this approach.

NOTE 2: During the deposition of coatings it is common for there to be relatively large residual stresses arising from thermal expansion coefficient mismatch between the coating and the substrate and / or stress induced by the coating growth process. Thus, a stress free surface would not normally be expected. Furthermore, stress gradients in coatings are not uncommon, so that by removal of excessive material during a remedial surface preparation stage may result in a significant departure from the "true" original surface state will be generated.

NOTE 3: Polishing will reduces the coating thickness and so the effects of the substrate will be enhanced when examined indenting in-plan. The data analysis requires as accurate knowledge of the coating thickness indented and so polishing may require re-measurement of coating thickness. This again emphasises the need to

carry out minimum preparation.

8.4 Surface cleanliness

Generally, provided the surface is free from obvious surface films, no special cleaning procedures are required. If cleaning is required, the surface shall be wiped with a lintless tissue soaked in the solvent to remove trapped dust particles thus and the surface shall be rinsed in a solvent which will remove contaminants picked up during exposure to the working environment, but which is chemically inert to the coating. The surface shall then be wiped with a lintless tissue soaked in the solvent to remove trapped dust particles.

9 TEST PROCEDURE

9.1 The instrument shall be calibrated according to the procedures set out in Annex A. Ensure that and all systems required for the test are operating correctly.

9.2 In all cases a reference material shall be introduced and initial indentation experiments shall be made with this material to ensure calibrations are valid and that no damage or contamination has occurred to the indenter tip.

9.3 The test procedure detailed in Annex A shall be used. Indenter geometry, maximum force and / or displacement and load displacement cycle (with suitable hold periods) shall be selected by the operator to be appropriate to the coating to be measured and the operating parameters of the DSI instrument used.

9.4 Indents shall be placed such that no two indents are closer than five times the diameter of the larger indent. In the case of indentation into a cross-section of the coating, the indent shall be placed such that it is more than three times the largest indent dimension from the coating - substrate and the coating - interfaces.

9.5 The condition of indenters should be monitored regularly for contamination or defects. For micro and nano range indenters, periodic optical inspection using an x400 microscope is recommended for detection of contamination and gross defects. Detection of sub-microscopic damage or contamination is possible by maintaining a good history of frequent indirect validations and/or routine checking on an appropriate reference material, or by scanned probe microscopy of indents or the indenter itself. If an indenter requires cleaning the following procedure is recommended:

Hold indenter firmly and indent into a freshly cleaved surface of expanded polystyrene several times. (The plasticisers make a good solvent and the foam like nature is unlikely to damage the tip of the diamond). Inspect using an optical microscope at x400 or greater and indent gently into a small cotton wool ball soaked in acetone or water free alcohol (e.g. high purity methanol or ethanol or iso-propanol) until there is no visible contamination. If contamination is not removed by repeating this process, indentation into aluminium, glass or a clean wooden spatula may dislodge the contamination sufficiently for removal using the

above cleaning procedure. N.B. care should be taken not to subject the indenter to excessive normal and in particular lateral forces during the indentations as this could damage the indenter. One method is to use a sample that weighs less than the usual forces experienced by the indenter and gently and slowly lower the sample onto the upturned indenter, thereby limiting the maximum force to that of the sample weight.

10 ANALYSIS OF LOAD DISPLACEMENT CURVES

10.1 The procedures described in Annex A shall be used for the determination of maximum displacement, h_{max} , contact depth, h_c , measured total stiffness, S_t, specimen stiffness, S and maximum force, F_{max}.

10.2 In the case of indentation in cross-section the analysis procedures in Annex A shall be applied.

10.3 For indentation in-plan, :
Test parameters for ductile and brittle coatings need to be considered separately. However, in both cases, an accurate measurement of coating thickness, t_c, is essential for reproducible measurement of coating properties. In both cases a set of trial indentations shall be performed (e.g. at two widely spaced forces) and analysed to enable estimates of force vs. indentation depth, h_c, and indentation radius, a, to be determined. For in-plan indentation, elastic deformation of the substrate will always occur for all coatings, even though this could be negligibly small for a thick compliant coating on a stiff substrate. Thus the measured modulus will be the composite modulus of the coating and substrate and the value obtained will be a function of indentation depth.

> Note: It is relatively easy to measure the hardness of ductile coatings or the elastic modulus of brittle coatings. It is more difficult to determine the hardness of brittle or hard coatings or the elastic modulus of ductile coatings.

10.3.1 For modulus measurement of **ductile coatings** a maximum hold period shall be used that is sufficiently long to eliminate creep effects. Apparent rate sensitivity is often dominated by creep. A combination of a long hold at maximum load and a high removal rate of the test force is the best strategy for minimising the effect of creep on the measurement of contact compliance and subsequent calculation of modulus. The coating modulus may be obtained by taking a series of measurements at different indentation depths and extrapolating a linear fit to indentation elastic modulus vs. a / tc gives to zero. This method provides a first approximation in the regime a / tc < 1.5.

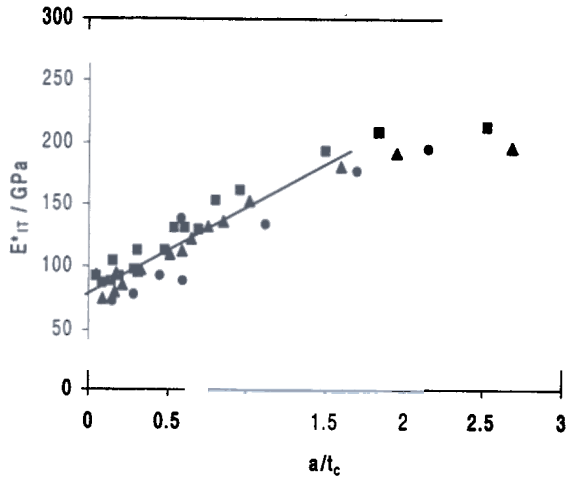


Figure 5.1b Indentation reduced elastic modulus vs. normalised coating thickness Au on Ni, selected data for spherical, Berkovich and Vickers geometries (INDICOAT

Similarly, for indentation hardness measurement of ductile coatings, a linear fit to indentation hardness vs. hc / tc gives a first approximation in the regime hc / tc < 1, providing the hardness of the substrate is not reached.

10.3.2 For **hard coatings** a linear fit to indentation elastic modulus vs. a / tc gives a first approximation in the regime a / tc < 2. However, in general, a non-linear relationship appears to apply and can be reproduced by FEA analysis. The exact nature of this non-linear relation is not known and so a linear fit over the restricted range indicated is a reasonable first approximation but is not applicable over a range wider than this.

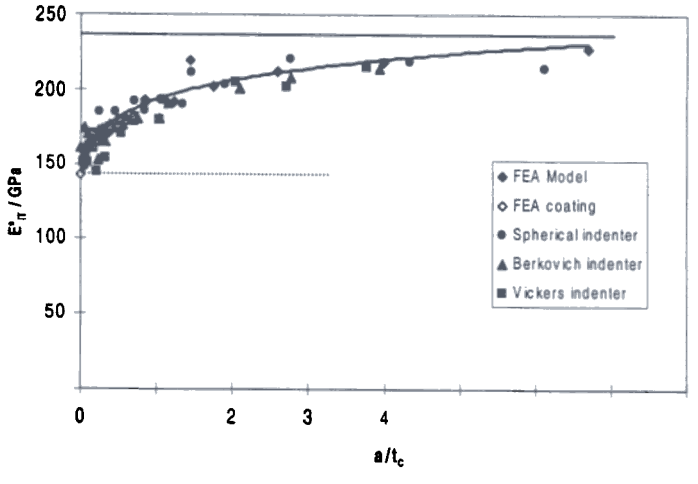


Figure 5.5b Indentation elastic modulus vs. normalised coating thickness DLC on Steel, selected data plotted with values calculated from FEA simulation. Solid line

The hardness of hard or brittle coatings can only be determined with a sharp (small tip radius) indenter that causes yielding within the coating. In general, this will only occur when hc / tc < 0.5. It is recommended that an elastic stress analysis of the coating/substrate system be undertaken using the approximation of a spherical indenter of a radius equivalent to the tip radius of the pointed indenter. This will determine whether the coating or the substrate

will yield first during indentation and if it is possible to determine the coating hardness at all. It is recommended that hardness values for the substrate be obtained for comparison, by testing if necessary. Delamination or fracture of the coating can be recognised by the hardness values obtained clustering at the substrate value, even at low hc / tc. Note, sharper indenters may cause fracture at lower loads than more blunt indenters.

NOTE 1: The extent of substrate plastic deformation will depend upon a number of factors including the relative difference in hardness and modulus between the coating and the substrate, adhesion, the coating thickness the indenter radius of curvature ('sharpness') and the maximum force.
Premature yielding of the substrate may be a particular problem only in the case of hard and stiff coatings on softer substrates. (However, if the film *modulus* is much less than the substrate *modulus* than, premature yielding of the substrate may also be caused e.g. SiO2 on W.)

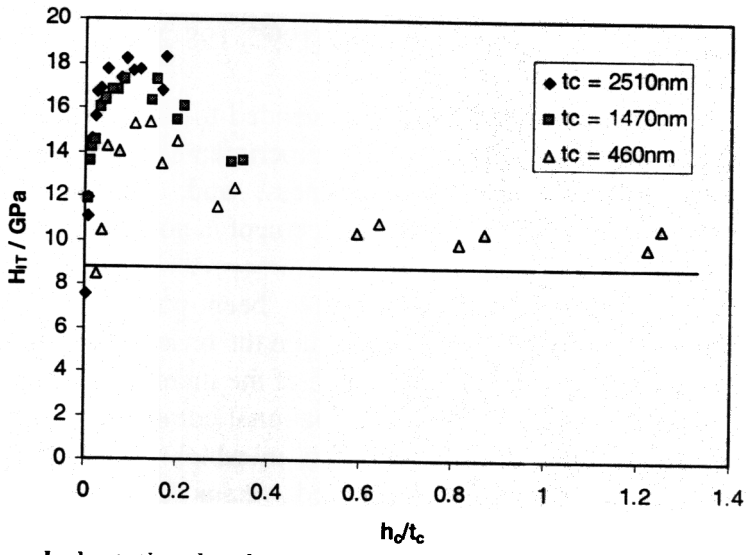


Figure 5.7b Indentation hardness vs. normalised coating thickness DLC on Steel, selected data showing the effect of substrate yield for the thinnest. Data from Berkovich and Vickers indenter geometries.

NOTE 2: The maximum penetration depth to prevent yielding of the substrate is a function of the indenter tip radius. If the indenter tip radius increases, then the maximum penetration depth to coating thickness ratio is reduced. (INDICOAT final report)

10.4 For in-plan indentation, elastic deformation of the substrate will always occur for all coatings, even though this could be negligibly small for a thick compliant coating on a stiff substrate. Thus the measured Young's modulus will be the composite modulus of the coating and substrate.

10.5 Three approaches strategies can be used to derive the coating hardness and Young's modulus:

a) For modulus measurement it is always preferable to perform perfectly elastic indentations. Thus a large radius of curvature indenter (e.g. spherical indenter) is recommended. In all cases ensure that the maximum force does not exceed a critical value for plastic deformation of the substrate and make indents that are as shallow as possible. Empirical guidelines are given in BS 5411 Pt 6 for hardness measurement of electroplated coatings on steels, and where it is recommended that the indentation depth does not exceed one tenth the thickness of the coating, while for paint films (ASTM D-1474) penetration of up to one third the coating thickness may be allowed.

NOTE 1: These are rough approximations which are It is believed that these approximations are unsatisfactory in many cases:

Y. Sun, T. Bell, S. Zheng, Finite element analysis of the critical ratio of coating thickness to indentation depth for coating property measurements by nanoindentation, Thin Solid Films 258 (1995) 198-204 .

b) For hardness measurement it is recommended to use as small a radius indenter (i.e. as sharp) as possible and determine experimentally the onset of substrate plastic deformation and the substrate hardness, and. tThen carry out indentation experiments such that the critical displacement is not exceeded.

NOTE 1: Different procedures have been published recently which suggest methods that may be used to determine the onset of substrate plastic deformation by the evaluation the loading branch of the indentation hysteresis curve, but none has yet been validated by the international community. These involve a method proposed by Rother and co-workers in which the differential of the load with respect to displacement is plotted versus displacement, and the point of inflection is taken to be the depth at which plastic deformation of the substrate occurs (Annex B, reference B8). Hainsworth and co-workers propose that departure from a linear relationship of force versus the square of displacement is also an indication of the onset of plastic deformation of the substrate (Annex B, reference B9). Similar effects were observed by Trindale and co-workers However, there is no guarantee that the yield or deviation detected is that of the substrate. Also, Tthere is always a slight deviation from the linear relationship especially for depths below 0.5μm where the tip rounding has an influence. Only for a depth above about 0.5μm (that means a film thickness of about 5μm) the deviation can be a clear indicator. when using a log-log plot (Annex B reference B21). In principle, all of these methods can be used but it should be kept in mind that they are not confirmed sufficiently and the results are not unequivocal.
Modelling provides an alternative for determining the onset of substrate plastic deformation. Our method works for the transition between elastic and first

plastic deformation. If there is already plastic deformation in the film (using pointed indenters) the method can not be used. Therefore I would not mention it here.

NOTE 2: Care should be taken when using the above approaches for multilayer or graded coatings.

NOTE 3:It is recommended to useThere is a compromise between: a) using a sufficiently high load (e.g. close to but not exceeding the limit corresponding to the onset of plastic deformation of the substrate), in order to obtain the maximum of force-depth data thereby improving the precision of the measurement; and b) indenting at a low enough displacement such that the plastic zone of the indentation does not interact with the substrate/coating interface – thus minimising the influence of the substrate on the measurement..

c) use an appropriate model such as described in 10.3 that allows calculation of the coating hardness and Young's modulus from the measured composite values.

NOTE 1: Both analytical and numerical models have been proposed. Analytical models are usually only applicable to elastic deformation. As with the experimental approach, none of these have yet been validated by the international community. Annex B, references B11 - B14, list some of the approaches being developed. *This section may need more input from the INDICOAT project WP 2.*

Further references for composite hardness:

B. Jönsson, S. Hogmark, Thin Solid Films, 114 (1984) 257

P. J. Burnett, T. F. Page, J. Mater. Sci., 19 (1984) 845

B. D. Fabes, W. C. Oliver, R. A. McKee, F. J. Walker, J. Mat. Res. 7 (1992) 3056

I. J. Ford, Thin Solid Films, 245 (1994) 122

D. Chicot, J. Lesage, Thin Solid Films 254 (1995) 123

N. G. Chechenin, J. Bøttiger, J.P. Krog, Thin Solid Films, 261 (1995) 219

A. M. Korsunsky, M. R. McGurk, S. J. Bull, T. F. Page, Surf. Coat. Technol. 99 (1998) 171

Further references for composite modulus:

H. Gao, C.-H. Chiu, J. Lee, Int. J. Solids Structures 29 (1992) 2471

J. Mencik, D. Munz, E. Quandt, E. R. Weppelmann, J. Mater. Res., 12 No. 9 (1997) 2475

NOTE 2: For multilayer coatings or coatings with a gradation in properties modelling is clearly much more difficult, and no generally accepted models are available.

NOTE 3: If wholly elastic measurements are possible, for instance using spherical indenters with a big enough radius, an exact calculation of the coating modulus from the measured composite value is possible (see references below)

T. Chudoba, N. Schwarzer, F. Richter, New possibilities of mechanical surface characterization with spherical indenters by comparison of experimental and theoretical results, Thin Solid Films 355-356 (1999) 284
N. Schwarzer, F. Richter, G. Hecht, Elastic Field in a Coated Half Space under Hertzian pressure distribution, Surf. Coat. Technol. 114 (1999) 292
T. Chudoba, N. Schwarzer, F. Richter, Determination of elastic properties of thin films by indentation measurements with a spherical indenter, Surf. Coat. Technol. 127 (2000) 9
T. Chudoba, N. Schwarzer, F. Richter, U. Beck, Determination of mechanical film properties of a bilayer system due to elastic indentation measurements with a spherical indenter, Thin Solid Films 377-378 (2000) 367-373

11 TEST REPORT

11.1 The test report shall be in accordance with EN 45001 and shall contain the following information:

a) name and address of the testing establishment;

b) date of the test, unique identification of the report and of each page, customer name and address;

c) a reference to this standard, iei.e. determined in accordance with ENV xxxx;

d) manufacturer and type of instrument;

e) description of the test material (material type, manufacturing code, batch number, date of receipt, and any other relevant information);

f) test piece condition (dimensions, coating thickness, coating type and number of layers, if known, test piece preparation procedure and surface roughness in R_a values and substrate composition, hardness and Young's modulus);

g) procedures adopted for calibration of force, displacement, instrument frame stiffness and indenter area function, including the choice of reference material used for calibration and checking instrument repeatability;

h) load / unloading cycle selected, including hold periods and state whether a correction for thermal drift was applied and if so the method used;

i) distance between indents;

j) method used to determine surface contact (zero point);

k) method chosen for the analysis of data to determine the contact depth and any models used to calculate coating properties;

l) the test data (hardness and modulus) together with an uncertainty statement at the 95% confidence limit which includes measurement and calibration errors; (see ISO GUM). Hardness values shall be expressed as H x/y/z, where x is the force in Newtons, y is the time in seconds for the force application and z is the hold time at maximum force in seconds.

m) any other relevant comments, noting, for example, where different procedures to those recommended have been used.

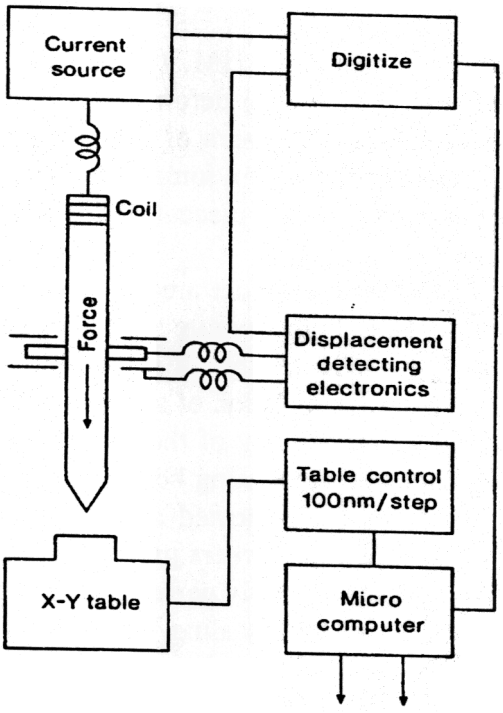


Figure 1 Schematic representation of a typical load displacement instrument - some instruments operate in the horizontal plane.

Annex A (normative)

Depth Sensing Instrumented Indentation (DSIIIT) Procedures

A1 Definitions related to DSIIIT

***A1.1 Hardness,* H:** resistance to **permanent** deformation *e.g. resistance to fracture damage is generally conferred by higher toughness and ductility, or lower H.* With DSIIIT, equation 1 below defines hardness as the maximum force, in Newtons, divided by the **projected contact area (cross-section)**, in square metres, that the indenter makes with the test piece at maximum force and thus has the units of Pa. This definition is in accord with that generally agreed and first proposed by Meyer (Annex B, reference B15), and it should be observed that the projected contact area is assumed to remain constant during elastic unloading. (see Figures A1 and A2). This is an approximation and refinements to this approach are being developed (ref. INDICOAT final Report)

> NOTE 1: The term Martens Hardness, **HM**, (previously Universal Hardness) has been recently agreed to describe the total deformation during indentation and is the maximum force divided by the surface area of the indenter penetrating beyond the initial surface of the test piece at maximum force. Thus, this definition includes both plastic and elastic deformation of the test piece. (see Figures A1 and A2).

> NOTE 2: Care is required to use the correct area function. Indentation modulus, E_{IT} and indentation hardness, H_{IT}, both require calculation of the cross-sectional (Projected) area, $A_p(h_c)$, of the indenter that is in contact with the test-piece whilst under maximum load. HM uses a calculation of surface area, $A_s(h_{max})$, of the indenter but does not attempt to model the bowing of the surface and makes the simplifying assumption that all of the indenter penetrating below the original surface is involved. Vickers hardness, HV, measures the projected area of the residual indent and then calculates the surface area of a perfect Vickers pyramid with the same projected area. This is roughly equivalent in cases of nearly perfectly plastic materials (e.g. metals) to a function $A_s(h_c)$ and so there can be a scaling factor equivalence between HV and HIT for certain materials. In practice, the blunt tip of real indenters means that, as indentation depths are reduced, there is a divergence - HV becomes infinite and HIT measures the mean pressure of indentation but ceases to be a measure of plasticity as the pressure drops below the plastic yield stress.

***A1.2 Stiffness,* S:** contact stiffness - resistance to elastic deformation, slope of the unloading curve at maximum force - see Figure A1.

***A1.3 Contact depth,* h_c :** the depth of the indenter in contact with the test piece at maximum force. This is commonly approximated by the tangent depth adjusted for indenter geometry $h_c = h_{max} - \varepsilon (h_{max} - h_r)$ where ε is 1 for a flat indenter, 0.73 for a conical and 0.75 for paraboloid - see Figure A1.

A1.4 Projected contact area, $\mathbf{A_c}$ *:* the projected area (cross-sectional area) of the indenter at the contact depth.

A1.5 Depth intercept of tangent to unloading curve, $\mathbf{h_r}$ *:* the extrapolation of the tangent to the elastic unloading curve at maximum force to zero load - see Figure A1.

A1.6 Residual penetration depth, $\mathbf{h_p}$ *:* the depth of the residual indentation - see Figures A1 and A2

A1.7 Frame stiffness, $\mathbf{S_f}$ *:* the stiffness of the instrument frame - see Section A3.2.5

A2 Principles of DSIIIT

A2.1 Determination of hardness and Young's modulus using depth sensing Instrumented indentation instruments allows direct measurement of these values indentation hardness and modulus from indentation experiments where the indentation process is continuously monitored with respect to force and, displacement and time. The experiments may be performed under either force or displacement control.

A2.2 This experimental method has two major advantages over conventional macro-hardness and micro-hardness test methods. Firstly, subjective estimation of the indent size normally needed for hardness measurement is eliminated from the test, and, secondly, from the same indentation experiment, analysis of the unloading curve (and input of an estimate for Poisson ratio) allows calculation of indentation modulus which Young's modulus, for isotropic homogenous materials, approaches Young's modulus.

Hardness, H, is defined as:

$$H = \frac{F_{\max}}{A_c} \qquad 1$$

where F_{max} is the maximum force and A_c is the projected **contact** area between the indenter and the test piece at maximum force.

A2.3 A_c is determined from the load displacement curve and a knowledge of the area function of the indenter - see Section A3.2.6.

A2.4 The area function of the indenter cannot be assumed to be that of the theoretical shape, since all pointed indenters will have some degree of rounding at the tip and spherically-ended indenters (spherical and conical) are unlikely to have a uniform radius. The determination of the exact area function for a given indenter is particularly important at small (< 500 6000 nm) indentation depths if the induced errors are to be kept below 1%.

A2.5 The reduced Young's indentation modulus, E_r, is defined as:

$$E_r = \frac{\sqrt{\pi}\ S}{2\sqrt{A_c}} \qquad 2$$

where E_r *is*

$$\frac{1}{E_r} = \frac{1-\nu_{IT}^2}{E_{IT}} + \frac{1-\nu_i^2}{E_i} \qquad 3$$

and S is the contact stiffness between the indenter and test piece, that is the derivative of the initial unloading curve after correction for frame stiffness at maximum force *(dP/dh)*, and E and ν refer to the Young's modulus and Poisson's ratio of the materials, respectively, where subscripts *IT* and *i* indicate properties of the test piece and indenter.

NOTE 1: Compliance is the reciprocal of stiffness.

NOTE 2: For diamond, the usual material used for indenters; accepted values of E_i and ν_i are 1140 GPa and 0.07, respectively, (Annex B reference B16)

A2.6 Figure A1 is a typical load / displacement curve showing the parameters to be derived for the determination of H and E. All values needed for calculation of hardness and Young's modulus can be derived directly from the load / displacement curve except the contact area. A full description is given in Section A5 on Analysis Methods.

A2.7 Indentation experiments may be performed with a variety of differently shaped indenters which are chosen to optimise the plastic and elastic deformation required for a given coating substrate system. Typically Vickers, Berkovich, conical, spherical and corner cube indenters have been used.

NOTE: For the determination of coating plastic properties, pointed indenters are recommended. The thinner the coating, the sharper the indenter should be. For the determination of coating elastic properties, spherical indenters are recommended. Ideally, an as small large as possible radius sphere is used which still enables indentation in the fully elastic regime over a reasonable indentation displacement. Too large a sphere and surface effects will dominate the uncertainties (roughness, surface layers etc). Too small a radius and the maximum load before plastic deformation results will be very low. The latter optimum can be verified by preliminary experiments or modelling (see section 10).

A3 Instrumentation

A3.1 General

A3.1.1 A variety of depth sensing indentation instrument types is commercially available which have a maximum force ranging between about 100 mN and 1000 mN; most of these can operate in either displacement or load control modes. Also many laboratory built instruments are in operation. A feature of suitable instruments in accordance with this Standard is that it must be possible to traceably measure force and displacement continuously during the load and unloading cycle. It is also important to be able to determine the point of contact with the test piece surface.

A3.1.2 While it is not a requirement, it is useful for an optical microscope to be incorporated in the instrument to allow selective positioning of the indents.

A3.1.3 Whatever the shape of the indenter chosen, it is unlikely that the theoretical shape is obtained thus each indenter area function shall be measured - see Section A3.2.6.

A3.1.4 Depth sensing indentation apparatus equipped with AFM to assess the indent shape allows the determination of possible pile-up or sink-in of the surface around the indent. These surface effects result in an increase (pile-up) or decrease (sink-in) of the contact area and hence may influence the measured results. Pile-up generally occurs for fully work hardened materials. Pile-up of soft, ductile materials is more important for thinner coatings due to the constraint of the stresses in the coating zone of plastic deformation. It has been reported that the piled up material results in an effective increase of the contact area for the determination of hardness, while the effect is less pronounced (about 50%) for the determination of Young's modulus, since the piled up materials behaves less rigidly

A. Bolshakov, G.M. Pharr, Influences of pileup on the measurement of mechanical properties by load and depth sensing indentation techniques, J. Mat. Res. 13 (1998) 1049-1058].

A3.2 Calibration procedures

A3.2.1 The instrument shall be traceably calibrated with respect to force, displacement, time, instrument frame stiffness and indenter area function. Particularly for calibration of force and displacement, it is probable that different calibration methods are required to take account of variations in instrument design. Instrument frame stiffness and indenter area function calibrations are not instrument specific when using an indentation based procedure so that these procedures shall be applied for all instrument types.

> NOTE: Some instruments measure displacement using a differential method in which the displacement difference between the indenter and test piece mounting block is recorded. While this largely eliminates the influence of instrument frame stiffness *per se*, any compliance associated with the test piece and indenter mounting system would remain, and thus calibration using a reference material mounted using the same mounting system as that employed for the test piece shall be carried out even where differential displacements are used.

A3.2.2 Force and displacement

Force is usually calibrated by use of calibrated weights, cantilevers or a microbalance. Displacement calibrations use either traceably calibrated sensors (e.g. linear variable displacement transducer (LVDT), or a capacitive system), step height standards or a laser interferometer system. Calibration procedures for both force and displacement shall be carried out using methods which provide traceability to National Standards.

> NOTE: The results of a project partially funded by the Bureau of Certified Reference Materials (BCR) on calibration procedures for depth sensing indentation instruments is available for guidance (Annex B reference B17). The paper is specific about four different instrument types, but the procedures described are believed to be of general applicability.

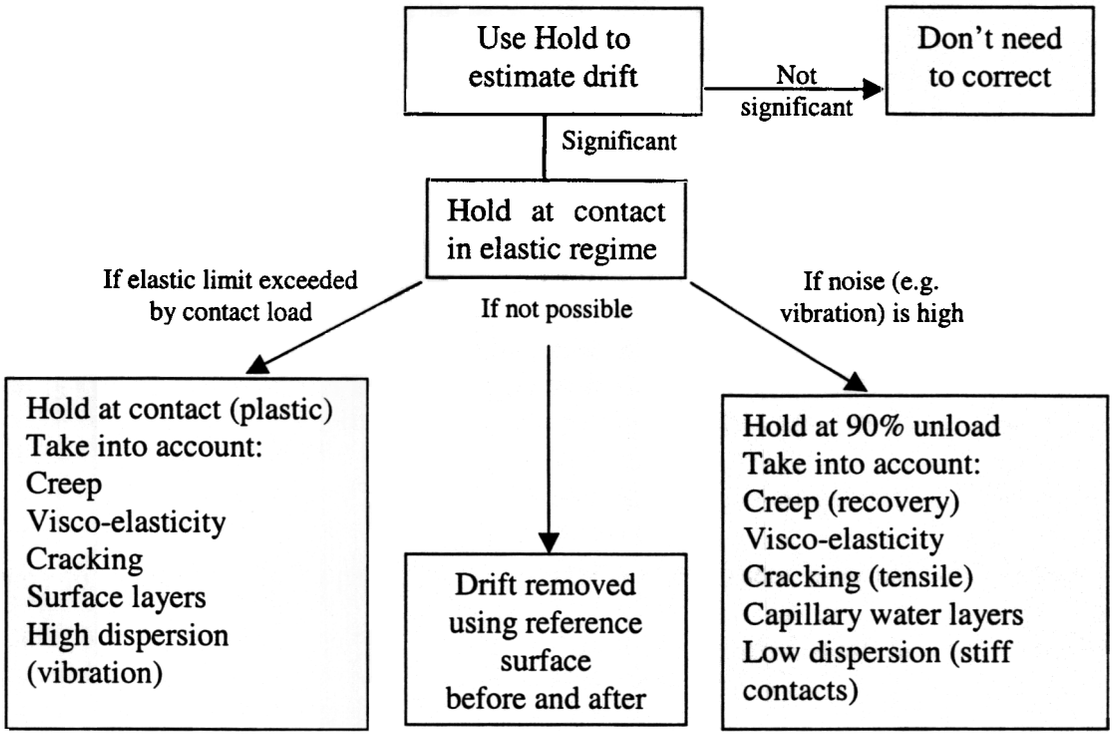
A3.2.3 The determination of instrument frame stiffness and indenter area function described below requires indentation experiments to be carried out. The depth sensing indentation instrument shall achieve optimum mechanical and thermal stability before starting an indentation cycle which may be under force or displacement control.

Force control experiments: A single loading and unloading cycle shall be used with a hold at as close to zero force as is practicable or at 90% unload for a sufficient time to allow determination of the drift in displacement due to temperature fluctuations. A further hold period shall be performed at maximum force to allow for completion of any time dependent deformation; this hold period shall be for a minimum of 10 30 s. Loading and unloading rates shall be the same and typical values are in the range 0.01-10 mN s^{-1}. Figure A1 is an example of such an indentation cycle.

> NOTE 1: If an elastic contact (contact in the fully elastic regime) can be obtained, a hold at initial contact is preferred. In this way, material influences (creep, visco-elasticity, cracking) can be avoided. If no elastic contact can be obtained, there is no generally recommendable method. Depending on the material under investigation, a hold at initial load (e.g. visco-elastic material) or at 90% unload (e.g. soft material) may be preferred. Because of the stiffer contact (higher contact area) at 90% unload, dispersion of the data when using this method is generally lower. For difficult materials, a hold period at both ends of the indentation cycle may be included. It is recommended that the hold period be for at least the loading time, and the first 10-20 s of the hold data should be discarded for the analysis since these initial data may be significantly influenced by time-dependent effects (material time-dependent deformation, formation of capillary surface layers) [reference to INDICOAT].
> The method for the determination of the surface position is described in my the article, already cited above:

T. Chudoba, N. Schwarzer, F. Richter, Determination of elastic properties of thin films by indentation measurements with a spherical indenter, Surf. Coat. Technol. 127 (2000) 9

A decision tree to assist in estimating the drift during the experiment is shown below



NOTE 2: Drift (as opposed to noise) in displacement values determined during the hold period at 90% unload or at close to zero is believed to result from temperature changes, and, in the absence of a better model, a linear correction is normally applied.

NOTE 3: The influence of the material creep behaviour on hardness and modulus results has been reported:
T. Chudoba and F. Richter, Investigation of creep behaviour under load during indentation experiments and its influence on hardness and modulus results, presented at the PSE 2000 Conference, Garmish-Partenkirchen, 17-21 September 2000

The results show that especially for materials with low hardness-to-modulus ratio (among them the most metals) the modulus results are not reliable if the hold period is too short. A modulus error, due to creep, of more than 50% may arise. The variation of the hold period produced a hardness change of 18 % at most. Hold periods are proposed in dependence on the material type that should be kept for high accuracy measurements, which range from 8 s for fused quartz to 187 s for aluminium. The criterion used was that the creep rate has decayed to a value where the depth increase in one minute is less than 1% of the indentation depth. The creep rate should be assessed in preliminary experiments. The unloading rate should be the highest possible that still ensures sufficient unload data for the subsequent analysis.

Displacement control experiments: Hold periods shall be imposed as for the load control experiments. In the case of temperature changes a drift in force will be observed, but similar linear correction procedures are normally used. Loading and unloading rates shall be the same and typical values are in the range 0.1 - 100 nm s^{-1}. Alternatively, some instruments are capable of holding at constant force to determine drift as for force controlled instruments.

A3.2.4 Calibration procedures detailed below require the use of reference materials of known Young's modulus and Poisson's ratio which shall be isotropic and homogeneous.

NOTE: Recommended materials are freshly polished single crystal tungsten and fused silica. If fused silica is used the force should not exceed the threshold at which cracking occurs (~80 - 100 mN).

A3.2.5 Instrument frame stiffness calibration

The reciprocal of the total measured stiffness, S_t , is the sum of the reciprocal of contact stiffness,
S, and the instrument frame stiffness, S_f, thus:

$$\frac{1}{S_t} = \frac{1}{} + \frac{1}{} \qquad 4$$

where S_t is derived from the derivative of the (uncorrected) unloading curve at maximum force

$$S_t = \frac{dP}{dh} \qquad 5$$

and S is the contact stiffness of the specimen material

$$\frac{1}{S} = \frac{\sqrt{\pi}}{2 E_r \sqrt{A_c}} \qquad 6$$

Thus

$$\frac{1}{S_t} = \frac{\sqrt{\pi}}{2E_r}\frac{1}{\sqrt{A_c}} + \frac{1}{S_f} \qquad 7$$

It is thus seen that if the Young's reduced modulus is constant, a plot of $1/S_t$ (uncorrected for frame stiffness) versus $1/\sqrt{A_c}$ is linear and intersects the stiffness axis at the frame compliance, $1/S_f$. Alternatively, if a reference material of known modulus is available, then by direct use of equation 7 and substituting values for E_r, A_c and S_t, S_f can be calculated. Thus a series of indentation experiments shall be performed using an isotropic reference material.

Four procedures can be used to determine instrument frame stiffness. The method selected is determined by the accuracy required balanced by the effort needed to obtain the data. The first method relies upon accurate knowledge of elastic properties of the reference materials and the indenter and the indenter shape, while the second method only requires that the indenter shape is known. The last two methods make no assumptions about the indenter shape but only require elastic properties of the indenter and the reference materials. Each of these methods requires analysis of the load displacement curve to determine the measured stiffness. The details of the analysis procedure are given in Section A5.

A3.2.5.1 The first method is to use indentations at sufficiently large displacements into a reference material. Indentation loads are typically in the 100 - 200 mN range. In this case the elastic properties of the reference material and those of the indenter are assumed and furthermore these are also assumed to be independent of depth. this method is that proposed by Meneve *et al* (Annex B references B18 and B23).

The frame compliance is determined using an iterative procedure that is itemised below. The analysis procedures are explained in section A5.

i) obtain indentation data of a material with known elastic properties;
ii) determine S_t and h_r (and hence h_c), and calculate A_c;
iii) calculate the frame stiffness using equation 7;
iv) correct indentation data for the frame compliance;
v) repeat until convergence.

NOTE 1: A minimum of ten replicate indentations is recommended to obtain statistically valid calibration values and tungsten is the preferred reference material because it is an elastically isotropic, homogeneous material, and it is less prone to handling damage compared to aluminium. Moreover, it has a high modulus and allows sufficient plastic deformation to give a high contact stiffness, yielding more robust values of the frame compliance.

NOTE 2: It is important for the accuracy of this method that the area function (at distances relatively far from the indenter tip) is well known, e.g. by independent AFM measurement (see Section 3.2.6), because the result is sensitive to that

input.

A3.2.5.2 The second procedure is based on the analysis by Doerner and Nix (Annex B reference B19). The frame stiffness is obtained by making replicate indentations in elastically isotropic and homogeneous material and assuming that the elastic properties are independent of depth. Maximum loads are typically in the 10 to 100 mN range The indenter shape is measured by an independent means, for example by atomic force microscopy, and by use of Equation 6, frame stiffness is determined from the intercept of the plot of the reciprocal of the measured stiffness against the reciprocal of the square root of the contact area.

NOTE 1: A minimum of ten replicate indentations at any single load is recommended to obtain statistically valid calibration values and tungsten or aluminium are considered to be suitable reference materials because large stiff indentations are obtained for the load range of interest.

NOTE 2: In this method, the area function must be known over a range of distances from the indenter tip, since different forces and hence different indentation displacements are used.

A3.2.5.3 The third method which has been proposed by Oliver and Pharr assumes **only** the elastic properties of the indenter and those of the reference materials and that the latter are independent of depth (Annex B Reference B20). In this method, a combined iterative procedure is used in which the frame compliance is determined as in A.3.2.5.2, while the area function is also calculated from indentations by rearranging eq. 7

$$A_c = \frac{\pi}{4}\frac{1}{E_r^2}\frac{1}{(C_t - C_f)^2} \qquad (8)$$

Aluminium and fused quartz are used as reference materials and indentation loads in the range 0.1 to 120 mN are used (3 to 120 mN in Al; 0.1 to 120 mN in fused quartz) with each loading experiment replicated ten times. Fused quartz is used to extend the area function to small distances from the tip.
In a more rigorous, self-consistent but laborious approach proposed by the same authors the frame compliance and indenter area function are determined assuming no specific value of elastic modulus, using a series of reference materials (Annex B Reference B20).

A.3.2.5.4 The alternative to the previous method as proposed by K Herrmann *et al* (Annex B Reference B23) is to use the procedure in A3.2.5.1 to determine the frame compliance in the same combined iterative procedure. Large indentations (100 - 200 mN range) shall be made into a stiff material (e.g. single crystal (100) tungsten) to obtain a value of the frame compliance and shallow indentations in fused silica (1 to 100 mN) to obtain the indenter area function. Using this approach, it was shown that after only a few iterations the frame compliance and indenter area function could be obtained, and the latter agreed to the area function by an independent AFM measurement.

A fifth method was proposed by T. Chudoba et al. which uses wholly elastic indentations

with a spherical indenter and two or three reference materials with different moduli. It is described in

T. Chudoba, N. Schwarzer, F. Richter, Determination of elastic properties of thin films by indentation measurements with a spherical indenter, Surf. Coat. Technol. 127 (2000) 9

NOTE: Ideally, reference materials are required with certified properties (Certified Reference Materials CRMs). CRMs are not yet available, but work has just started on their development. The literature values of the Young's modulus of tungsten and fused silica should be used where CRMs are not available. The need for CRMs arises from the fact that surface layers that are present on most materials will have an increasing influence on the elastic properties at small indentation depths and thus accuracy of the indenter area function and frame compliance values will decrease.

A3.2.6 Determination of indenter area function

Three methods of determining the area function are possible;

i) direct measurement using, for example, a traceably calibrated atomic force microscope (AFM), scanning electron microscope or even an optical microscope.

NOTE
The standard procedure used in the past for determining area functions has been to make a series of indentations at various depths in materials in which the indenter displacement is predominantly plastic and measure the size of the indentations by direct imaging. Using the contact depths computed from the indentation force-displacement data, an area function is then derived by empirically fitting a function to a plot of the imaged areas versus the contact depths. Clearly, the imaging technique must have sufficient contrast, resolution, and precision to accurately determine the areas. Optical imaging works well for larger indentations, but cannot be used exclusively since it is usually necessary to characterize the area function well into the sub micron range. Scanning electron microscopy is also of limited value for small indentations because the shallowness of the hardness impressions results in very poor contrast. TEM replication methods have proved useful, but they are tedious, time-consuming, and require equipment and expertise which may not be available in all laboratories. AFM is possible, but the image dilation effect caused by the finite size of the AFM probe requires correcting.

ii) indirectly by utilising indentation into a material of known Young's modulus, (see A3.2.5.3 and 4).

iii) for relatively large indentations, Trindale Trindade *et al* (Annex B reference B21) have proposed that by observing the departure from the expected linear behaviour of the plot between the calculated plastic depth using the procedure defined by Doerner and Nix (Annex B reference B19) and the depth observed by direct observation the

offset normally found for a Vickers indenter can be calculated.

The second method is similar to that used for the determination of S_f described in Section A3.2.5 above and requires a knowledge of S_f, and thus by using Equation 6 A_c can be derived for a specific **contact** depth, h_c (see Section A5.2 for the determination of **contact depth**). The load range shall be selected to encompass the full range of displacements to characterise the indenter's normal working range. For force controlled indentations some preliminary experiments are required to establish the load range needed to produce appropriate displacements in the reference material. A series of at least ten different loads shall be chosen to span the range of interest and for each load ten indentations shall be made into the reference material and the mean value used to determine A_c. Thus a plot of A_c versus indentation **contact** depth, h_c, is obtained. The method works under the assumption that no pile up exists.
If Martens Hardness is to be determined $As(h_{max})$ shall be determined in an equivalent manner, but in this case, the area function is derived from a plot of A_{max} A_s versus the maximum displacement, h_{max}.
N.B. This method does not work well for the Martens hardness because the hardness result depends on the E/H ratio and therefore on the reference material. There is no direct connection between the true physical surface area function and the apparent area, obtained at h_{max}. To prevent this situation minimise this discrepancy I it is recommended to use that only very plastic materials like Al are used as an HM reference, which would give a first approximation to the correct contact stiffness.

NOTE 1: The area function is normally expressed as a mathematical function relating the projected area to the distance from the tip of the indenter. Where a relatively simple (cubic or polynomial) mathematical function is unable to describe the area function then an estimate may be made either graphically or by using a look-up table. Alternatively a different area function can be used to describe different parts of the indenter, i.e. by use of a spline fitting routine.

A4 Test Method

A4.1. The surface of the test piece should be flat. A useful guideline is that the R_a value should be less than one tenth (I would recommend <5%) the maximum displacement.

A4.2 Generally surface preparation of the test piece should be kept to a minimum, and if possible, the test piece should be used in the as-received state if surface flatness is consistent with the criteria given in A4.1 above.

A4.3 The sample shall be mounted using the same methods as employed for determination of the instrument frame stiffness, and shall be such that the surface is normal to the axis of the indenter.

A4.4 The instrument to be used shall have been calibrated according to the procedures described in Section A3.2, and the experiments shall include a check on calibration by

indentation into a material of known properties. This check shall be carried out at the beginning of each test series.

A4.5 Indentation cycles shall be selected and where multiple indentations are planned, each indent shall be separated from the next by at least 5 diameters of the neighbouring indent.

A4.6 Determination of the zero point. For accurate determination of the displacement it is essential to be able to determine the point at which the indenter first touches the surface of the test piece (zero load on the displacement force curve). The zero-point is determined directly by observation of the first increase of either the test force or the contact stiffness during the loading cycle. Various instruments use different methods to determine the zero point, but the step size in force or displacement during the approach and subsequent loading shall be small enough to allow determination of the zero point to the required uncertainty.
Other instruments where an initial force must be applied prior to indentation, the zero depth datum is determined by post-facto back-extrapolation of the initial loading part to zero force. The initial load may vary from a few μN to several tens of μN. The errors involved in such procedure may amount to 5 - 10 nm, depending on the test material, presence of surface layers, initial load data available, and type of fit.
The back extrapolation method should also be used when direct methods fail due to uncertain contact conditions (surface roughness, vibration, surface layers) or low resolution.

NOTE 1: In case initial data in the fully elastic regime are obtained, the determination of the zero depth datum by back-extrapolation can be done with high accuracy, with uncertainties in the range 0.1 to 2 nm, using the Hertzian analytical relationships for spherical indentation.

T. Chudoba, N. Schwarzer, F. Richter, Determination of elastic properties of thin films by indentation measurements with a spherical indenter, Surf. Coat. Technol. 127 (2000) 9

(also in the case of pointed indenters in which case the tip radius typically varies between 100 and 400 nm). In this all cases the back-extrapolation method may be even better than direct methods since the latter may beconsideration should be given to the likely influence on the surface detection or definitiond byof (capillary) surface films. These can act to place additional unmeasured forces on the indentation and hence do not represent the real material response.

NOTE 2: The back-extrapolation method should be carried out with the smallest possible initial force, corresponding to the minimum extrapolation towards zero force. The uncertainty in the thus determined zero depth datum can be estimated from the uncertainty of the fit through the linearised initial depth vs. load data.

NOTE 3: First estimates of the depth offset for a given initial force can be derived from elastic theory. In the table below, elastic displacements for a range of material Young's moduli and indenter radii are given for initial contact forces of 1 μN, 5 μN and 10 μN. N.B. this is a minimum estimate assuming no plasticity.

Diamond indenter: E=1140 GPa, ny=0.307

E=5 GPa, ny=0.3	Elastic indentation depth [nm] for different indenter radii [nm]					
Load /μN	50	100	200	500	1000	10000
1	7.22	5.72	4.55	3.35	2.66	1.23
5	21.11	16.75	13.30	9.80	7.78	3.61
10	33.51	26.60	21.11	15.55	12.34	5.73
E=20 GPa, ny=0.3	Elastic indentation depth [nm] for different indenter radii [nm]					
Load /μN	50	100	200	500	1000	10000
1	2.89	2.30	1.82	1.34	1.07	0.49
5	8.46	6.71	5.33	3.93	3.12	1.45
10	13.42	10.66	8.46	6.23	4.95	2.30
E=70 GPa, ny=0.3	Elastic indentation depth [nm] for different indenter radii [nm]					
Load /μN	50	100	200	500	1000	10000
1	1.29	1.03	0.81	0.60	0.48	0.22
5	3.78	3.00	2.38	1.76	1.39	0.65
10	6.01	4.77	3.78	2.79	2.21	1.03
E=100 GPa, ny=0.3	Elastic indentation depth [nm] for different indenter radii [nm]					
Load /μN	50	100	200	500	1000	10000
1	1.04	0.82	0.65	0.48	0.38	0.18
5	3.04	2.41	1.91	1.41	1.12	0.52
10	4.82	3.82	3.04	2.24	1.78	0.82
E=200 GPa, ny=0.3	Elastic indentation depth [nm] for different indenter radii [nm]					
Load /μN	50	100	200	500	1000	10000
1	0.69	0.55	0.44	0.32	0.25	0.12
5	2.02	1.61	1.27	0.94	0.75	0.35
10	3.21	2.55	2.02	1.49	1.18	0.55
E=400 GPa, ny=0.3	Elastic indentation depth [nm] for different indenter radii [nm]					
Load /μN	50	100	200	500	1000	10000
1	0.48	0.38	0.30	0.22	0.18	0.08
5	1.41	1.12	0.89	0.65	0.52	0.24
10	2.23	1.77	1.41	1.04	0.82	0.38

A4.7 Load displacement cycles shall be performed and results calculated using the analysis method described in Section A5. The values of hardness and modulus derived shall be checked for their reasonableness.

A5 Analysis Method

A5.1 Introduction

The parameters to be determined are h_c and S. S is derived by determining the tangent to the unloading curve at F_{max} after correcting for the frame compliance (equation 4). h_c is required for the determination of the projected contact area which is given from the indenter area function [$Ap(h) = f(h_c)$]. Hardness and Young's modulus are then computed by use of equations 1, 2 and 3.

A5.2 Determination of contact depth

Figure A2 shows schematically the different depths monitored during the indentation experiment and these are related to a typical load unloading curve in Figure A1. The theoretical basis of the method for the determination of contact depth is given in Annex B reference B20. The contact depth is derived from the unloading curve using the tangent depth, h_r, and the maximum displacement, h_{max}, via the surface displacement, h_s, as

$$h_c = h_{max} - h_s \qquad 7$$

follows:
and following Sneddon's elastic analysis for a conical indenter (Annex B reference B22)

$$h_s = \frac{(\pi - 2)}{\pi}(h_{max} - h_p) \qquad 8$$

and, also for a conical indenter and elastic deformation

$$(h_{max} - h_p) = 2\frac{F_{max}}{S} \qquad 9$$

thus

$$h_s = \varepsilon \frac{F_{max}}{S} \qquad 10$$

where the geometric constant ε is 1, 2(□ - 2)/□ or 0.75 for, respectively, a flat punch,

conical or paraboloid of revolution. These ε values were theoretically derived for wholly elastic deformations. If additionally plastic deformations occur, the contact pressure distribution is changing below the indenter and this will correspond to the pressure distribution of a conical nor to that of a spherical tip in the elastic case. However it has been confirmed that ε for elasto-plastic deformations is close to the value of 0.75, independent of the indenter shape. Therefore it this value can be used as a reasonable estimation.

Thus combining (7), (10) and from Figure A1, where it can be seen that F_{max} / S equals $(h_{max}-h_r)$,

$$h_c = h_{max} - \varepsilon(h_{max} - h_r) \qquad 11$$

h_s and therefore ε depends depending on the pressure distribution that is established after the plastic deformation. h_t h_r is derived from the force displacement curve and is taken to be the tangent to the unloading cycle at F_{max}

NOTE 1: For a Berkovich or Vickers indenter ε is usually taken as 0.75 because of the fact that most indenters have a rounded tip.

Annex B (informative)

List of References

B1 P J Burnett and D S Rickerby, *Thin Solid Films.* **157** (1988) 233
B2 P J Burnett and D S Rickerby, *Thin Solid Films.* **154** (1987) 403
B3 P J Burnett and D S Rickerby, *Thin Solid Films.* **148** (1987) 41
B4 P J Burnett and D S Rickerby, *Thin Solid Films.* **148** (1987) 201
B5 T F Page and S V Hainsworth, *Surf. Coat. Technol.*, **61** (1993) 201
B6 H Lai, *J. Mater. Res.*, **8**(5) (1993) 1028
B7 N J McCormick, M G Gee and D J Hall, "The calibration of the nanoindenter". *Mat. Res. Soc. Symp. Proc.* **308** (1993) 195-200
B8 B Rother, T Lunow and G Leonhardt, *Surface Coatings and Technology,* **71** (1995) 229
B9 S V Hainsworth, H W Chandler and T F Page, *J Materials Research,* **11** (1996) 1987
B10 J J Vlassk and W D Nix, *Phil. Mag. A*, **67** (1993) 1045
B11 H F Wang and H Bangert, *Mat. Sci. & Eng.* **A163** (1993) 43
B12 K Mao, Y Sun and T Bell, *Surface Engineering*, **10** (1994) 297
B13 J C Pivin, D Lebouvier, H M Pollock and F Fielder, *J Phys. D.*, **22** (1989) 1443
B15 E Meyer, *Z. Ver. Dtsch. Ing.* **52** (1908) 645
B16 J E Field and R H Telling, Research Note "The Young's modulus and Poisson Ratio of Diamond", PCS Cavendish Laboratroy, Dept of Physics, Madingly Road, Cambridge CB3 0HE, UK, February 1999.
B17 S R J Saunders *et al* "Calibration Guidelines for Load Displacement Indentation Instruments and Procedures for Round-Robin Experiments" NPL Report CMMT(D)10, 1995.
B18 J Meneve, J F Smith, N M Jennett and S R J Saunders, *Applied Surface Science*, **100/101** (1996) 64
B19 M F Doerner and W D Nix, "A method for interpreting the data from depth-sensing indentation instruments", *J Mater. Res.*, **1**, (1986) 601-609
B20 W C Oliver and G M Pharr, "An Improved technique for the determining the hardness and elastic modulus using load displacement sensing indentation experiments", *J Mater. Res.*, **7**, (1992) 1564-1583
B21 A C TrindaleTrindade, A Cavaleiro and J V Fernandes, *J Testing and Evaluation*, **22** (1994) 365
B22 I N Sneddon, "The relation between load and penatrationpenetration in the axisymmetric Boussinesq problem for a punch of arbitaryarbitrary profile ", *Int. J. Engng. Sci.*, **3** (1965) 47-57
B23 K Hermann, N M Jennett, W Wegener, J Meneve, K Hasche and R Seemann, *Thin Solid Films,* in press.

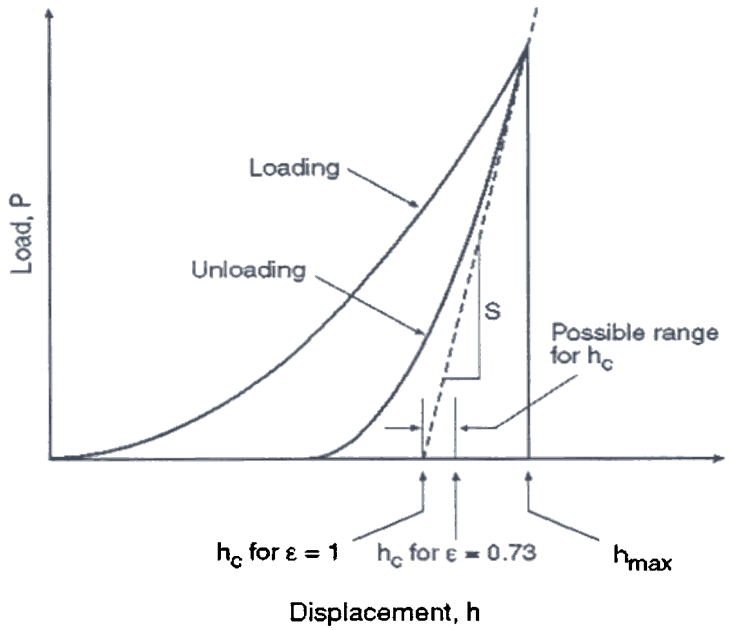


Figure A1 Schematic load displacement curve showing the quantities used in the analysis as well as a graphical interpretation of the contact depth (after reference B20).

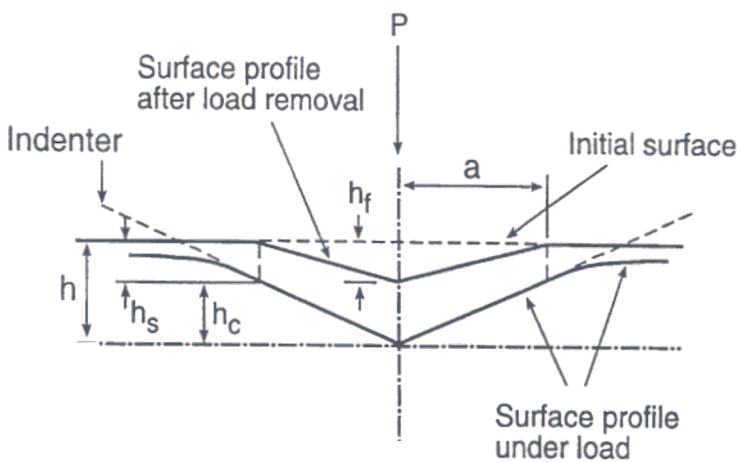


Figure A2 A schematic representation of a section through an indentation showing the various quantities used in the analysis (after reference B20)

Appendix 3 Intercomparison Instructions

Intercomparison

The intercomparison consists of three phases:

Phase one – qualification.

Participants should ensure that their instruments are recently calibrated for force, displacement, frame compliance and have a recent and valid area function for the actual shape of their indenter(s). Participants wishing to maximise the performance of their instrument may subject their instrument to a full direct calibration according to ISO/DIS 14577 part 2, however this is not compulsory. Please document any deviation from the environmental specifications of ISO/DIS 14577 or indicate where these are unknown.

Once participants are satisfied that their instrument is traceably calibrated, they will perform indentations into the two reference materials, Fused Silica and Single crystal Tungsten, according to the indirect verification in ISO/DIS 14577 part 2 section 5. Use only the samples that have been supplied under the INDICOAT project. The applied forces are not specified in the standard, but NPL suggests using 10mN and 100mN (except for Fused Silica where a lower force, such as 75 mN may be required if cracking is observed) and the cycles specified in Phase two for JDQ.

Phase two - Preliminary indentations

Participants will perform prescribed indentation cycles into the test samples using a **Berkovich indenter**. The data generated will help quantify laboratory to laboratory and sample to sample reproducibility and the data will also be useful to participants in designing the phase three indentations. The **individual results** of these experiments will be entered into a separate copy of the supplied spreadsheet. The results shall also be averaged and expressed in the ISO format in a report conforming to ISO/DIS 14577 part 1.

The prescribed cycles are as follows:
For JDQ (and phase one reference) samples:

1. Approach to contact
2. Hold for 60 seconds to measure thermal drift (optional if hold at segment 6)
3. Increase test force to maximum at a constant rate over 30 seconds
4. Hold at Max. Test Force for 30 seconds
5. Decrease test force to 90% of maximum at a constant rate over 27 seconds
6. Hold for 60 seconds to measure thermal drift (compulsory unless hold at contact)
7. decrease test force to zero over 3 seconds.

For JDR and JDS samples:

1. Approach to contact
2. Hold for 60 seconds to measure thermal drift (optional if hold at segment 6)
3. Increase test force to maximum at a constant rate over 60 seconds
4. Hold at Max. Test Force for 60 seconds

5. Decrease test force to 90% of maximum at a constant rate over 54 seconds
6 Hold for 60 seconds to measure thermal drift (compulsory unless hold at contact)
7. decrease test force to zero over 6 seconds.

Two maximum loads are to be used on each sample: 100mN and 10mN. Thermal drift should be calculated by discarding the first 20 seconds of the hold data and fitting a linear drift rate to the remaining data. It is recommended that the maximum data rate be used for all segments of the indentation cycle or at least 2 data points per second. IF your software is unable to discard data from a thermal drift segment, it is permissible to split the hold into two segments, one immediately following the other, and fit the data for the second segment to calculate the thermal drift correction.

Phase three - determination of H and E for the coatings

Participants will perform additional calculations and/or indentations to assign a value to the coating hardness and modulus for each test sample. Should participants wish to use non-Berkovich geometry indenters for this phase, they shall repeat phase one for the different indenter and report the data obtained on the reference materials. In all cases, the data will be corrected for thermal drift by using hold periods as in phase two.

Method 1 - compulsory

The coating hardness, H, or modulus, E, will be determined by performing indentations at least **five** suitable contact depths, h_c less than the nominal coating thickness and plotting the results obtained as a graph of H or E vs. h_c. The function obtained will be fitted with a straight line and extrapolated to $h_c = 0$ to obtain an estimate of the coating only value of H or E. It is recommended to use phase two data to determine the most suitable indentation depths. For Modulus, it is important to determine ranges of indentation depth where the substrate does not plastically deform. This may be done by a number of methods depending on the geometry of indenter used, e.g. this may include differentiating the loading curve or plotting suitably linearized functions, (e.g. $F^{0.5}$ vs h for Berkovich).

Method 2 - optional

It is possible that a laboratory may have other methods that they consider should be compared. This section is intended to allow participants to return their best estimate of the coating properties by these methods. Methods may include fitting an alternative function to the data obtained in method 1, or other methods, which the participant shall describe fully in the report.

Appendix 4 Research Profile of Partners

National Physical Laboratory

The National Physical Laboratory is the UK's Standards laboratory for physical quantities (mass, length, time, etc.), and within the Materials Centre has responsibility for the development of test methods for materials. The Laboratory has ISO 9000 quality accreditation and has a broad experience in research projects funded by the European Commission, many of which have been sponsored by Brite/Euram, JOULE and BCR. The Centre carries out research on a broad range of topics covering most aspects of materials with the general remit to develop improved measurement methods. It has about 50 graduate level staff plus 25 support staff as well as consultants and guest workers.

The researchers working on the indicoat project included Dr. Nigel Jennett, Dr Stuart Saunders, Dr Tony Maxwell, Dr Roger Hunt and Dr Neil McCartney. Stuart Saunders was the former chairman of VAMAS-TWA22, is a member of CEN/TC184/WG5 and the author of the CEN ENV on hardness and modulus testing of thin ceramic coatings by depth sensing indentation.

Related EC Contracts that NPL have participated in include:

> BCR project, MAT1-CT92-0027, "Hardness (mechanical property) testing of surfaces" - completed 1996
>
> BCR project, MAT1-CT-94-0045 "Development and Validation of Test Methods for Thin Hard Coatings (FASTE)" - current.

VTT Manufacturing Technology

VTT Manufacturing Technology is one of VTT´s nine research institutes. It has 320 staff members, of whom 180 are university graduates. The Institute can provide its customers and collaborators with easy access to the very wide expertise of VTT´s almost 3000 specialists.

Turnover in 1999 was about EURO 25 million, three quarters of which coming from contract work and joint research programmes. Foreign income is more than 12 % of the turnover.

VTT Manufacturing Technology carries out research and development work in collaboration with its customers and the best technology providers with the aim of enhancing the competitiveness of engineering, energy and process industries. More generally, the Institute develops the infrastructure necessary for more effective product development and manufacturing.

The Institute's high level of knowledge is maintained by means of its own research initiatives and extensive networking with international technology providers. On the other hand our close collaboration with experts in the corporate world guarantees the industrial relevance of our research and development work. We serve our SME customers in conjunction with local service providers, forming an expanding network.

VTT Manufacturing Technology has been and is participating in many Nordic and European research programmes, such as FP5 GROWTH, BRITE-EURAM, ESPRIT, EUREKA, TACIS/PHARE and COST. It has good resources as well as versatile, long and acknowledged experience and expertise in carrying out and co-ordinating research work in it's competence areas.

Surface Engineering Profile

The surface engineering group consists of 19 staff members specialised into various aspects of surface engineering. The number of researchers in the group is 13. The area of interest cover surface treatment, coating, surface analysis and testing. Several projects in these fields have been assigned to companies and conducted in large national and European projects.

In more detail the group has expertise in the following subjects:

Surface treatment processes: Pre-treatment methods, electrode-position, painting, thermal spraying (HVOF, wire arc), plasma assisted deposition (PVD, PSII), hot dip galvanising, laser surface coating, HIP- and weld cladding.

Advanced coatings: Physical vapour deposion (pulsed vacuum arc, rf plasma deposition) plasma source ion implantation (PSII), High Velocity Oxy-Fuel (HVOF), wire arc spray, thick coatings by HIP, SHS and weld cladding.

Surface characterisation and failure analysis: Scanning electron microscopy (EDS/WDS), optical microscopy, nano-indentation and micro hardness, CER-measurements (contact electric resistance), material failure mechanisms determination, optical emission spectroscopy.

Coating selection and testing: accelerated environmental testing (salt spray, weather test, gas corrosion), erosion corrosion testing (slurry pot, high temperature oxidative erosion), high temperature corrosion testing (effect of gasses and salt deposits), abrasive wear testing

Environmental aspects: Three valent chromium plating, vacuum coating, surface treatment plant waste water management, electrical discharge polishing, electroplating modelling.

PTB Research profile

The key staff of PTB comes from the section Micro- and nanotopography. The research profile of this section is divided in following fields:

- Hardness
- Roughness and topography
- Layer thickness
- Scanning probe microscopy

In the field of hardness the following tasks are fulfilled:
- calibration of hardness reference blocks and indenters for macro-, small force and microhardness
- further development and investigation of hardness standard machines
- Investigation and development of methods for the calibration of hardness reference blocks for macro-, micro- and nanohardness
- Investigation of the geometry of indenters used for nano- and microindentation with scanning force microscopy

The key staff of PTB:
Dr. Herrmann, head of section, is secretary of IMEKO TC 5 "Hardness measurement". He is member of the DIN standardization committee NMP 141 on hardness testing and chairman of the DIN standardization committee NMP 161 on layer thickness measurement. In the framework of the German calibration service DKD he carries out the accreditation of hardness laboratories.
Dipl.-Ing. Frank Pohlenz has over 10 years of experience in dimensional and hardness metrology (macro-, micro- and nanohardness, automatization of of measurement processes, form measurements, laser interferometry, scanning force microscopy).
Dipl.-Phys.(FH) Febo Menelao has over 3 years experience in material testing including metallography and other preparation techniques. He is specialized in micro- and nanohardness measurements.

VITO, (Flemish Institute for Technological Research)

VITO is a non-university multidisciplinary RTD organisation with expertise in the fields of advanced materials, energy, and the environment. Ir. J. Meneve, of the Materials Technology Centre, is a senior research engineer with a profound expertise in the field of mechanical and functional characterisation of hard wear resistant surface coatings. He is an active member of the European Standards Committee CEN TC184/WG5 'Test Methods for Ceramic Coatings'. VITO has a national responsibility in this field of standardisation.
The Surface Technology Group of the Materials Technology Centre is an established centre of excellence for the development, characterisation and testing of thin surface coatings, particularly in the area of DLC and related materials. A NanoTest 550 depth-sensing indentation instrument is extensively used to assess the surface mechanical properties of coated components. All aspects of surface engineering are covered which range from surface preparation to functional property evaluation, and the results of this research are regularly published.

Selected Relevant publications and patents:
Dekempeneer, R. Jacobs, J. Smeets, J. Meneve, L. Eersels, B. Blanpain, J. Roos and D.J. Oostra, *'R.f. plasma assisted chemical vapour deposition of diamond-like carbon: physical and mechanical* properties', Thin Solid Films, 217 (1992) 56.

Meneve, J.F. Smith, N.M. Jennett and S.R.J. Saunders, *'Surface mechanical Properties by depth sensing indentation'*, Applied Surface Science, 100/101 (1996) 64.

Dekempeneer, J. Smeets and J. Meneve, 'Method for applying a diamond-like carbon coating on steel, iron or alloys thereof', Patent number: EP 0 600 533 B1.

Joint Research Centre, Institute for Advanced Materials, Ispra

The Joint Research Centre, now DG-JRC of the Commission of the European Communities, forms an integral part of the European Union's science and research initiative, playing a neutral role whilst being closely integrated into the European network of science and technology programmes. It executes scientific and technical research in 7 institutes located in 5 different sites in Belgium, Germany, Italy, the Netherlands and Spain. Total statutory staff is 1860 from which 1110 are scientific-technical staff. In addition 325 non permanent staff including grant holders, post-doctoral fellows and visiting scientists are present at the JRC. During 1993, the Council of the European Union and the European Parliament made a JRC participation in European Commission sponsored shared cost actions possible.

Within the framework of the JRC, the Institute for Advanced Materials (IAM), with sites both in Petten and Ispra executes the specific research programme on Advanced Materials, support to the Commission services, and operates the High Flux Reactor. Furthermore, the IAM is also involved in competitive activities such as work for third parties on a contractual basis, mainly for industries.

At JRC-IAM Ispra several laboratories are operational: a Surface Modification Centre (5 kW C02-laser, Nd-YAG laser, ion implanter), a Cyclotron Laboratory, a Mechanical Testing Laboratory, a Thin Film Deposition Laboratory, a Non-Destructive Testing (Ultrasonics) Laboratory, a Photothermal Methods Laboratory, a Plasma Spraying Laboratory, and a Sensors Laboratory. IAM Ispra is equipped, in addition, with many facilities for compositional, microstructural, tribological and morphological analysis (scanning and transmission electron microscopes with microanalysis, ESCA/Auger spectroscopy, plasma etching, scratch and wear testing, indentation and nanoindentation, standard and glancing angle X-ray analysis, IR spectroscopy, etc.).

Because of their neutral and international position, many JRC staff members participate in the working groups and technical committees of CEN as observers and advisers. The voting members of these groups and commitees are nominated by the national organisations. Moreover, JRC have through BCR indirect relations with CEN concerning reference materials.
IAM/JRC Petten has connections with the CEN-STAR working group dealing with general problems of standards and research, and participates in the CEN-TC 184: "Advanced technical ceramics" technical committee working group WG 5: "Methods of testing of ceramic coatings".

The thin films group of IAM/JRC Ispra (directly involved in this proposal) participated in the BCR project MAT 1-CT 92-0027: "Hardness testing of surfaces" concerning the mechanical properties of coated surfaces.

The project manager for INDICOAT was Dr Neil GIBSON a Research Scientist in the "Thin Films Sector" of the "Surface Engineering Unit". Gibson has over 10 years experience of materials analysis and characterisation, surface analysis techniques, nanoindentation, thin film deposition. He is an experienced project manager and an established scientist in his field with over 50 publications, manuscripts and EUR or DL Technical reports to his name, recent publications include:-

1. ULTRAHARD Ti-B-N AND Hf-B-N COATINGS: PREPARATION AND CHARACTERIZATION, T. Friesen, J. Haupt, P.N. Gibson and W. Gissler, 12th Italian Conf. on "Vacuum Science and Technology" (XII Congresso Nazionale sulla Scienza e Tecnologia del Vuoto), 23-26 March 1993, Bolzano (I), Vuoto **23** no.2 (1994) pp.28-31

2. TITANIUM BORON NITRIDE COATINGS OF VERY HIGH HARDNESS, P. Hammer, A. Steiner, R. Villa, M. Baker, P.N. Gibson, J.Haupt and W. Gissler, Surface and Coatings Technology **68/69** (1994) pp.194-198

3. A COMPARATIVE STUDY OF THE TRIBOLOGICAL BEHAVIOUR OF HOMOGENEOUS AND MULTILAYER Ti-B-N COATINGS, T.P. Mollart, M.A. Baker, P.N. Gibson, J. Haupt and W. Gissler, Int. Conf. on "Metallurgical Coatings and Thin Films" (ICMCTF '96), San Diego (CA) USA, 22-26 April 1996, to be published in Surface and Coatings Technology

4. PHASE COMPOSITION AND TRIBOLOGICAL BEHAVIOR OF TITANIUM BORON NITRIDE COATINGS, W. Gissler, M.A. Baker, J. Haupt, P.N. Gibson, R. Gilmore and T.P. Mollart, Diamond Films and Technology **7** no.3 (1997) pp.165-180

5. TRIBOLOGY AND MICROSTRUCTURE OF PACVD B-N-C COATINGS, E. Dekempeneer, V. Wagner, P.N. Gibson, J. Meneve, S. Kuypers, L. van Ijzendoorn, J. Smeets, J. Geurts and R. Caudano, Diamond Films and Technology **7** no.3 (1997) pp.181-193

Royal Institute of Technology (KTH)

KTH is a major centre for the study of all aspects of materials science. The Division of Ceramics frequently collaborates with industry on topics such as mechanical properties of multilayer coatings on cemented carbide cutting tools, wear-resistant materials and coatings, thin metallic lines on Si substrate. The Department is host to many overseas students and staff who participate in courses and training programmes at all levels, Area of special teaching expertise include microstructural analysis, phase diagrams and mechanical behaviour.

The Division of Ceramics has an extensive range of modern facilities for processing ceramics and evaluation of their properties and microstructure. Indentation equipments are one of the special features in the new mechanical testing laboratory, which includes

a Nano-indenter, Micro-indenter and Macro-system which can all capture load-penetration curves. Over the last five years, there has been extensive research activity related to the modelling and analysis of indentation load-penetration curves. The research has lead to an analysis methodology to derive the mechanical properties of bulk materials from load-penetration curves, including hardness, modulus, yielding strength, strain hardening, and damage modulus. A new method to analyse DSI unloading curves to get elastic modulus has also been derived.

The researchers involved in Indicoat are involved in a project on numerical modelling (finite element method) of sharp indentations on coatings and have participated in Round Robin intercomparisons organised as part of the VAMAS TWA 22 project - Mechanical Properties of Thin Films and Coatings and the EC SMT Project on Development and Validation of Test Methods of Thin Hard Coatings (FASTE). A Selection of recent publications are listed below:

P.-L. Larsson, A.E.Giannakopoulos, E.Söderlund, D.J.Rowcliffe, and R.Vestergaard, 1996. Analysis of Berkovich Indentation, Int. J. Solid Structures, Vol. 33, No.2, pp.221-248.

K.Zeng, E.Söderlund, A.E.Giannakopoulos, and D.J.Rowcliffe, 1996, Controlled Indentation: A General Approach to Determine Mechanical Properties of Brittle Materials, Act mater., Vol.44, pp.1127-1141.

K.Zeng and D.J.Rowcliffe, 1996, Analysis of Penetration Curves Produced by Sharp Indentations on Ceramic Materials, Phil. Mag., A, Vol.75, 1107-1116.

E.Söderlund and D.J.Rowcliffe, 1994, Analysis of Penetration Curves Produced by Depth-sensing Indentation Systems, J.Hard Mater., Vol.5, 149-177.

University of Coimbra

University of Coimbra is a University Laboratory which is part of the Mechanical Engineering Department of the Faculty of Sciences and Technology of Coimbra University (DEM-FCTUC). It is involved in the processing and characterization of materials. It's main interests are related to the modification of the surface of materials, particularly by deposition of thin coatings using sputtering techniques. The laboratory has the usual structural, chemical, morphological and thermal characterization of the coatings, but mechanical tests (hardness, scratch-test, wear tests) have been the most important for the Group, in particular those which allow the evaluation of the elastic-plastic characteristics of the films. For several years, an extensive research programme has been conducted concerning the analysis of the plastic deformation behaviour of materials, either by experimental techniques (e.g. TEM) or by finite elements modelling. At first, efforts were concentrated on the problems arising in technologies using plastic deformation for materials processing, but now the requirement to understand the plastic behaviour under hardness indentations has been one of the main aims of the Group.

LAIN (Laboratoire d'Analyse des Interfaces et de Nanophysique)

LAIN is part of the EEE Department of the University of Montpellier II. At the present time, 42 researchers (staff and PhD students) are involved in the field of micro acoustics. With 20 years of experience in micro acoustics, more than one hundred publications, proceedings and patents on this topic, about fifty national, European and industrial projects in micro acoustics, the laboratory has become a leader in the field. Its budget (acoustics team only) is about 200kECU/year since the beginning of the 80s. The research topics are :

- Microanalysis of the elastic moduli using the spatial acoustic signature.
- V(z) and frequency acoustic signature V(f) for layered systems.
- Micro echography and micro interferometry.
- Near field acoustic microscopy (super resolution).
- Specific acoustic lenses and transducer designing.
- Application to microelectronics, metallurgy, glass, biomedical...

Dr J.M. Saurel, CNRS senior researcher and Dr L. Robert will be personally responsible of the technical and scientific tasks executed within the present programme.

References

R. da Fonseca, L. Ferdj-Allah, G. Despaux, A. Boudour, L. Robert and J. Attal
" Scanning Acoustic Microscopy "
Recent Applications in Material Sciences Advanced Materials, Vol.5, pp. 508-519, (1993).

R. da Fonseca, L. Robert, J.M. Saurel, Foucaran, Camassel, Massone, Taliercio, Boumaiza
" Acoustic investigation of porous silicon layers " J. Materials Science, 30, p. 35-39, (1995).

A. Ramdani, F. Augereau, G. Despaux
" Etude de l'efficaciti des modes de Lamb dans la signature acoustique V(z) d'une couche mince par la thiorie de la risonance " J. Phys. III France 6, p. 571-595, (1996).

M. Amlouk, N. Brunet, B. Cros, S. Belgacem et D. Barjon
" Study by means of acoustic microscopy of Ag2S thin film deposited by spray "
J. Phys. III France 7, p. 1741-1753 (Septembre 1997).

University of Oxford

University of Oxford is a world renowned centre of academic research excellence. The Dept of Materials has extensive experience of thenano-measurement techniques and has collaborated with NPL, VITO and LAIN on the other EU programmes including the EC SMT project "FASTE" developing the use of acoustic techniques for coating property measurement.

Oxford has a unique experience of Surface Brillouin spectroscopy for the independent determination of elastic properties of thin films and coatings.

The dedicated apparatus for the SBS measurements is now commercially available (Bede Scientific Ltd., Durham, UK). It was developed in collaboration with the acoustic microscopy group of the Oxford University, which has all the expertise in the design, application, and calibration of the system. The physical values involved in the measurement of the SAW velocity are length of the Fabri-Perot interferometer (manufacturer - Queensgate, UK) angle of the incident beam, absolute frequency of the laser and use the constant of the speed of light in air, making the procedure of tracing the measured values to the national standards a relatively straightforward task.

1. Surface Brilluoin scattering—extending surface wave measurements to 20 GHz. P. Mutti, C.E. Bottani, G. Ghislotti, M. Beghi, G.A.D. Briggs and J.R. Sandercock. Advances in Acoustic Microscopy 1 (Ed Andrew Briggs) Plenum Press, New York (1995) 249-300.

2. "Acoustic microscopy for imaging and characterization". G.A.D. Briggs and O.V. Kolosov. MRS Bulletin, October 1996.

Fraunhofer Institute for Material and Beam Technology (FhG-IWS)

Research activities:
IWS is an institute of the Fraunhofer Society for Applied Research. It works in the field of surface engineering by using and developing laser assisted techniques. Many efforts are performed to deposit super-hard films as diamond-like carbon films for industrial applications. Since there is a lack of robust mechanical test methods for super-hard films in the sub-micrometer range, FhG-IWS used its long experience in laser-acoustics to develop and commercialise a laser-acoustic equipment for testing thin films. This is presently the only commercially available laser-acoustic test equipment for thin films in the world. It is based on laser induced acoustic surface waves. It measures the dispersion spectrum of this wave mode that is very sensitive to surface films. The inverse solution of the dispersion relation yields the Young's modulus of the film material. The technique enables the elastic modulus of film with thickness down to less than 50 nm to be measured on substrate materials showing low ultrasonic attenuation. Few test methods are currently available for mechanical testing films in this thickness range.

Unique contribution:
The laser-acoustic test method is an interesting alternative method for testing mechanically thin films. It is based on other physical principles and, therefore, complements the introduced techniques. The developed equipment can be easily operated, is completely non-destructive, has a good reproducibility, and does not need special specimen preparation. It can be applied to support the surface engineering in the

field of fundamental research, optimising the technology, and controlling the film quality.
Therefore, our institute is a partner of many scientific groups from all over the world for testing thin films by the laser-acoustic technique.
For example:

- Pof. Russell Messier, Pennsylvania State University, 277 Materials Research Lab. University Park, PA 16802, USA
- Prof. Allan Matthews, RCSE, University of Hull, Hull HU6 7RX, UK
- Prof. Jan - Eric Sundgren, Department of Physics, Linköping University, S-58183 Linköping
- Andrey Voevodin, Wright Patterson Airforce Base, Wright Lab, Matls Dircectorate, WL/MLBT, 2941 P Street Bld 654, Ohio OH 45433 - 7750, USA
- Shi Xu, Nanyang Technological Univ., School of EEE, Block S1, Research Lab. 6, Nanyang Avenue Singapore 639798
- Tai Kumagai, Nanotec Corporation, Nishi 8-19-8, Shiraoka, Minamisaitama Saitama 349-02, Japan
- Prof. Y Lifshitz, Soreq NRC, Yavne 81800, Israel

The method was mostly used to investigate diamond-like carbon films, since deposition of such films for industrial application is a main field of FhG-IWS. However, many other film materials were tested as SiC, ZrO_2, BN, TiN, TiC, (Ti,Al)N, CrN, Al_2O_3, hard chromium, nickel, nitrided coatings, polyamide, etc.

Appendix 5 Partners Contact Details

Role	Organisation Name and Address	Type	Country	Contact Person
Coordinator Partner 1 NPL	National Physical Laboratory Materials Centre, Queens Road, Teddington Middlesex , TW11 0LW, UK	ROR5	GB	Dr Nigel M Jennett Tel:+44-181-943 6641 Fax:+44-181-943 6177 E-mail: nigel.jennett@ npl.co.uk
Partner 2 VTT	VTT Manufacturing Technology P.O.Box 1703 Metallimiehenkuja 2-4 Espoo, FIN-02044 VTT, Finland	ROR5	FI	Dr Jari Koskinen Tel:+358 9 456 5413 Fax:+358 9 463 118 E-mail:Jari.Koskinen@vtt.fi
Partner 3 VITO	Vlaamse Instelling vor Technologisch Onderzoek Boeretang 200, B-2400 Mol Belgium	ROR	BE	Ir Jan Meneve Tel:+32-14-33 5620 Fax:+32-14-32 1186 E-mail:menevej@vito.be
Partner 4 JRC-IAM	Institute for Advance Materials TP 750 Joint Research Centre 21020 Ispra (VA) Italy	IND	IT	Dr. Neil Gibson Tel:+39-(0)332-789 5616 Fax:+39-(0)332-785 036 E-mail:neil.gibson@jrc.it
Partner 5 KTH	Royal Institute of Technology Valhallavagen 79 Stockholm 100-44 Sweden	EDU	SE	Dr David Rowcliffe Tel:+46-8-790 8322 Fax:+46-8-790 8322 E-mail:david@met.kth.se
Partner 6 QMW	Queen Mary and Westfield College Mile End Road London, UK E1 4NS	EDU	GB	Dr Andy Bushby Tel:+44-171-975 5276 Fax:+44-181-981 9804 E-mail:a.j.bushby@qmw.ac.uk
Partner 7 TUC	Technische Universität Chemnitz Institut für Physik Reichenhainer Strasse 70 (Weinholdbau) D-09107 Chemnitz, Germany	EDU	DE	Dr. Thomas Chudoba Tel:+49-(0)371-531 3210 Fax:+49-(0)371-531 3042 E-mail: t.chudoba@physik.tu-chemnitz.de
Partner 8 UC	Departamento de Engenharia Mechanica Faculdade de Ciencias e Tecnologia da Universidade de Coimbra Pinhal de Marrocos, Coimbra 3000, Portugal	EDU	PT	Prof. Albano Cavaleiro Tel:+351-39-790700 Fax:+351-39-790701 E-mail:albano.cavaleiro@mail.dem.uc.pt
Partner 9 PTB	Physikalisch-Technische Bundesanstalt P.O.Box 1132 Fürstenwalder Damm 388 Berlin, D-12562/D-12587, Germany	ROR/6	DE	Dr.-Ing. Konrad Herrmann Tel:+49-30-6441 291 Fax:+49-30-6441 488 E-mail:konrad.herrmann@ptb.de
Partner 10 CSEM	Centre Suisse D'Electronique et de Microtechnique SA Case Postale 41, Jaquet-Droz 1 Neuchatel 2007, Switzerland	ROR4	CH	Mr Bertrand Bellaton Tel:+41-32-720 5560 Fax:+41-32-720 5730 E-mail:bertrand.bellaton@csemne.ch
Partner 11 LAIN	Laboratoire d'Analyse des Interfaces et de Nanophysique, Uni. Montpellier, Place Eugene Bataillon Montpellier, F34095 CEDEX 05, France	EDU	FR	Dr Jean-Marc Saurel Tel:+33(0)-4-67 14 42 82 Fax:+33(0)-4-67 52 15 84 E-mail: saurel@lain.univ-montp2.fr

Partner 12 UOX-Mat	University of Oxford Dept. of Materials Parks Road, Oxford, UK, OX1 3PH	EDU	GB	Dr Oleg Kolosov Tel:+44(1865)273-735 fax:+44(1865)273-789 E-mail:oleg.kolosov@materials.ox.ac.uk
Partner 13 FhG-IWS	Fraunhofer Institut für Werkstoff und Strahltechnik Winterbergstrasse 28 01277 Dresden Germany	ROR	DE	Dr. Dieter Schneider Tel:+49-(0)351-2583 451 Fax:+49-(0)351-2583 300 E-mail:schneider@iws.fhg.de